# High-Temperature Corrosion Phenomena in Waste-to-Energy Boilers

Shang-Hsiu Lee

Submitted in partial fulfilment of the

Requirements for the degree

of Doctor of Philosophy

in the Graduate School of Arts and Sciences

**Columbia University**

**2009**

# Abstract

High-Temperature Corrosion Phenomena in Waste-to-Energy Boilers

Shang-Hsiu Lee

Waste-to-Energy (WTE) technology is an essential part of sustainable waste management. It generates electricity by combusting municipal solid waste (MSW) under controlled conditions. There are over 600 WTE facilities globally combusting over 170 million tons of MSW annually. However, high temperature corrosion of boiler tubes remains an operational and economic problem for the WTE industry.

Past research work concentrated on reducing corrosion in WTE boilers either by improving the process conditions in the boiler, or by developing alloys that can withstand better the relatively high chlorine concentration in the combustion gases (400-600 ppm HCl).

This research examined the corrosion mechanisms in WTE boilers by conducting laboratory tests under conditions that simulated the WTE environment. The controlling variables in the tests were based on the analysis of data provided by over fifty U.S. WTE facilities in response to a corrosion survey that was distributed by the Waste-to-Energy Research and Technology Council, an academic-industry organization headquartered at Columba University. This study also explored the feasibility of a novel procedure that aimed to reducing the hydrogen chloride concentration in the combustion gases flowing through the boiler.

The research effort included (1) an in-depth analysis of the survey on high temperature corrosion; (2) laboratory tests that, for the first time simulated the large temperature gradients encountered across the wall of WTE heat exchanging metal surfaces and clarified the mechanism and kinetics of chlorine induced corrosion and the effect of hydrogen chloride gas concentrations on corrosion rates; and (3) laboratory tests on the sequestration of chlorine in the WTE process gas by means of injecting chemicals into the furnace.

The corrosion survey showed that the most common waterwall tubing was low-carbon steel SA178A (>99%Fe) cladded with Inconel 625 (58%Ni-20-23%Cr-8-10%Mo) applied. Low-carbon, intermediate-chrome alloys SA213 T11 (Fe-1.05%Cr-0.08%C) and T22 (Fe-2.21%Cr-0.1%C) were mostly used as superheater tubing.

In the experimental corrosion tests, the stainless steel alloy NSSER-4 (Fe-17.3%Cr-13.1%Ni-2.5%Si) that is produced by a Japanese company showed excellent corrosion resistance. Although NSSER-4 is not available in the U.S. steel industry now, it is highly recommended for superheater tubing where higher metal temperatures are required. The low-carbon, intermediate-chrome steel SA213 T11 exhibited acceptable corrosion resistance at metal temperatures up to 540$^{o}$C. The low carbon steel SA178A had the worst corrosion resistance among all alloys tested.

Increasing the HCl concentration in the synthetic gas flow through the experimental apparatus increased the corrosion rates of test coupons. The HCl effect was amplified with increasing metal temperature. In addition, the presence of HCl promoted the formation of sulfate salts and increased the corrosion. The results of the

chemical rate test showed that the overall reaction process of alloy SA178A during the 100-hour test followed the parabolic time dependence which was often found in high temperature oxidations. The overall apparent activation energy of alloy SA178A within the 100-hour test was 178kJ/mol which was determined from multiple tests. The calculated activation energy of alloy SA178A after a single 100-hour test was 149kJ/mol, which was close to its overall activation energy showing that the 100 hours of exposure was suitable for the corrosion test. From the comparison of activation energies of three test materials, it was inferred that the corrosion of the low-carbon steel, SA178A was more kinetically controlled while the stainless steel, NSSER-4 was more diffusion controlled.

The injection of calcium hydroxide slurry droplets, in order to react with $HCl/Cl_2$ and thus lower the effective chlorine concentration in the gas, was shown to reduce appreciably the corrosion rate of the metal coupons in the test chamber. The observed reduction of overall mass loss ranged from 0.3-18% for three different metal alloys. These accelerated corrosion tests were conducted at metal temperatures of $700^{o}C$, that is appreciably higher than the temperature gradient tests (450-$580^{o}C$). Even under these conditions the stainless steel alloy, NSSER-4, exhibited vastly superior performance to the steel alloys that are commonly used in the WTE industry. Its overall mass loss per surface area was 64 times lower than SA178A and 70 times lower than SA213 T11.

# Table of Contents

Page

# List of Figures

Page

# List of Tables

Page

# Acknowledgements

I would like to express my deep gratitude to Dr. Nickolas J. Themelis and Dr. Marco J. Castaldi for their invaluable advice and supports through this graduate work. I would also like to thank my dissertation committee members Dr. Paul F. Duby, Dr. I. Cevdet Noyan, and Dr. Raimondo Betti for their helpful guidance and suggestions.

I also gratefully acknowledge the financial support of the Waste-to-Energy Research and Technology Council (WTERT) of Earth Engineering Center at Columbia University and the scholarship awards of the ASME Solid Waste Processing Division (SWPD).

I would also like to thank my friends who helped me in many different aspects during the study at Columbia University. Thanks to Liliana Themelis, Dr. Eilhann Kwon, Dr. Forrest Zhou, Federico Barrai, Dr. Heidi Butterman, Dr. Scott Kaufman, Peter Rennee and Gary Hill for their supports.

I would also like to thank engineers from Covanta Energy Corp., Veolia Environmental Services, and Wheelabrator Technologies Inc. for their valuable suggestions and discussions.

Finally, I would like to give my deepest and sincerest gratitude to my parents, parents-in-law, my wife Paofan, my daughter Audrey, and the rest of my family.

# 1. Introduction

## 1.1. Industrial Significance

Waste-to-Energy (WTE) is one of the principal means of the Integrated Waste Management (IWM) of municipal solid wastes (MSW) and the only alternative to landfilling of post-recycling wastes. The other means, higher in the hierarchy of IWM are waste prevention, minimization, reuse, recycling and composting of source-separated organics. In WTE facilities MSW is combusted under controlled conditions, and heat from the combustion gases is transferred through heat exchanging metal surfaces to generate steam that powers turbines that produce electricity. There are over 600 WTE facilities globally combusting over 170 million tons of MSW annually. In the US, there are currently 88 WTE facilities processing 29 million short tons of MSW annually and generating 2.3 GW of electricity. Every ton of MSW processed in a WTE facility avoids the mining of about one quarter ton of coal or the importation of one barrel of oil [1, 2].

Metal tube corrosion in WTE facilities is generally categorized as high-temperature corrosion. It is a major operating problem of WTE facilities because it results in downtime and periodic shutdowns in plants and accounts for a significant fraction of the total operating cost of WTE plants. High temperature corrosion has also environmental impacts. Metallic coatings and corrosion resistant alloys such as stainless steels and nickel-base alloys are often used to protect boilers from corrosion and

represent a large use of valuable resources. In addition, plant shutdowns due to corrosion increase the cost of WTE processing, impede further expansion of the WTE technology, and perpetuate the annual disposal of about 250 million short tons of MSW in the U.S. to landfills that add considerably to greenhouse gas emissions [3].

In WTE boilers, higher steam temperature in the superheater represents higher energy recovery, but the accompanied higher metal temperature of the superheater tubes also leads to higher corrosion rates. The trade-off indeed involves not only the economic perspective but also the environmental and social perspectives. Therefore, it is critical for WTE operators to find out what are the best operating parameters and the most cost-effective protection methods of boiler tubes.

### 1.1.1. Waste-to-Energy Technologies

Based on the fuel characteristics WTE technologies can be categorized into two groups: (a) mass burn or burn as received and (b) refuse derived fuel (RDF). Stoker or "mass burn" is the dominant WTE technology globally, and the most common grate technologies are reverse-acting stoker grate, roller grate, step-down reciprocating grate, and water-cooled rotary gate. In mass burn WTE facilities, oversize objects (e.g. mattresses) are removed, but there is no other pre-treatment such as shredding or material separation. The MSW is then fed into the combustion chamber and combusted over the grate. The advantage of mass burn is its lower capital cost of construction and

simplicity of operation while the disadvantage is that the combustion conditions are less uniform due to the variety of MSW content. The combustion residue, called bottom ash, falls off the end of the grate and drops into a water quench bath to lower its temperature and to avoid fugitive emission. The de-watered bottom ash is either disposed in landfill or re-used as construction materials. After combustion, the process gas flows through the combustion chamber where the sensible heat in the gas is recovered through a series of heat transfer surfaces that include the waterwall tubes, superheater tube bundles, evaporator tubes and economizer tubes. Then the cooled flue gas is cleaned by air pollution control (APC) equipment to remove fine particulates (fly ash), acid gases and remaining traces of organic compounds. A variety of APC equipments is adopted in WTE facilities to clean the flue gas, mainly a dry or semi-dry scrubber, activated carbon injection to remove volatile metals and organic traces, and fabric bag filters. The APC residue and fly ash contain potentially harmful materials such as heavy metals and organic pollutants, and therefore are not suitable to reuse. They are usually stabilized before being sent to the landfill.

Figure 1-1 shows a schematic of a conventional stoker-type waste-to-energy facility. The main sections of a WTE facility include entrance zone with weighing facility and refuse receiving area, refuse holding pit and feeding section, the grate and the combustion chamber, combustion chamber integrated thermal equipment for heat recovery (boiler with water steam system and steam turbine), flue gas treatment system,

residue treatment equipment, electrical installation and control system, and auxiliary equipment and buildings.

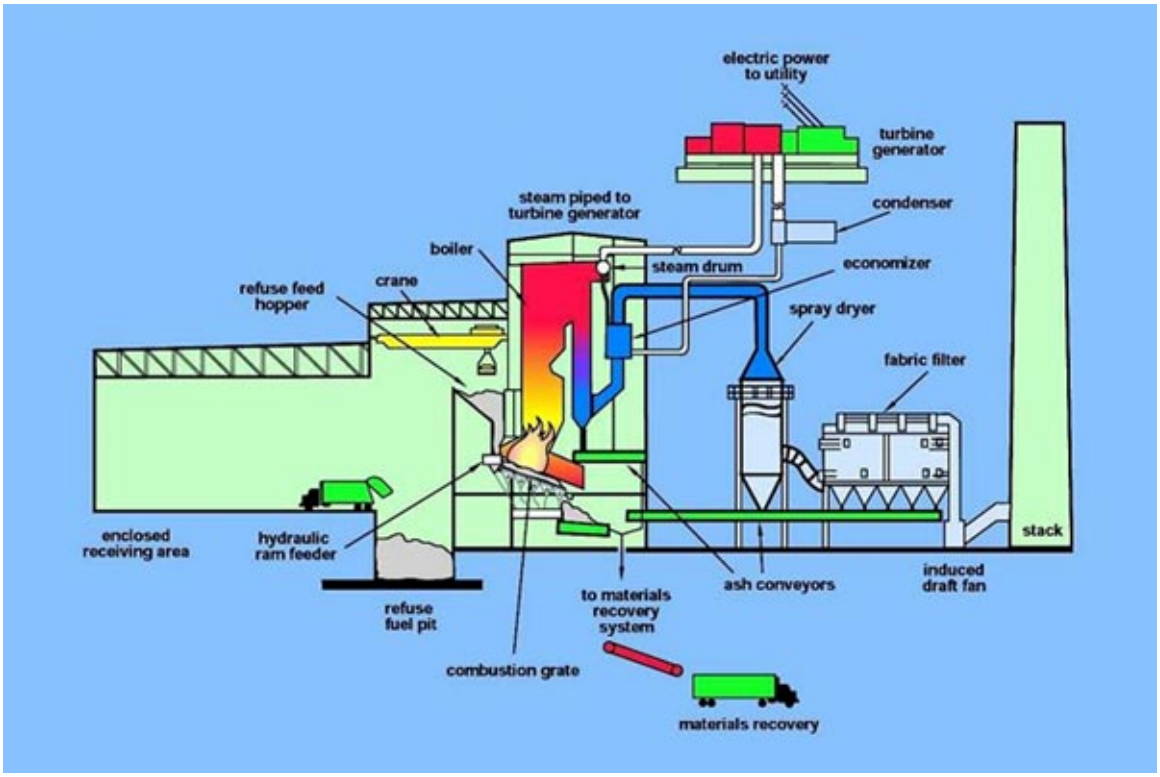


Figure 1-1 Schematic diagram of a typical waste-to-energy facility [2]

### 1.1.2. High Temperature Corrosion in Waste-to-Energy Facilities

In a WTE facility, as the hot combustion gases flow over the heat transfer surfaces, such as membrane water tubes (waterwall), tube bundles of evaporator, screen, superheater and economizer, heat is transferred from the gases to the water

vapor within the tubes. The superheated steam is then used to rotate the steam turbine generator. The efficiency of conversion of steam energy to electricity increases with higher steam temperature and pressure. However, with increasing steam temperature, the heat transfer surfaces are subjected to severe high temperature corrosion, caused both by the high concentration of hydrogen chloride (HCl) and sulfur dioxide ($SO_2$) in the process gas and the chlorides and sulfate salts in the ash particles deposited on the tubes. The chlorine and sulfur concentration in the combustion gas depends entirely on the MSW composition and varies somewhat from region to region.

Table 1.1 shows that the chlorine content in three types of MSW varied from 0.47 to 0.72% [4]. Approximately, one half of the chlorine content of MSW is due to natural organics and the other half to chlorinated plastics, mostly PVC. During combustion, nearly all of the chlorine content in the various components of the MSW, both natural organics and chlorinated plastics is volatilized and converted to HCl gas. Assuming that the MSW contains 0.5% of chlorine, the HCl concentration can be calculated to be about 580 ppmv [5]. Also, the typical concentration of $SO_2$ in WTE process gas is about 100-150 ppm according to the corrosion survey made by the author and his colleague.

In comparison to WTE boilers, coal-fired power plants have much lower chlorine but higher sulfur contents in the process gas. For example, a typical U.S. coal contains 0.05% of chlorine and 2.5% of sulfur. Since the process gas associated with the combustion of coal amounts to about 10,000 standard cubic meters per ton of coal, the

corresponding concentration of HCl in coal combustion gas is 29 ppm and of $SO_2$ is 795 ppm (shown in Table 1.2). Since coal-fired power plants can operate at higher steam temperatures and exhibit higher thermal efficiencies (30-35%) than WTE boilers (20-27%) while suffer less corrosion problems than WTEs, chlorine's effect upon resulting in the corrosion has shown to be critical.

In general, high temperature corrosion in WTE facilities typically occurs in three areas: top of the refractory lining in the first pass (including the waterwall tube), transition of the first to the second pass (including the boiler roof), and tube bundles of the screen, evaporator and superheater [6]. The first area is subjected to corrosion by high temperature impingement, low-melting deposits of molten chloride and sulfide salts, and corrosion/erosion due to high flue gas velocity. The rest of the areas are subjected to corrosion/erosion due to high flue gas velocity, high-temperature gaseous oxidation, and molten chloride and sulfate corrosion. Corrosion causes rapid wall thickness reduction in these areas and the failure of a single or multiple tubes, necessitating an immediate shutdown of the facility for repair.

Table 1-1 Chlorine concentration in MSW [7]

| | ***New York City MSW*** | ***U.S. typical MSW*** | ***U.K. typical MSW*** |
|---|---|---|---|
| ***Total Cl, g/kg*** | 4.71 | 7.26 | 4.53 |
| ***Cl wt. %*** | 0.471 | 0.726 | 0.453 |
| ***HCl conc. in process gas, ppm*** | 540 | 832 | 519 |

Table 1-2 Chlorine and sulfur concentration in WTE facilities and coal-fired power plants

| | *WTE facilities* | *Coal-fired power plants* |
|---|---|---|
| ***Total Cl wt. %*** | 0.5 | 0.05 |
| ***HCl conc. in process gas, ppm*** | 580 | 29 |
| ***Total S wt. %*** | 0.24 | 2.5 |
| ***$SO_2$ conc. in process gas, ppm*** | 150 | 795 |

## 1.2. Research Objectives and Scope

This research is co-sponsored by the Earth Engineering Center (EEC) of Columbia University and the Waste-to-Energy Research and Technology Council (WTERT). WTERT is a technical group that brings together engineers, scientists, and managers from industry, universities, and government with the objective of advancing the goals of sustainable waste management globally. In 2004, WTERT sponsored a graduate student to conduct the literature research on the theory and experience of corrosion phenomena in WTE facilities. The literature research also carried out a corrosion survey to WTE operating companies in the United States, but the survey results were not retrieved completely upon the graduation of the student.

The present study continues the investigation of the corrosion phenomena on waterwall and superheater tubes of WTE facilities. It incorporates and completes an in-depth analysis of the survey on high temperature corrosion, the laboratory tests that,

for the first time simulate the large temperature gradients encountered on WTE heat exchanging metal surfaces and clarify the mechanism and kinetics of chlorine induced corrosion and the effect of hydrogen chloride gas concentrations on corrosion rates, and invention of reducing the corrosive agents in the flue gas by means of injecting chemicals into the furnace and subsequently reducing corrosion.

# 2. High Temperature Corrosion Mechanisms

## 2.1. Principals Mechanisms and Corrosion Factors

Metals corrode at high temperatures in the absence of a liquid electrolyte, which is required in the case low-temperature of aqueous corrosion. The term oxidation is ambivalent because it can either refer to the formation of oxides or to the mechanism of oxidation of a metal. Strictly speaking, high temperature oxidation is only one type of high temperature corrosion, but it is the most important high temperature corrosion reaction [8]. The corrosion mechanism is indicated by the most abundant corrosion deposits observed on the metal after corrosion, i.e. oxidation by metal oxides, sulfidation by metal sulfides, sulfidation/oxidation by mixtures of sulfides and oxides, carburization by metal carbides, and chlorination by metal chlorides. In general there are two principal mechanisms of high temperature corrosion [7]:

**(1) Active oxidation**: This mechanism occurs at metal temperatures above 450$^{o}$C (840$^{o}$F) and comprises several steps: (a) reaction of HCl in the gas with oxygen to form chlorine at the tube surfaces; (b) penetration of chlorine through the metal oxide (scale) to the scale/metal interface; (c) reaction of chlorine with iron or other metal component of the tube to form metal chlorides; (d) diffusion of metal chloride vapor outward through the scale covering the tube; (e) reaction of the metal chloride with available oxygen in the gaseous layer surrounding the tube to form metal oxide and chlorine. In

step (e) chlorine is released and diffuses to the bulk gas. However, parts of the liberated chlorine migrate back to the scale/metal interface to react with the metal and form metal chlorides again. Therefore, a cycle is formed that provides a continuous transport of metal away from the metal surface towards the higher oxygen partial pressure, and the rate of this cycle depends on the rate of diffusion of chlorine between the gas phase and the metal.

**(2) Corrosion due to deposits by molten slats**: Gases containing HCl and also gaseous alkali chlorides, such as NaCl and KCl can accelerate the rate of active oxidation mentioned above. Also, when volatilized chloride salts in the combustion gases come into contact with the cooler tube surface they condense and form either liquid or solid deposits. The deposits contribute to corrosion in two ways: (a) the chlorinated species in the deposit cause a reaction similar to the gas phase active oxidation described above; (b) the presence of chlorides in the deposits may result in the formation of low melting point eutectics (i.e., salt solutions characterized by the lowest possible melting point) which may dissolve ("flux") the oxide layer that is protecting the metal surface.

The corrosion sensitive areas in the WTE facility are the waterwall and superheater tube bundles. Because the gas and metal temperature are different in these two areas, the corrosion mechanisms are not exactly the same. The waterwall metal temperature is operated in the range of 200-300°C, while the superheater metal temperature is in the range of 400-530°C. A schematic of the influence of metal temperature on different corrosion mechanisms is illustrated in Figure 2-1.

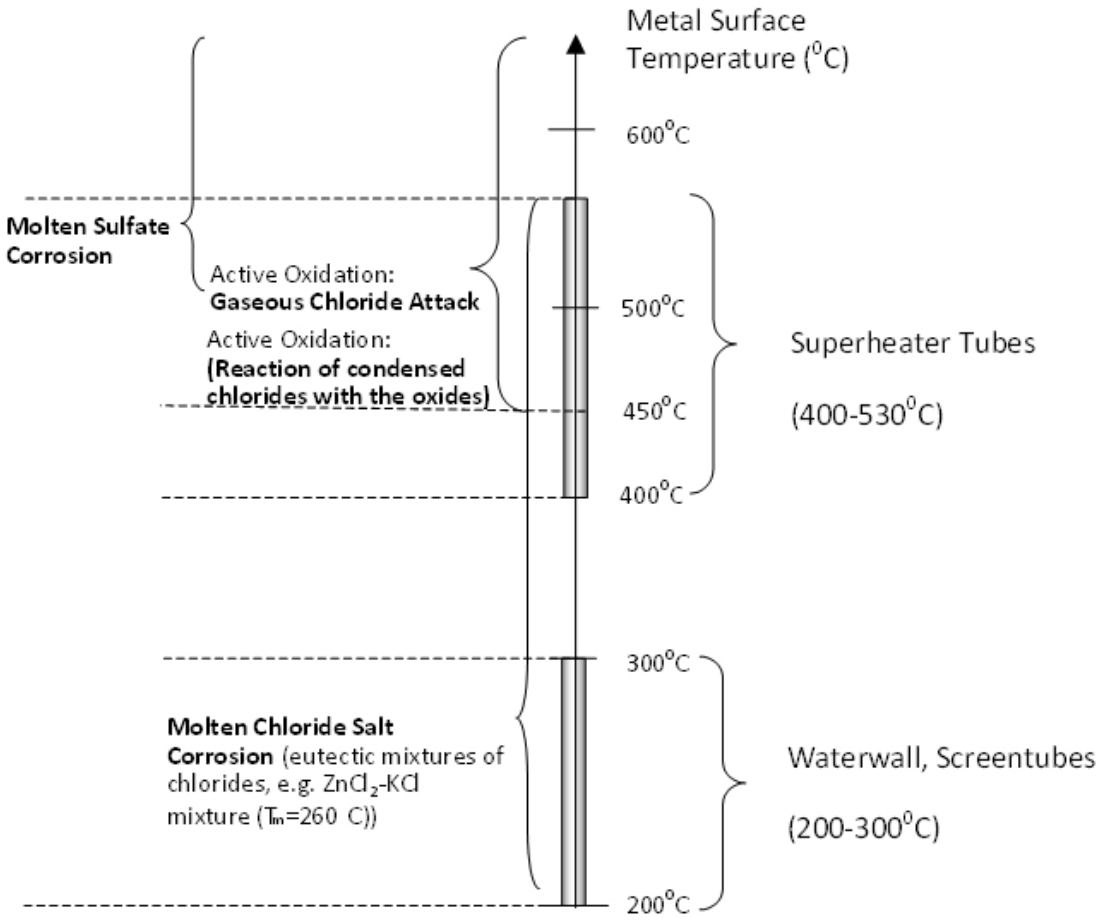


Figure 2-1 Schematic on the influence of temperature on different corrosion mechanisms on boiler tubes [7]

Various factors can affect the corrosion rate in WTE boilers, such as the concentration of chlorine and sulfur in the MSW, the operating temperatures of the combustion chamber and boiler, temperature fluctuations at a particular location that may disrupt the protective oxide layer, the method used for periodic cleaning of the fireside of the tubes, and the design of the boiler that should avoid extremely high

temperatures (e.g. horizontal vs. vertical disposition of superheater tube arrays). The influence of some important factors can be summarized as follows [9]:

**(1) Metal surface temperature:** High temperature of the metal surface, due to high radiation fluxes and/or inadequate heat transfer rate to the steam flow inside the tube, results in the melting of deposits and acceleration of the corrosion rate. In general, the metal temperatures of waterwall and superheater tubes are maintained at temperatures below 300$^{o}$C (570$^{o}$F) and 450$^{o}$C (840$^{o}$F), respectively [10]. As mentioned earlier, operation at higher superheater temperatures can increase the thermal efficiency of the steam turbine, but also cause severe corrosion at the same time.

**(2) Gas temperature:** The temperature of the combustion gases can affect the deposition rates and also the composition of the deposit and thus accelerate corrosion. The temperature gradient between the gas temperature and metal surface temperature is a driving force for the condensation of vaporized species, such as metal chlorides, on the cooled surface [11]. When the temperature gradient is large, the chloride concentration in the deposit is high and the melting point of the salt decreases. Also, thermal stresses induced by the temperature gradient across the deposit and the metal wall can affect the adhesion of oxide scales on the metal surface, thereby resulting in fracture of the protective oxide layer followed by spalling and increase of point defect diffusion within oxide scales [12-14].

**(3) Temperature fluctuation:** The non-homogeneous physical and chemical composition of the MSW fuel and the corresponding fluctuation in heating value with time result in pronounced fluctuations of the gas temperature within the combustion chamber. Experimental studies have confirmed that the corrosion rate increased several times because of wide temperature fluctuation [15].

**(4) Characteristics of molten salt deposits**: As already noted, diffusion of chlorine through the cracks and pores of deposits enhances the rate of corrosion [7]. The presence of chlorides, sulfides, and alkaline and heavy metal components in deposits affects both chemical and physical properties of deposits, such as gas permeability of deposits. In some cases, the corrosion rate also increases with an increase in thickness of deposits [15].

A particular reaction that is beneficial in reducing the corrosive effect of chlorine and chloride salts is the sulfation of volatilized alkali salts in the flue gases. This reaction transforms chlorides into sulfate salts and the released chlorine then reacts with water vapor to form hydrochloric gas. Sulfate salts are less aggressive since sulfate corrosion occurs at higher temperature [6]. In WTE boilers, the character of deposits is affected by feed composition and the gas-metal temperature gradient.

## 2.2. Corrosion Kinetics

The first step in high temperature oxidation is the adsorption of oxygen on the surface of the metal, followed by oxide nucleation and the growth of the oxide nuclei into a continuous oxide scale covering the metal substrate. Defects, such as microcracks, marcocracks, and porosity may develop in the scale as it thickens. Such defects tend to render an oxide scale nonprotective, because, in their presence, oxygen can easily reach the metal substrate to cause further oxidation [8].

### 2.2.1. Rate Equations of Metal Oxidation [8, 16]

Reaction rates and corresponding rate equations for the oxidation of a metal depend on a number of factors such as temperature, oxygen pressure, elapsed time of reaction, surface preparation and pretreatment of the metal. Although the rate equations along are insufficient for interpretations of oxidation mechanisms, these equations may be used to classify the oxidation behavior of metals and may as such often limit the interpretation to a group of alternative mechanisms. The number of possible mechanisms may be reduced further, or the proper mechanism may be elucidated by correlation with other studies.

Three rate equations: (1) logarithmic rate equations, (2) parabolic rate equations, and (3) linear rate equations are commonly used to describe the oxidation of metals. It is important to bear in mind that these laws are based on relatively simple oxidation

models. Practical oxidation problems usually involve alloys and considerably more complicated oxidation mechanisms and scale properties than considered in these simple analyses. Deviations from these rate equations and intermediate rate equations are also often encountered. In many instances it may be difficult to fit data to simple rate equations.

**(1) Logarithmic rate equations:** It is an empirical relationship that has no fundamental underlying mechanism. This law is characteristic of the oxidation of a large number of metals at low temperatures that reaction is initially quite rapid and then drop off to low or negligible rates. The oxidation rate either follows a direct or inverse logarithmic law:

$$Direct\ logarithmic\ law \qquad x = K_1 log t + A \qquad (2\text{-}1)$$

and

$$Inverse\ logarithmic\ law \qquad 1/x = K_2 log t + B \qquad (2\text{-}2)$$

where x may alternatively represents the thickness of the oxide film, the amount of oxygen consumed per unit surface area of the metal, the amount of metal transformed to oxide etc., t denotes the time, $k_1$ and $k_2$ represent the rate constants, and A and B are integration constants.

**(2) Parabolic rate equations:** At high temperatures the oxidation of many metals is found to follow the parabolic time dependence. The differential and integral forms of the parabolic equation are:

$$dx/dt = K_p\ /x \tag{2-3}$$

$$\mathrm{x}^2 = \ 2K_p t \ + \ C \tag{2-4}$$

where $K_p$ denote the parabolic rate constant and C is the integration constant.

As a rule, high temperature parabolic oxidation signifies that a thermal diffusion process is rate determining. Such process may include a uniform diffusion of one or both of the reactants through a growing compact scale or a uniform diffusion of the gaseous reactant (e.g. oxygen) into the metal.

**(3) Linear rate equation:** It is also an empirical relationship that is applicable to the formation and build-up of a non-protective oxide layer:

$$dx/dt = K_l \tag{2-5}$$

$$\mathrm{x} = \mathrm{K_l\,t} + \mathrm{D} \tag{2-6}$$

where $K_l$ is the linear rate constant and C the integration constant.

In contrast to the parabolic and logarithmic equations, for which the reaction rates decrease with time, the rate of linear oxidation is constant with time and is thus independent of the amount of gas or metal previously consumed in the reaction. If the relationship is linear, a surface or phase boundary process or reaction may be rate determining. This may involve, for example, a steady state reaction limited by the supply at surface, a reaction governed by a steady state formation of oxide at the metal/oxide interphase, or diffusion through a protective layer with constant thickness.

## 2.3. Current Methods of Protection

Over several years of operating experience, the WTE industry has developed general approaches to reduce corrosion that can be classified as primary and secondary measures. Primary measures seek to eliminate corrosion by influencing the process conditions in the boiler. Some of these methods include [7]: (1) improvement of process control, in particular minimizing fluctuations in gas temperature; and (2) design modifications, such as process gas recirculation to alter flow dynamics, enhancing gas mixing through the use of process gas recirculation, and designs of the boiler system (e.g. horizontal vs. vertical boiler).

Secondary methods of protection are applied to extend the lifespan of the boiler tubes. In the past ten years, many kinds of corrosion-resistant material systems have been tested and applied to actual boilers. For example, high chromium - high molybdenum nickel-base alloys and high chromium - high silicon ferronickel alloy tubing products are used in WTE plants. Furthermore, coating systems such as high velocity oxygen fuel (HVOF) thermal spray and weld overlay have been developed and applied to advanced WTE boilers. Other secondary measures include a new technology named Targeted In-Furnace Injection which by means of injecting chemicals, such as MgO, into the combustion chamber to make the ash deposits more friable and easy to remove, and the extensive use of high conductivity refractory lining and ceramic tiles in the lower half or the entire height of the combustion chamber.

Some of these methods require either the retrofit of existing WTE boilers or the redesign of boilers of new WTE facilities. In the case of retrofits, the construction time for making equipment changes is a very important parameter since the required shutdown can affect the economic viability of the WTE facility. Details of these methods that have been applied in WTE facilities or are under investigation are described in the following section. The actual cost of each method is not shown due to limited available information.

**(1) Adoption of Inconel Alloy 625 cladding:** Waterwall areas that are not protected by a refractory lining and the superheater tubes are the most corrosion prone areas. Cladding consists of overlaying a layer of Inconel 625 (21Cr-9Mo-3.5Nb-Ni base) on tubes to protect them from the attack of corrosive gases. This method has been used successfully in the waterwall tubes and part of the superheater tube bundles in many WTE facilities. The key element regarding the cost is how much and where the Inconel 625 should be applied. Some researchers have shown that Inconel 625 applied on waterwall tubes provides excellent corrosion resistance [10, 17]. Although the price of Inconel 625 is higher than that of a protective refractory lining, the cost of Inconel 625 is partly compensated by avoiding the cost of refractory maintenance. Besides, Inconel 625 has higher thermal conductivity than refractory materials and therefore can reduce gas temperature in the first gas pass.

The application of Inconel 625 on superheater tubes is more complicated because the performance of the cladding depends on the metal temperature reached

during operation. One study showed that Inconel 625 does not provide protection above 400–420$^{o}$C (750-840$^{o}$F) [18]. Another study indicated that at metal temperatures about 540$^{o}$C (1000$^{o}$F), the wastage rate of Inconel 625 was 0.2 µm/h (0.069 inch/year) [19]. The boilers of some of the existing WTE facilities have been designed to operate at lower temperatures and therefore can apply Inconel 625 on superheater tube bundles. However, problems still arise because the lifetime of Inconel 625 cladding is unpredictable. It may last as much as two years, or as little as three months. According to data that the authors obtained from a WTE facility, the cost of replacing the superheater tube bundle with Inconel 625 cladding is $350,000/unit; and only $250,000/unit without Inconel 625 cladding. The labor cost of installation is $75,000/unit. If the lifetime of the superheater tube bundle with Inconel 625 cladding is sufficiently longer, the additional cost of this cladding can be compensated by the avoided costs of shutdown and replacement of tubes. For new WTE facilities, where boilers are designed to operate over 420$^{o}$C, cladding of superheater tubes with Inconel 625 cladding is not recommended.

**(2) HVOF and thermal sprayed coatings:** Apart from the selection of corrosion resistant metals for cladding, the technologies used to apply these materials on metal tubes also affect the lifetime of protection layers. Technologies such as weld overlay and thermal spray processes that consist of high velocity oxygen fuel (HVOF) and thermal plasma sprayed coatings have been used in WTE boilers. Weld overlay is mostly applied in severe corrosive environment, but one major concern regarding weld overlay is that

repeated applications at the same area may cause embrittlement of the old overlay and lead to cracks that will propagate into the overlaid tube [20].

Thermal spray processes can provide hard, dense, sufficiently thick, and tightly coatings for long time protection of erosion [21]. With practice, the porosity of HVOF coatings has been reduced to less than 1%, which is much lower than the typical range of 3% to 5% encountered in flame or arc spraying overlays [22]. Experimental tests have indicated that both HVOF and plasma coatings have good erosion resistance because they produce homogeneous and low microstructure coatings [21]. The application of corrosion resistant materials like Inconel 625 by means of the HVOF or plasma coating processes has shown the best combination of erosion-corrosion resistance among all other thermal spray processes [21, 23]. In practical applications, NiCrSiB alloy HVOF coatings and Inconel 625 plasma sprayed coatings have been used successfully on waterwall tubes while $TiO_2$-$Al_2O_3$/625 cement HVOF coatings applied on superheater tubes show long-term durability of more than 3 years [24].

**(3) Design of flue gas pass of boilers:** In general, there are two major flow-pass designs of boilers: vertical and horizontal. With regard to the erosion-corrosion issue, the design objectives are to obtain a uniform gas flow pattern, minimize impact velocity on the tubes, and provide for smooth transition from the $1^{st}$ pass (combustion chamber) to the $2^{nd}$ pass of the boiler. Under the same operating conditions, superheater tube bundles in a vertical design boiler, which has fewer gas passes (upper left in Figure 2-2) will have more critical corrosion problems than the tubes in a horizontal design boiler

(bottom in Figure 2-2), because the former are subjected to higher metal temperatures and flow velocities of flue gas. The disadvantage of the horizontal design is that it needs more floor space than the vertical design. In practical terms, the determination of vertical vs. horizontal set-up and the number of gas passes depends also on other factors, such as space, thermal efficiency, past operating experience, and cost.

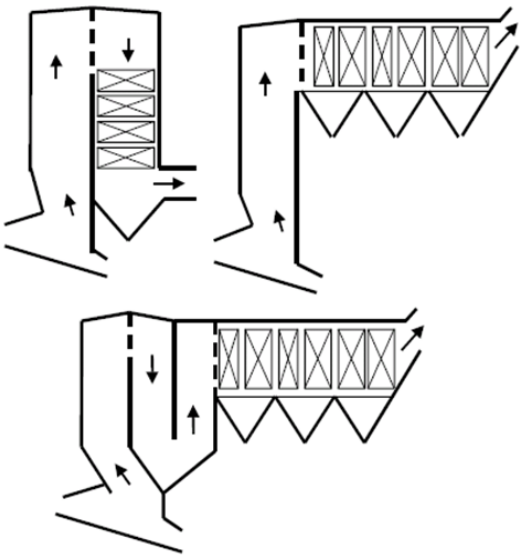

Figure 2-2 Schematic diagram of vertical and horizontal boilers [10]

**(4) The Seghers Prism:** The Seghers Prism [6] is a prism-shaped tubular structure equipped with several nozzles through which secondary air is injected into the combustion gases as they rise above the combustion grate. It is inserted horizontally through the center of the combustion chamber at the lower end of the first radiant boiler pass (Figure 2-3). It is water-cooled and refractory lined. Corrosion phenomena

can be reduced since the function of the prism is to mix the combustion gases, increase turbulence and decrease temperature fluctuation, thus minimizing hot spots. The advantage of the prism is that it can be implemented in existing plants as a retrofit. However, the retrofit requires a long plant shutdown [6].

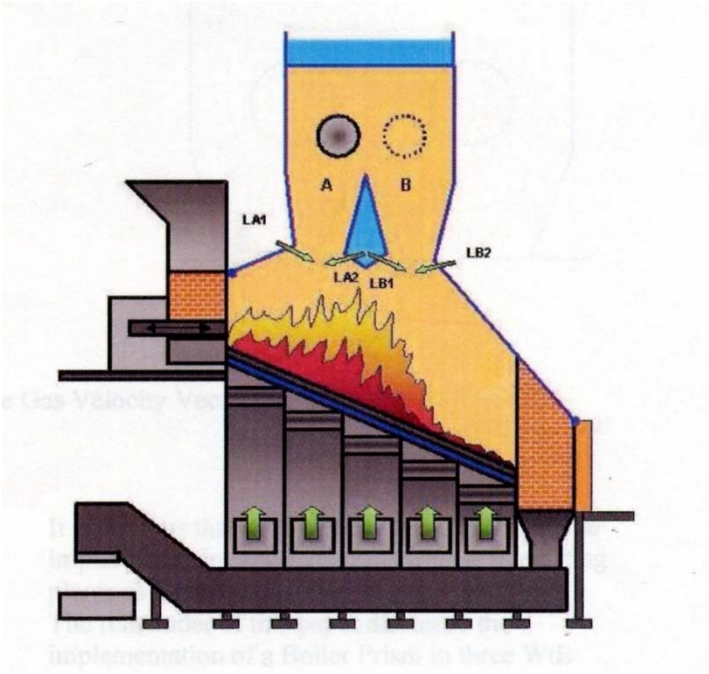


Figure 2-3 Schematic diagram of the Seghers Boiler Prism [6]

**(5) Recirculation of flue gas:** In some of the most recent WTE facilities, e.g. the Brescia plant in Italy, part of the flue gas is recirculated through secondary tuyeres in the combustion chamber. This has similar beneficial effects (better mixing, increased turbulence, fewer hot spots) as those claimed for the Seghers Boiler Prism.

**(6) Injection of chemicals into combustion chambers:** The objectives of injection of chemicals such as $Ca(OH)_2$ or $Mg(OH)_2$ into combustion chambers are to (a) decrease HCl concentration in the flue gas; (b) facilitate the removal of deposits and decrease their corrosion potential. This method is still under investigation, but preliminary results have shown it to be effective [25]. The disadvantage is that continuing injection of chemicals is required and this increases the cost of operation and also the amount of fly ash.

**(7) Improvement of cleaning method:** On-line methods for cleaning heat exchanger tubes, such as high pressure water washing and explosive cleaning have been developed in order to limit the build-up of deposits and shorten plant downtime. These cleaning methods are effective in removing the ash deposits; however they also may cause increased erosion-corrosion at some locations of the superheater tubes. Furthermore, some cleaning methods require WTE plants to come off-line for complete cleaning. Therefore, development of cleaning methods that are less harmful to tube life without reducing cleaning efficiency is needed. A new technology named Targeted In-Furnace Injection (TIFI) has been invented by Fuel Tech Inc. [26] and applied to some WTE facilities for deposit removal and fouling control. This technique injects the deposit control agent such as MgO directly to the problem area to react with ash deposits and makes them more friable and easy to remove; by doing so, the performance and cost effectiveness of the tube cleaning process are improved [26].

# 3. Corrosion Survey and Analysis

## 3.1. Corrosion Questionnaire

In order to understand better the actual operating parameters, corrosion problems and current trends of protection methods, Waste to Energy Research and Technology Council (WTERT), the major sponsor of this corrosion research, conducted a corrosion survey by sending questionnaires to the WTE facilities that are owned or operated by three major companies in the U.S. WTE industry: Covanta Energy, Veolia Environmental Services and Wheelbrator Technologies. The survey included six categories: (1) basic information of the facility, (2) waterwall tube data, (3) superheater tube data, (4) furnace and boiler data, (5) combustion air, $NO_x$ reduction and clean technologies, and (6) overall operating information. The questionnaire is shown in Appendix 1.

The questionnaire was distributed in November 2004. The results were analyzed by the author and presented in the following sections. In order to keep the confidentiality agreement with the participants of the survey, a plant code is assigned to each participating WTE plant in terms of WTE company, plant name and grate technologies. The description of the plant code is shows below:

Plant (“capital letter” “number”, “lowercase letter”), e.g. Plant A3,d,

where capital letter (A,B,C…) denotes WTE operating companies (A, B, and C), number denotes different facilities of a certain company, and lowercase letter represents different types of grate, e.g. a: rotary chamber, b: roller grate, c: Detroit Stoker Reciprocating grate, d: Steinmuller Reciprocating grate, e: Segher, and f: Martin.

After receiving the responses, the author communicated with the survey respondents to ensure the accuracy of the information. The responses of each question in the survey are summarized in Appendix 2.

## 3.2. Results and Analysis

**(1) Waterwall**

The most popular waterwall tubing was SA178A, and its average wastage rate was 1.62 mm/y (63.8 mils/y). All of the WTE facilities participated in the survey applied Inconel 625 to the waterwall, with the average wastage rate of 0.14 mm/y (5.5 mils/y). This showed that Inconel 625 did offer good protection against corrosion. As mentioned in the previous chapter, it is critical for operators to decide how much Inconel 625 should be applied from the perspective of cost performance index. From the author's interviews with several WTE operators and engineers, the average lifetime of the Inconel 625 cladding in waterwall is in the range of 5-10 years, with few exceptions that last longer than 10 years. Also they pointed out that regardless of the percentage of the cladding coverage, the intersection of the refractory lining and the cladding above it is

the most susceptible area to corrosion attack. Figure 3-1 shows the relation between the cladding percentage of waterwall (1st pass) and the wastage rate of Inconel 625 cladding. With the exception of Plant A2, a, all plants showed that higher cladding percentage led to lower wastage rate. This might be because the higher wastage rate of some area, e.g. the lower part of the 1st pass which suffered more serious corrosion, was averaged out by the lower wastage rate from the rest of the 1st pass. Figure 3-2 shows a nearly positive correlation between the cladding percentage of waterwall (1st pass) and the wastage rate of un-clad base tubing. This behavior showed that most WTE plants operators tended to apply more Inconel 625 when plants encountered higher wastage rates of the waterwall base tubing.

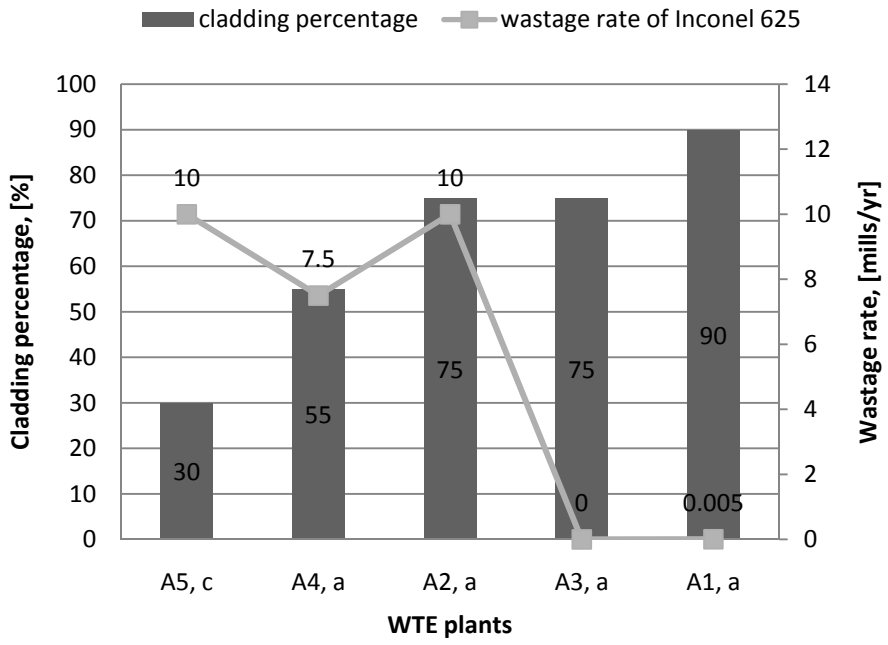


Figure 3-1 Waterwall cladding percentage and wastage rate of Inconel 625

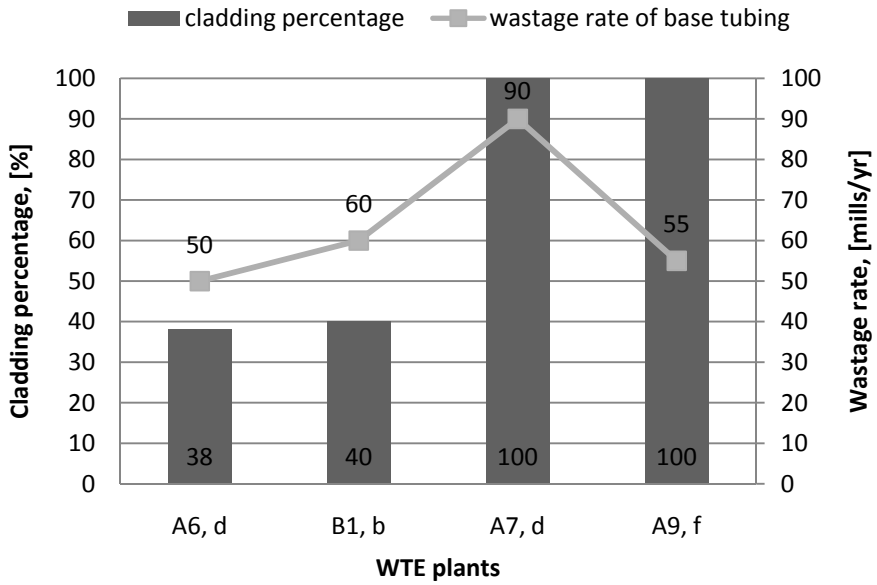


Figure 3-2 Waterwall cladding percentage and wastages rate of the base tubing

Figure 3-3 and 3.4 show the relations of the cladding percentage of waterwall ($1^{st}$ pass) as function of HCl and $SO_2$ concentration in the process gas. In most plants, higher HCl and $SO_2$ concentration led to higher coverage of Inconel 625 cladding. Figure 3-5 shows that, with the exception of Plant A9, f, higher HCl/$SO_2$ ratios (either be the case of higher HCl or lower $SO_2$) led to higher corrosion rate. If the coverage of Inconel 625 cladding is taken as an indicator of the corrosion rate, we can describe higher HCl and $SO_2$ concentrations as the contributors to higher corrosion rates. However, since the usage of Inconel cladding may have originated in the initial plant design and is not always direct related to the degree of corrosion, we would not draw firm conclusions on these relations.

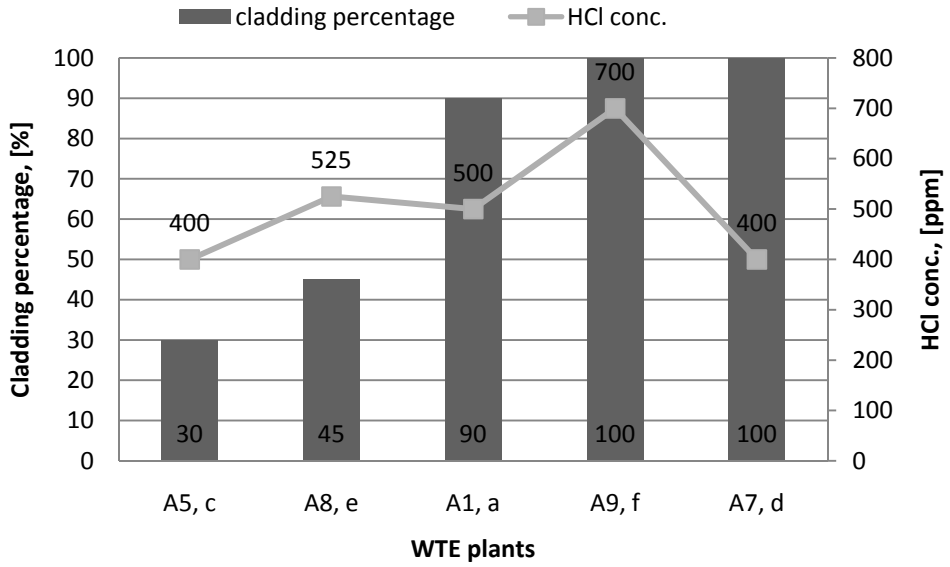


Figure 3-3 Waterwall cladding percentage and HCl conc. in process gas

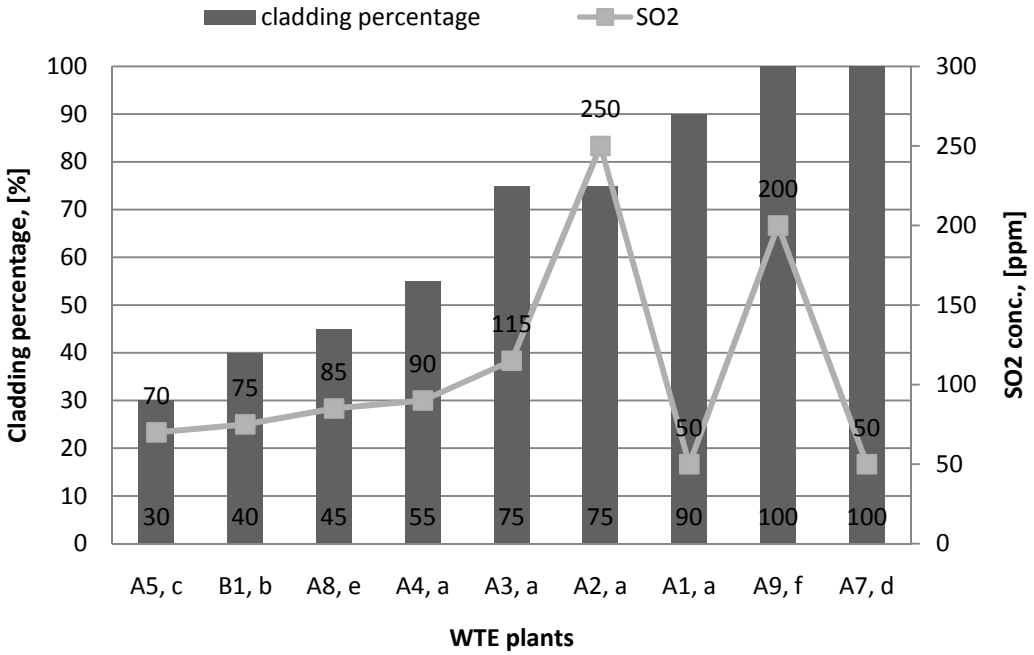


Figure 3-4 Waterwall cladding percentage and $SO_2$ conc. in process gas

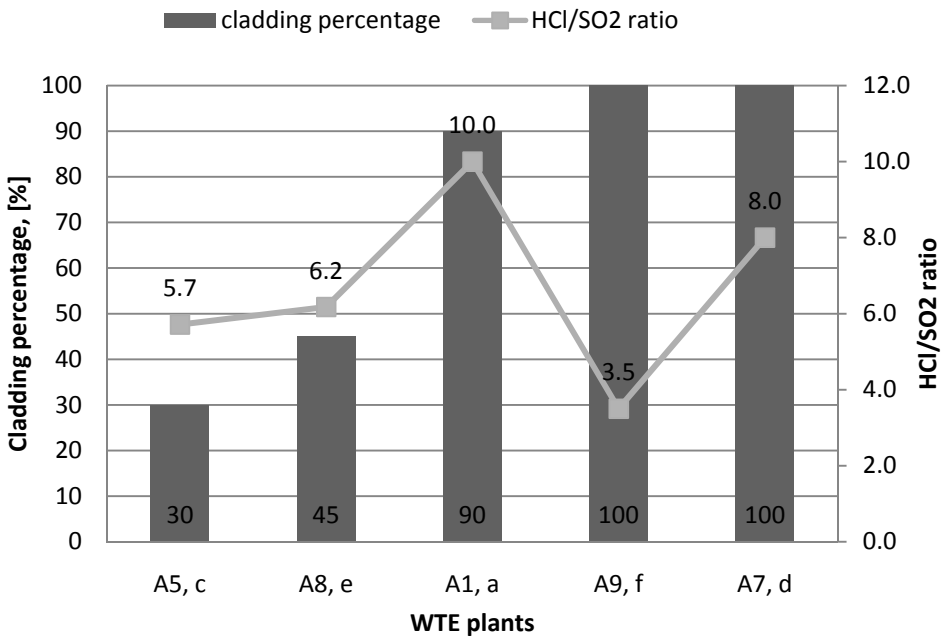


Figure 3-5 Waterwall cladding percentage and $HCl/SO_2$ ratio

According to the literature, waterwall tubes are generally attacked by molten chloride salts [7], so it is expected that higher HCl concentration will lead to higher wastage rate. However, on the basis of Figure 3-6 and 3.7, neither the wastage of Inconel 625 nor that of base tubing showed a positive correlation to the HCl concentration. Regarding the effect of $SO_2$ concentration on corrosion rate, Figure 3-8 shows that in most plants higher $SO_2$ concentration led to higher corrosion rate of Inconel 625, while Figure 3-9 shows that higher $SO_2$ concentration was less harmful to the base tubing of waterwall.

As described in previous chapter, a particular reaction that is beneficial in reducing the corrosive effect of chlorine and chloride salts is the sulfation of volatilized

alkali salts in the flue gases. This reaction transforms chlorides into sulfate salts and the released chlorine then reacts with water vapor to form hydrochloric gas. Sulfate salts are less aggressive especially in waterwall since sulfate corrosion occurs at higher temperature [6]. Therefore, operators believe that maintaining a certain level of $SO_2$ in the flue gas actually helps reduce the corrosion on waterwall area. This theory is in agreement with the result shown in Figure 3-10; higher levels of $SO_2$ (and therefore lower $HCl/SO_2$ ratios) resulted in lower wastage rate of waterwall base tubing. However, in Figure 3-11, the $HCl/SO_2$ ratio had an opposing effect on the corrosion rate of Inconel 625.

Based on the analysis of the survey results, Table 3-1 summarizes the correlations of wastage rates of Inconel 625 and waterwall base tubing, HCl concentration, $SO_2$ concentration and $HCl/SO_2$ ratio. Somehow some of the correlations, such as the HCl concentration versus the wastage rate, showed different trends than the generally accepted theories of the corrosion mechanism. One of the reasons might be because the number of responses on this point was not big enough to effect a correlation.

Table 3-1 Correlation between the wastage rates of Inconel 625/base tubing and HCl, $SO_2$ concentrations and $HCl/SO_2$ ratio

| | *Wastage rate of Inconel 625* | *Wastage rate of Base tubing* |
|---|---|---|
| **"higher" HCl concentration** | lower | lower |
| **"higher" $SO_2$ concentration** | higher | lower |
| **"higher" $HCl/SO_2$ ratio** | lower | higher |

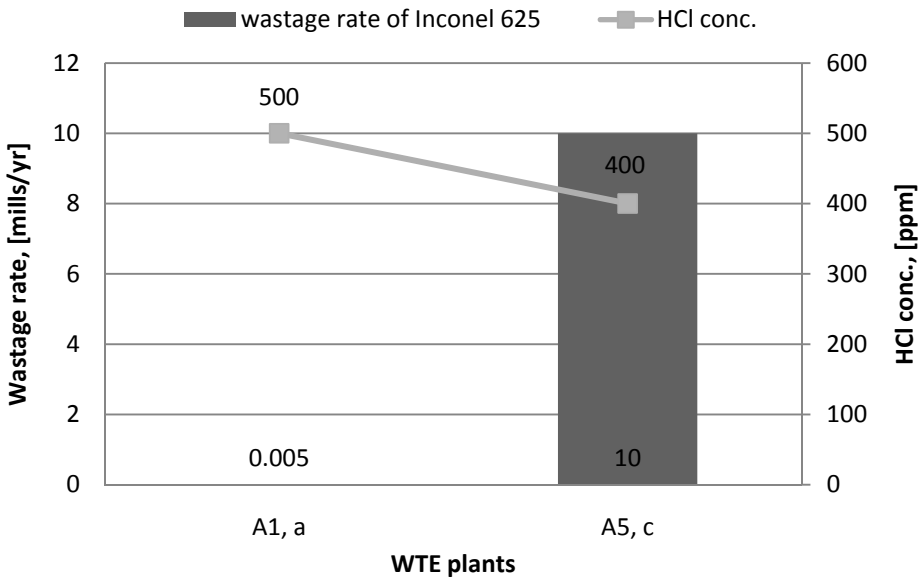


Figure 3-6 Wastage rates of Inconel 625 and HCl conc. in process gas

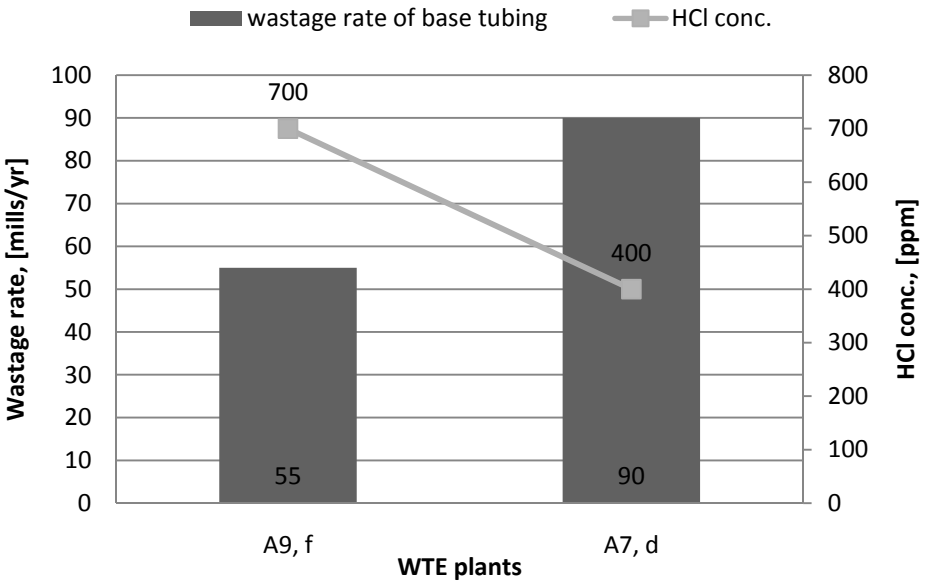


Figure 3-7 Wastage rates of waterwall base tubing and HCl conc. in process gas

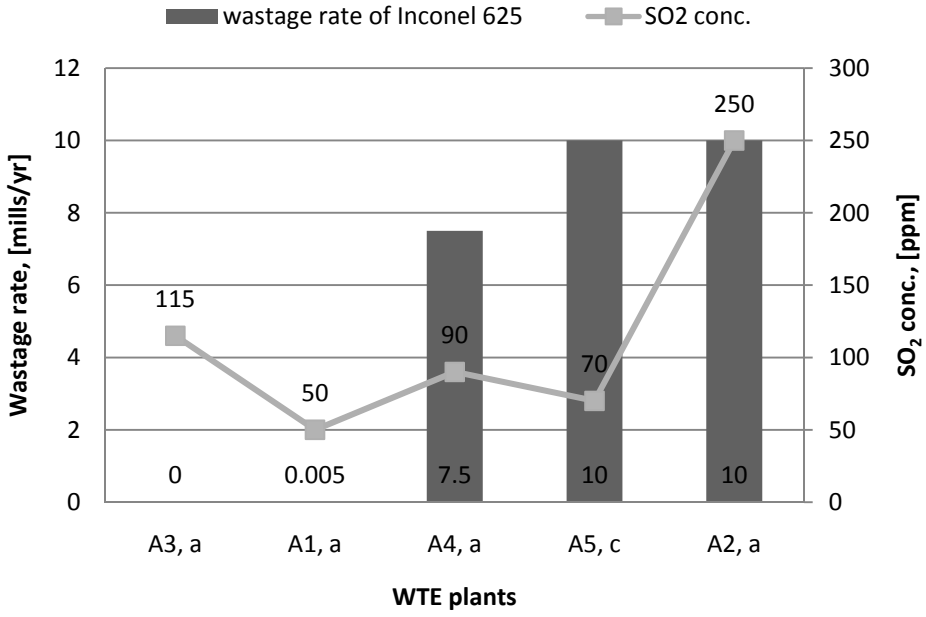


Figure 3-8 Wastage rates of Inconel 625 and $SO_2$ conc. in process gas

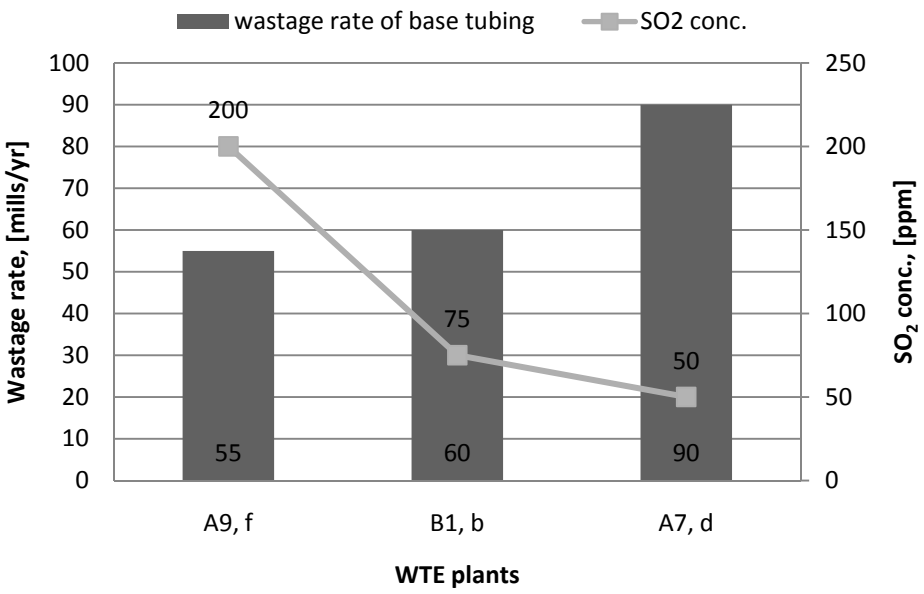


Figure 3-9 Wastage rates of waterwall base tubing and $SO_2$ conc. in process gas

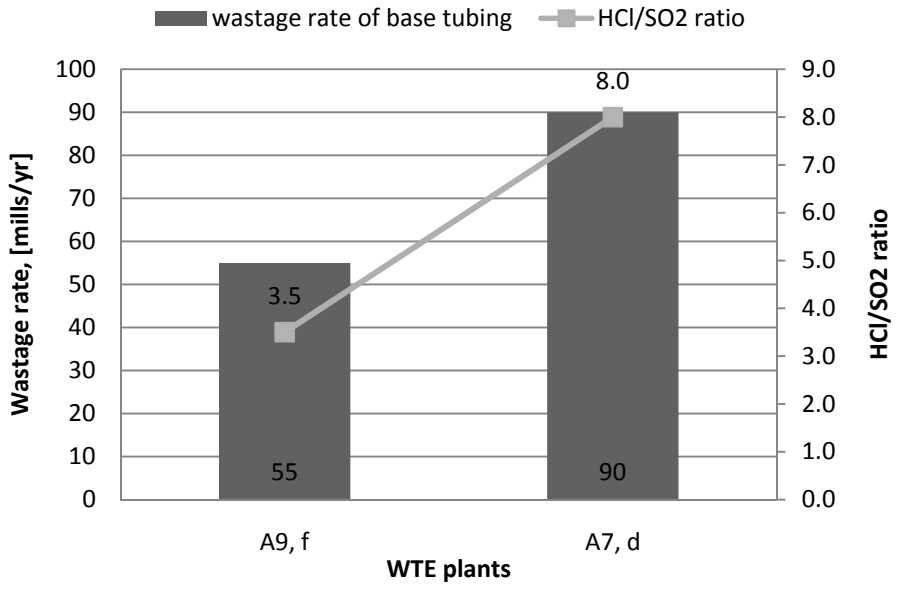


Figure 3-10 Wastage rates of waterwall base tubing and $HCl/SO_2$ ratio

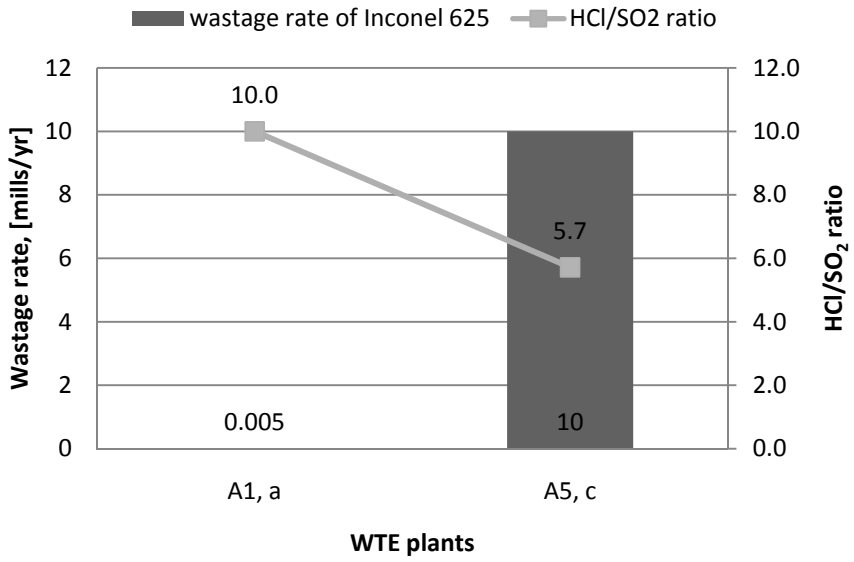


Figure 3-11 Wastage rates of Inconel 625 and $HCl/SO_2$ ratio

Figure 3-12 and 3.13 show the relations of wastage rate of Inconel 625 and waterwall base tubing in the combustion chamber (1st pass) with flue gas temperature and the saturation temperature within the waterwall tubing, respectively. The average flue gas temperature of 1st pass was 806°C with approximate 8% fluctuation. The flue gas temperature did not exhibit any relation to the wastage rate of Inconel 625, but it seemed to present a positive correlation with the wastage rate of waterwall base tubing. The average saturation temperature in the steam/water mix in the waterwall tube was 266°C and did not alter too much among plants. This temperature did not demonstrate any effect on the wastage rates of Inconel 625 and waterwall base tubing.

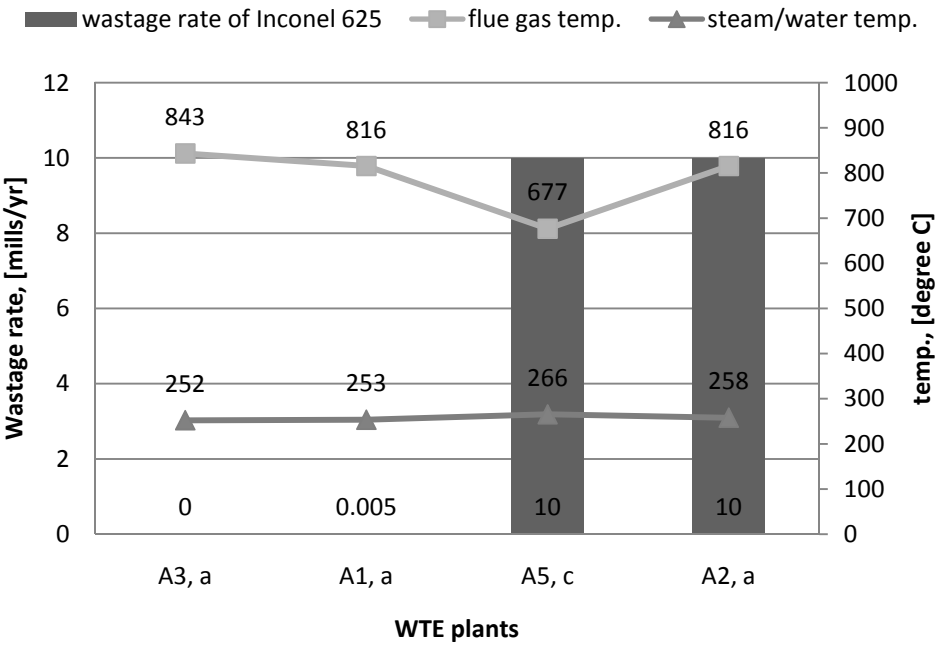


Figure 3-12 Wastage rates of Inconel 625, flue gas, and steam/water temperatures

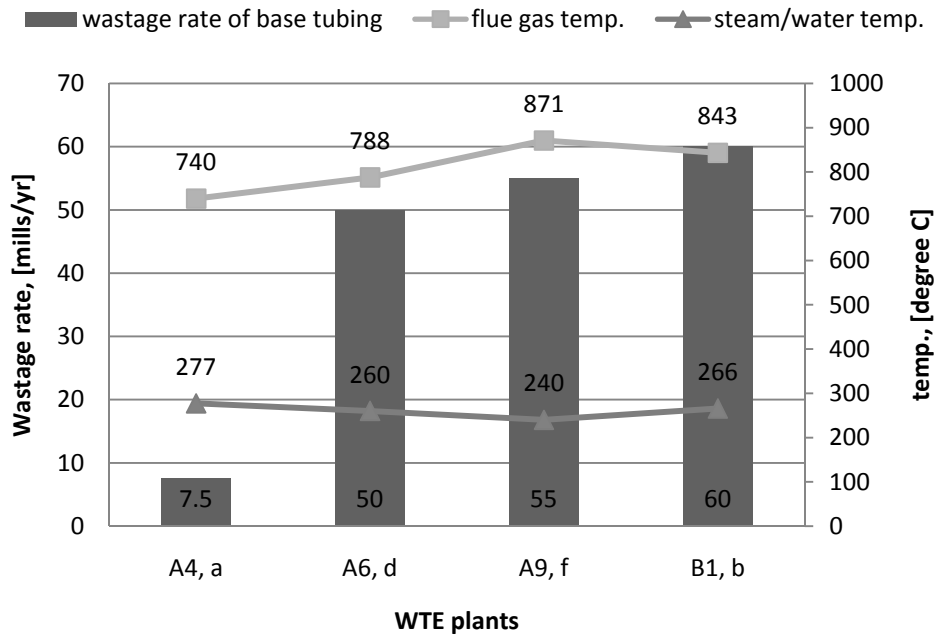


Figure 3-13 Wastage rates of waterwall base tubing, flue gas, and steam/water temperatures

**(2) Superheater**

Alloys SA213 T11 and SA213 T22 were the most wildly used for superheater tubes. The average wastage rate varied from 5 X $10^{-5}$ to 3.81 mm/y (0.002 to 150 millls/y) (Ave.: 1.32 mm/y (51.8 mils/y), StdDev: 1.41 mm/y (55.4 mils/y)) among WTE facilities. Some WTE facilities applied a small portion of Inconel 625 on superheater. Several WTE engineers and operators mentioned in interviews with the author that unlike the waterwall, the lifetime of superheater tubes was more unpredictable; they might last as long as two years, or as little as three months. Besides, it was generally agreed that the application of Inconel 625 did not improve performance too much. This experience is consistent with the theory described in previous chapter that Inconel 625 does not provide protection above 400–420$^{o}$C (750-840$^{o}$F) [18].

The superheater tube corrosion is either due to gaseous chloride attack and deposits containing chloride salts or to a combination of molten chlorides and molten sulfates [7]. Figure 3-14 and Figure 3-15 show the relation of wastage rate of superheater base tubing with HCl and $SO_2$ concentration, respectively. These results are in agreement with the generally accepted theories of corrosion mechanism that both higher HCl and $SO_2$ concentration lead to higher wastage rate. In addition, Figure 3-16 shows that lower HCl/$SO_2$ ratio (i.e., higher level of $SO_2$) led to higher wastage rate. This result is in contrast to the waterwall tubing where lower HCl/$SO_2$ ratio decreased corrosion. This is because the metal temperature of superheater tube is much higher than that of waterwall and has reached the melting point of the sulfate salts that are

transformed from chlorides. This means that even as the molten chloride attack is reduced, the corrosion threat remains because attack of tube metal by the molten sulfate salts occurs.

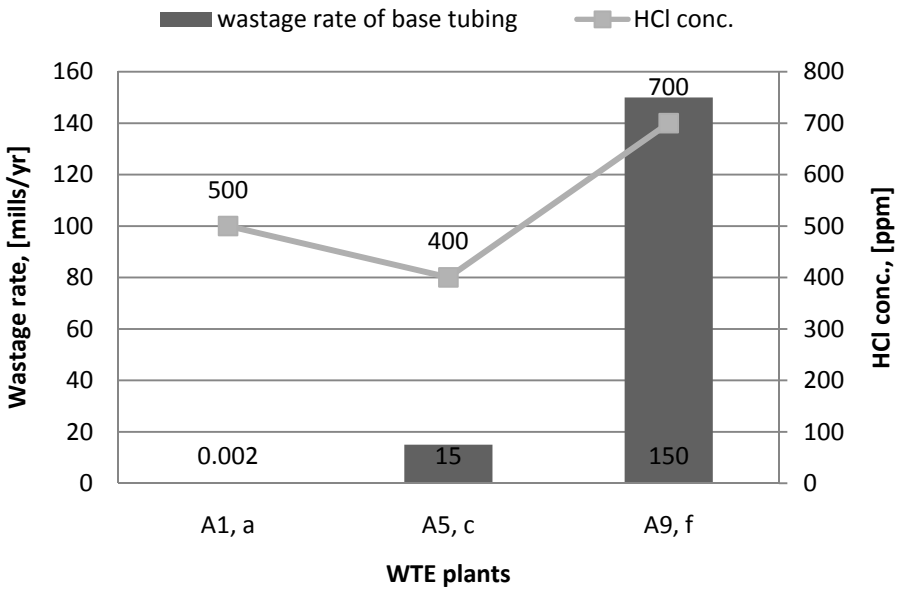


Figure 3-14 Wastage rates of superheater base tubing and HCl conc. before in process gas

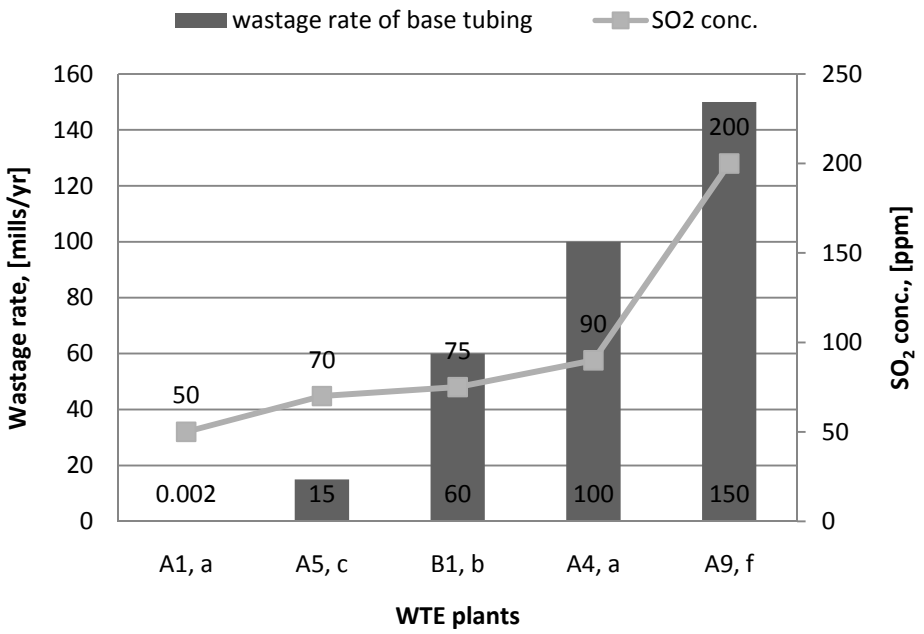


Figure 3-15 Wastage rates of superheater base tubing and $SO_2$ conc. before in process gas

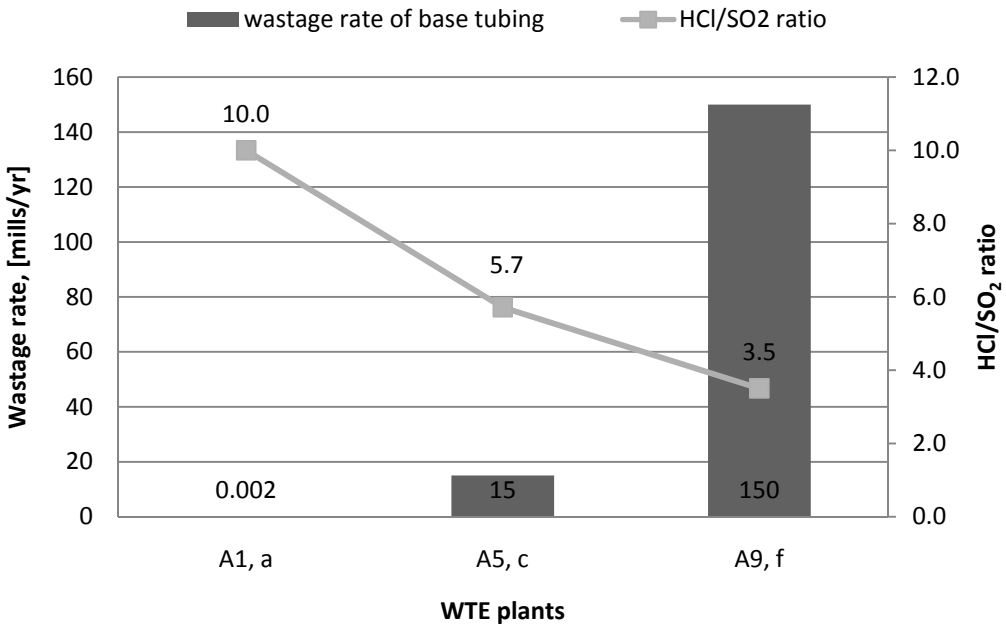


Figure 3-16 Wastage rates of superheater base tubing and $HCl/SO_2$ ratio

Figure 3-17 shows the relation of wastage rates of base tubing as a function of 1st superheater flue gas, steam inlet, and steam outlet temperature. The average flue gas temperature in 1st superheater pass was 699°C. The average temperature of steam inlet and steam outlet was 261°C and 398°C, respectively. The reported level of these temperatures did not show any direct relation to the wastage rate of superheater.

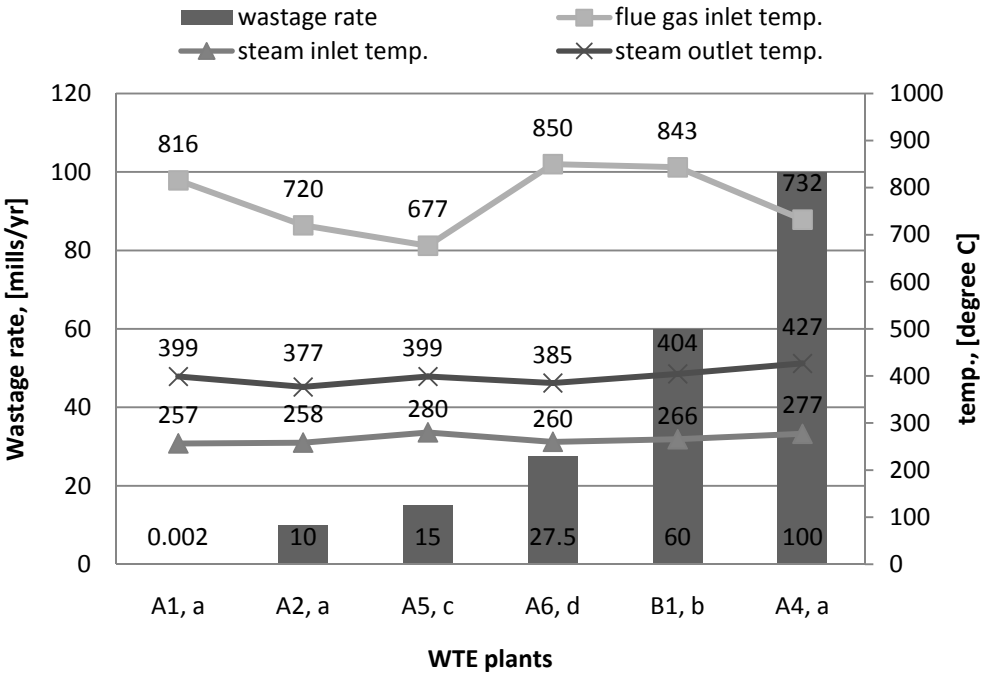


Figure 3-17 Superheater wastage rate, flue gas inlet, steam inlet and outlet temperature

**(3) Overall operating information**

From the survey results, the yearly maintenance cost per boiler unit due to corrosion ranged from $18K to $1,200K and the maintenance cost due to corrosion

ranged from $0.23 to $8.17 per ton of MSW combusted, as shown in Figure 3-18. The typical cost is in the range of $4 per short ton of MSW combusted. In Figure 3-18, the maintenance cost of Plant A4, a, was much higher than those of other plants. The author have checked with the facility manager and found that the cost was due to the recent replacement of the boiler and corrosion has been the major issue to the boiler failure.

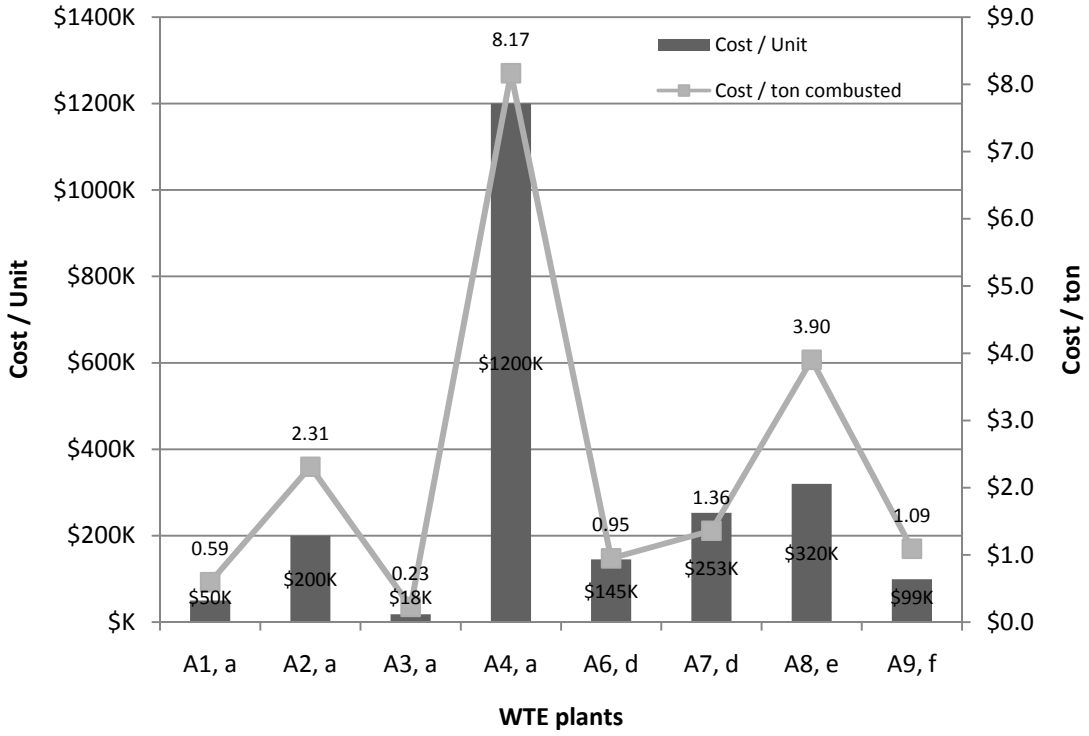


Figure 3-18 Yearly operating cost due to corrosion

The percent distribution of costs of a German WTE facility is shown in Figure 3-19. Capital cost and maintenance cost account for approximately 60% and 15% of the yearly cost of a WTE facility respectively. Therefore, the corrosion problems will cost a WTE plant approximately 5% of its yearly total cost, if the corrosion/total maintenance cost ratio of 1/3 applies. The actual cost will be even higher if the revenue loss due to shutdowns because of corrosion is taken into account.

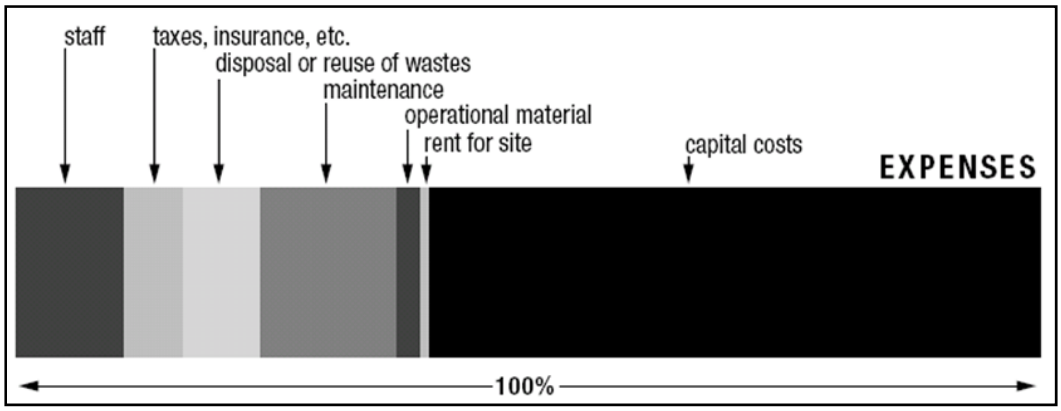


Figure 3-19 Expenses and revenues of a German WTE facility [27]

# 4. Experimental Section

## 4.1. Overview of the Experimental Work

Past studies on high temperature corrosion mechanisms have identified important factors that affect the corrosion rate [10, 28-30]. In addition, there have been many laboratory tests that have sought to classify the effects of these corrosion factors where metal coupons were subject to corrosion at constant furnace temperature [31-33]. However, these tests may not be useful in forecasting long term and synergistic effects of various corrosion factors on the tube life. In particular, some dynamic factors such as fluctuations in the flue gas temperature and thermal gradient between the gas and metal surface are difficult to reproduce and control in laboratory tests. However, these factors have been found to be accountable for the breakdown of the protective oxide scales on the metal surface and the resultant increased corrosion rate due to such breakdown [11]. Additionally, the thermal gradient between the gas and metal surface has been observed to strongly influence the deposition behavior and rates of formation of molten salts that contain corrosive compounds resulting from WTE combustion [28].

In order to elucidate the synergistic effects of these corrosion factors, the author developed an apparatus that could maintain a thermal gradient between a representative WTE combustion gas and test samples that were maintained at representative waterwall and superheater temperatures. The experimental work that

utilized this apparatus included 1) the verification of chlorine induced corrosion mechanisms, 2) the effects of HCl concentrations on corrosion rates, and 3) the corrosion kinetics.

In addition to elucidating the corrosion mechanism, this research study aimed to find out ways to reduce corrosion phenomena in WTE facilities. The experimental work investigated the feasibility of the $HCl/Cl_2$ sequestration in the combustion gases by means of injecting chemicals into the furnace.

## 4.2. Experimental Procedure and Apparatus

The flowchart shown as Figure 4-1 indicates the experimental procedure the corrosion test. First, samples were cleaned and measured by following the ASTM standard. After the 100-hour test, samples were cooled down in the furnace and prepared for post test analyses. The first analysis was surface and cross-sectional metallographic analysis by scanning electron microscope (SEM). The second analysis was elementary analysis of corrosion products by energy dispersive spectroscopy (EDS). In the final step, samples were cleaned with chemical solutions, and the mass loss was measured. Details of each process will be described in the following sections.

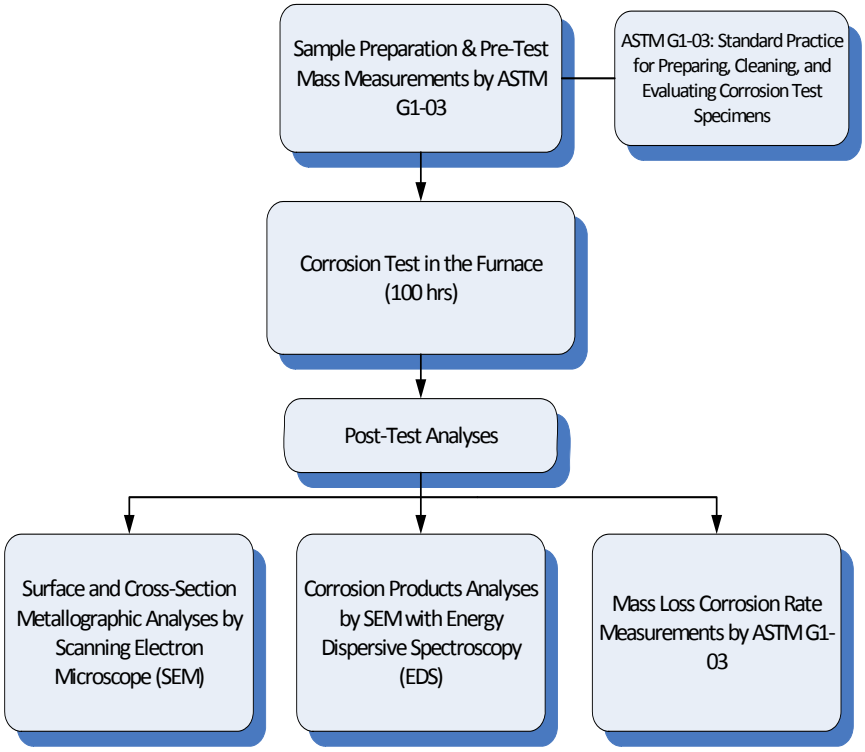


Figure 4-1 Experimental procedures of the corrosion test

### 4.2.1. Test Materials and Sample Preparations

Three commercial steels, NSSER-4 (Nisshin Steel, Inc., Japan), SA213 T11, and SA178A have been studied in this research. It is well known that SA213 T11 and SA178A have been widely used as the base metal in the manufacture of waterwall and superheater tubes. NSSER-4 was developed by a Japanese steel company that claims it offers good resistance to chlorine corrosion. The chemical compositions of these materials are summarized in Table 4-1. The three steel coupons were cut to dimensions of 2.54 cm X 2.54 cm X 0.20 cm (1” X 1” X 0.08”) using a water–cooled saw machine.

The preparation of samples followed the standard ASTM G1-03 procedure that included (1) imprinting the designation code into the sample surface using hardened steel stencil stamps hit with a hammer; (2) grinding the sample (the edges and faces) with 120-grit SiC paper; (3) degreasing with acetone in ultrasonic baths; and (4) drying at $100^{o}$C for one hour. After these steps, the clean, dry sample was measured and weighed.

Table 4-1 Chemical Composition (wt. %) of test samples

| Steel | C | Si | Mn | P | S | Ni | Cr | Mo | Fe | Nb+Ta | Cu | Al | Ca | N | Ti | V | W | B |
|---|---|---|---|---|---|---|---|---|---|---|---|---|---|---|---|---|---|---|
| ***SA178A*** | 0.07 | 0.06 | 0.47 | 0.01 | 0.004 | 0.054 | 0.016 | 0.01 | bal. | 0.002 | 0.119 | 0.026 | 0.001 | 0.008 | 0.003 | 0.002 | - | - |
| ***SA213 T11*** | 0.08 | 0.28 | 0.43 | 0.014 | 0.002 | - | 1.05 | 0.52 | bal. | - | - | - | - | - | - | - | - | - |
| ***NSSER-4*** | 0.04 | 2.5 | 0.8 | - | - | 13.1 | 17.3 | 2.5 | bal. | - | - | - | - | - | - | - | - | - |

### 4.2.2. Apparatus of Corrosion Tests

Corrosion tests were carried out in a laboratory furnace at the gas temperature of 700-750$^{o}$C for 100 hours. Figure 4-2 shows the configuration of the apparatus. The furnace (Barnstead Thermolyne, FA 1638-1) was well insulated and had a constant temperature zone of 33 cm in which the test samples were maintained. A sample carrier consisting of a stainless steel tube with a square cross section (2.5 cm X 2.5 cm) was placed in the furnace (Figure 4-3). Cooling air was passed through the sample carrier and maintained its upper surface, on which the coupons rested, at a constant temperature that differed from the temperature of the synthetic flue gas flowing through the furnace. The synthetic flue gas was injected into the furnace from the front and exited from the four holes on the same side of the entrance (Figure 4-3). Therefore, the furnace enclosure could be seen as a continuous stirred-tank reactor (CSTR).


Figure 4-2 Configuration of the apparatus

The schematic cross section of the furnace and the sample carrier is illustrated in Figure 4-3. The sample carrier had six relief locations on which samples could be placed, and each indent was equipped with a K-type thermocouple (Omega Engineering, Inc., KQXL-116U-18) to monitor the sample temperature. Lowering of the sample temperature to the desired value was achieved by controlling the flow rate of the cooling air through the sample carrier. This enabled the test to simulate an induced thermal gradient between the gas and metal surface.

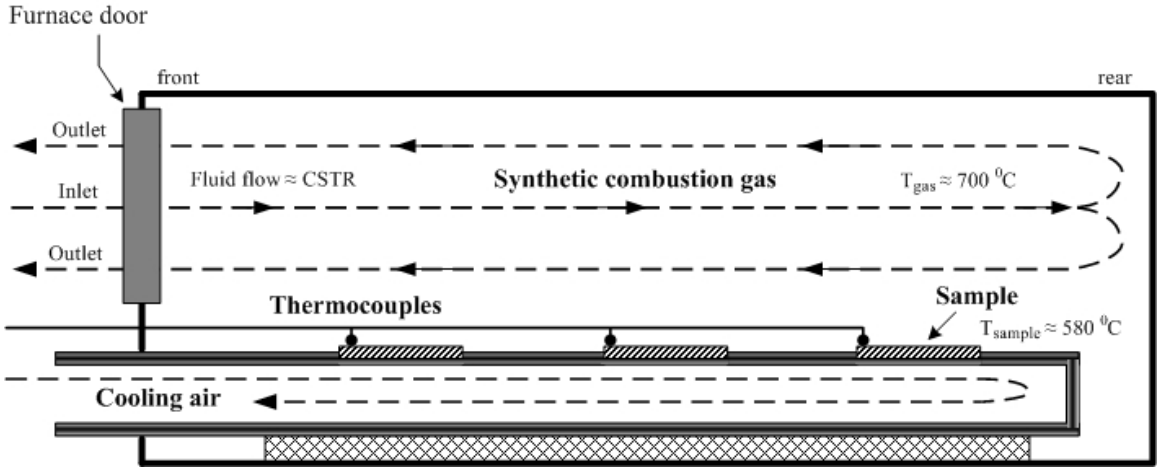


Figure 4-3 The schematic cross-section of the furnace and sample carrier

The temperature profile of six samples and their average temperatures during the test (when the furnace temperature was set at 750$^o$C) is shown in Figure 4-4. During the 100-hour test, each sample was maintained at stable temperature. By controlling the flow rate of the cooling air, surface temperatures of the six samples varied from 500-630$^o$C, whit the thermal gradient (at furnace temperature of 750$^o$C) ranging from

120-250$^{o}$C. This setup enabled a single 100-h test to yield five temperature versus time results with one duplicate set for comparison.

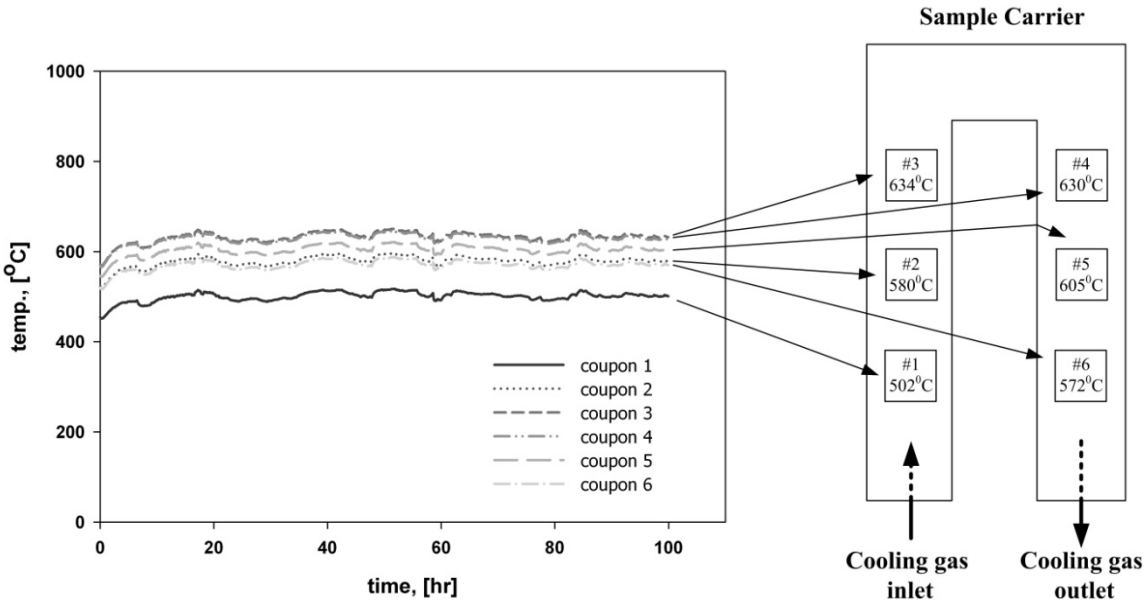


Figure 4-4 Temperature profiles of six samples on carrier

The composition of synthetic flue gas in the test was suggested by WTE engineers and consisted of 8% $O_2$, 12% $CO_2$, 0-1000 ppmv HCl, 100 ppmv $SO_2$, 15% water vapor, with a balance of $N_2$ for a total gas flow rate of 500 ml/min (mass flow control: Aalborg Instruments and Controls, Inc., SKUW-183356). The synthetic flue gas was preheated to 350$^{o}$C with heat tapes (Omega Engineering, Inc., FGS101-060) before being injected into the furnace.

### 4.2.3. Apparatus of $HCl/Cl_2$ Sequestration Tests

The $HCl/Cl_2$ sequestration tests utilized a laboratory scale of injection system to inject the calcium hydroxide slurry into a tube furnace, together with the synthetic flue gas. The tube furnace (Carbolite GHC 12/900) had a heated chamber length of 106.7 cm (42") (zoned 15.3 cm – 76.2 cm – 15.3 cm (6" – 30" – 6")) and was equipped with a quartz process tube (15.0 cm ID X 16.5 cm OD X 106.68 cm (5 7/8" ID x 6 1/2" OD x 42") long). During the test, the furnace heated to 750$^{o}$C to represent the flue gas temperature of WTE facilities. The samples were hung at the end zone of the process tube to ensure the maximum contact time of the slurry and flue gas. The duration of the test was 50 hours. The schematic of the experimental setup is shown as

Figure 4-5. Figure 4-6 shows the configuration of the tube furnace and injection system.

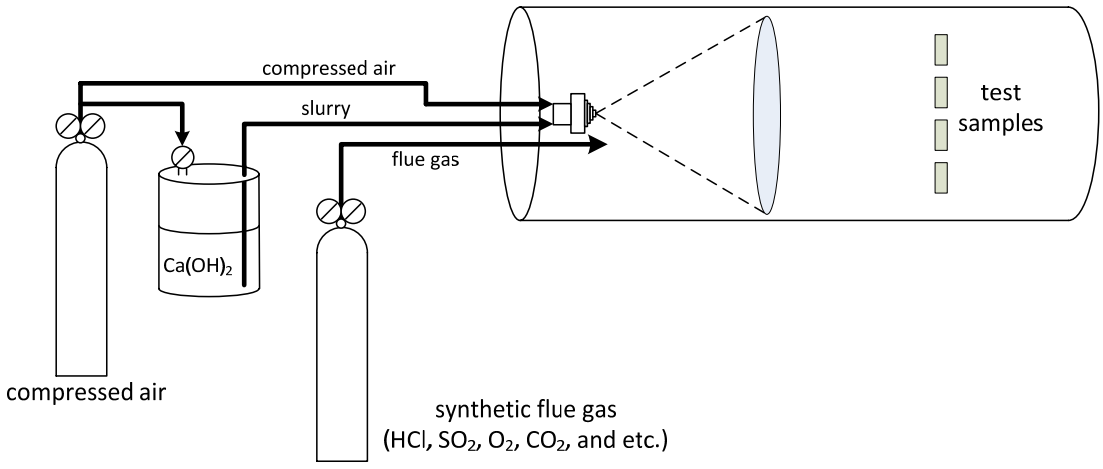


Figure 4-5 Schematic of the experimental setup

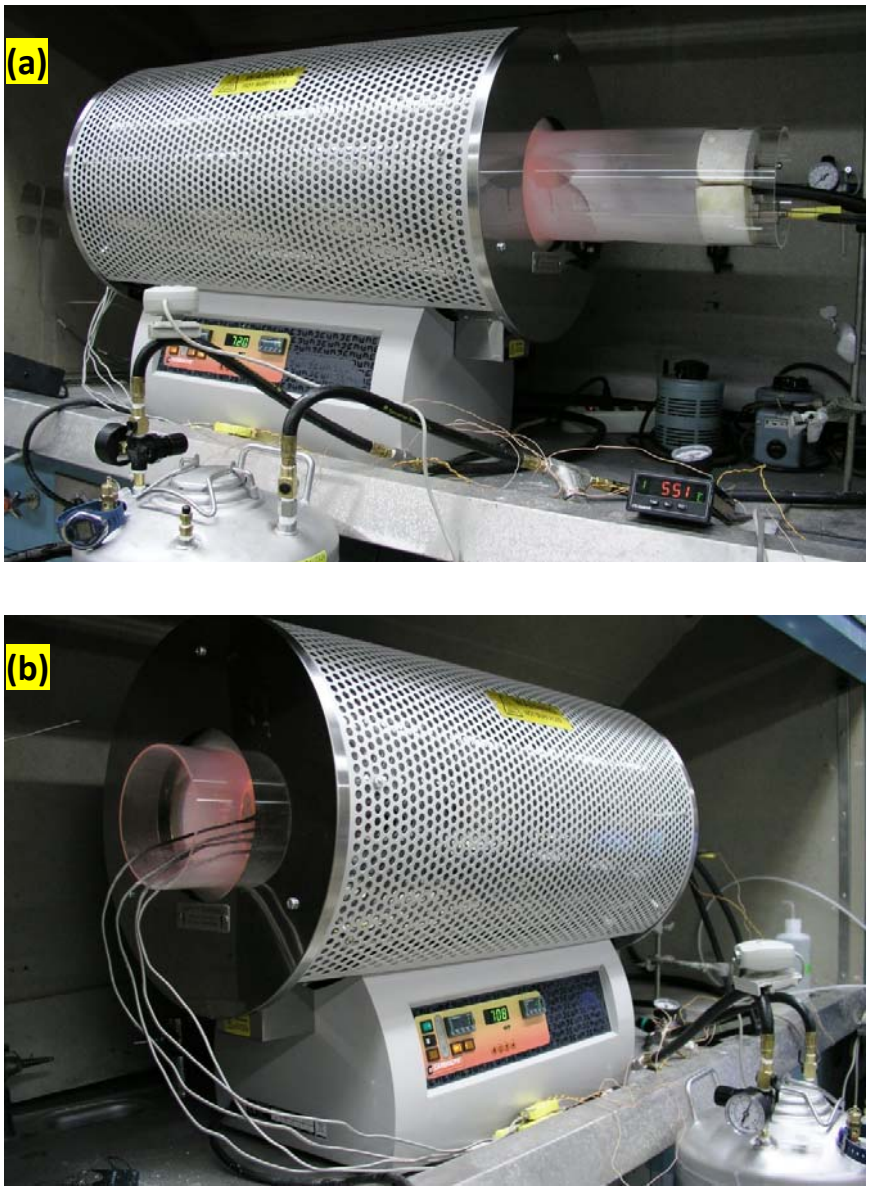


Figure 4-6 Configuration of the tube furnace and injection system; (a) seen from the right side and (b) seen from the left side of the furnace

The injection system consisted of a air atomizing nozzle (Spraying System Co., 1/4JBC-SS+SUE15B-SS), air pressure regulator with gauge (Spraying System Co., 111438-250S), air filter (Spraying System Co., 11438-1), air shut-off valve, liquid pressure regulator with gauge (Spraying System Co., 11438-45S), liquid strainer, liquid shut-off

valve, and pressure tank (Spraying System Co., 22140-10-304SS) (Figure 4-7). The atomization was produced by a combination of air and liquid pressures, and the flow rate and shape of the spray was controlled by adjusting these pressures. The pneumatic nozzle featured internal impingement atomization to assist fine drop formation. Finer atomization was accomplished by increasing the air pressure and/or lowering the liquid pressure, resulting in a higher ratio of air flow rate to liquid flow rate. When the air pressure was controlled at 68.9 kPa (10 psi), the drop size that corresponded to the fluid capacity of 18.9-75.7 $cm^3$/min (0.005-0.02 gal/min) is 20-100 µm. Figure 4-8 shows the configuration of the nozzle and synthetic gas inlet. The nozzle and gas inlet were mounted on a cylindrical ceramic section. Figure 4-9 shows the spray pattern in the tube furnace (furnace temperature: 750$^{o}$C) when the air and fluid pressures were controlled at 20.7 kPa (3 psi) and 13.8 kPa (2 psi), respectively.

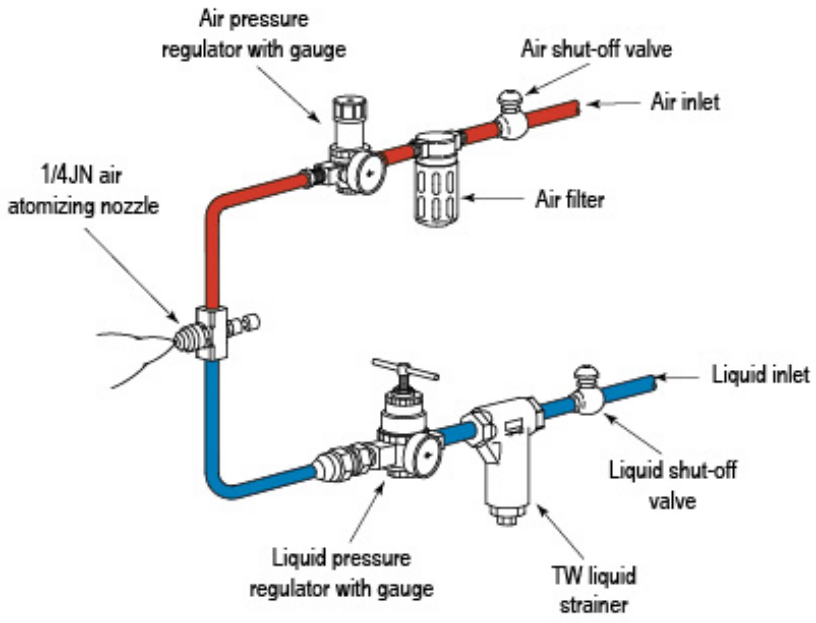


Figure 4-7 The schematic of the injection system [34]

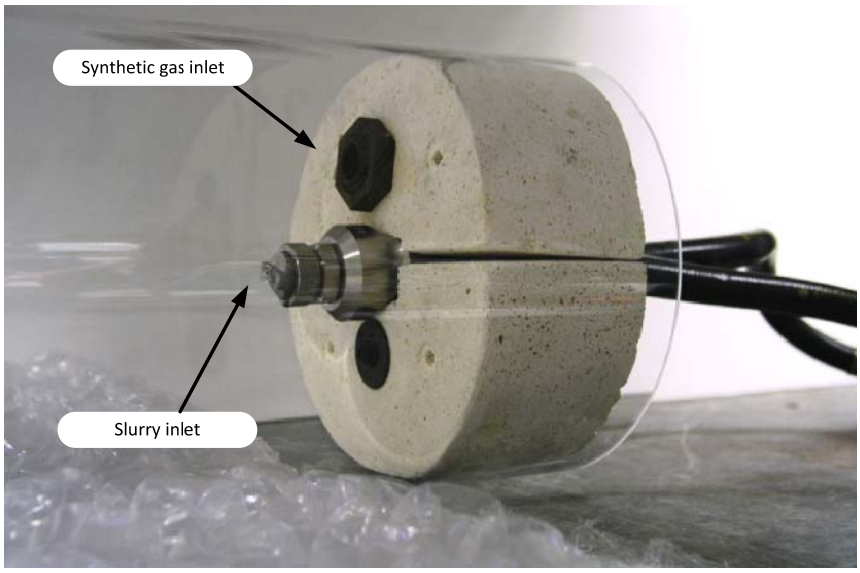


Figure 4-8 The configuration of the nozzle and synthetic gas inlet

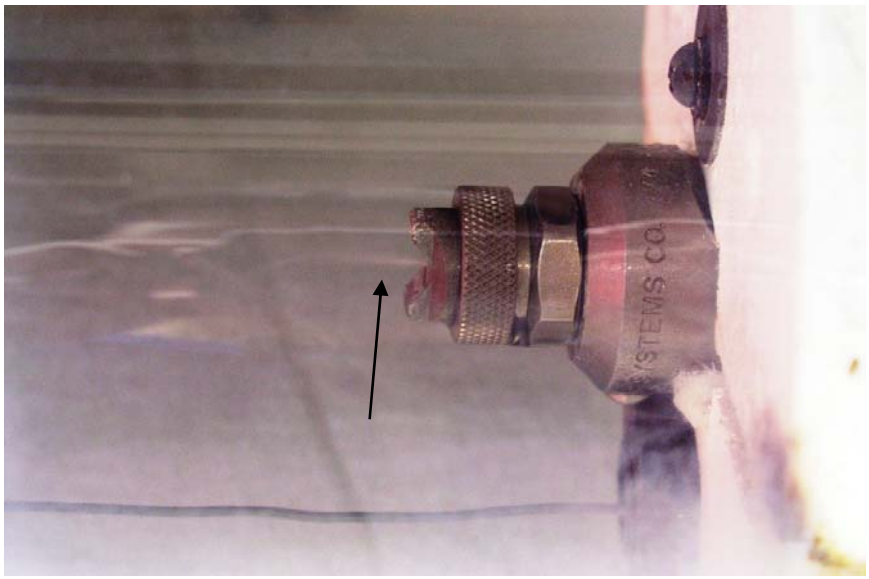

Figure 4-9 The spray pattern generated with air and fluid pressure at 3 and 2 psi, respectively

### 4.2.4. Post Test Analysis

After each corrosion test, the samples were left to cool in the furnace. They were then prepared for corrosion product analysis, metallographic corrosion rate observations, and mass loss corrosion rate measurements. Analysis of the surface morphology and elemental composition of the corrosion products was conducted by using a scanning electron microscope (SEM, Hitachi S-4700) equipped with an energy dispersive spectroscopy (EDS) unit.

The measurement of mass loss corrosion rate followed the ASTM G1-03 guidelines. A cleaning cycle that combined procedures of light brushing, ultrasonic cleaning, chemical cleaning, and mass loss measurement was repeated several times until the corrosion products were completely removed. Removal was confirmed by examination with a low power microscope (e.g. 7X to 30X). Final sample weights were measured to the nearest 0.001 g and adjusted for blank weight losses in the cleaning process. Once the mass lost during the test was determined, the average corrosion rate was converted by the following equaition:

$$\text{Corrosion Rate} = (K \; X \; W) \; / \; (A \; X \; T \; X \; D) \qquad (4\text{-}1)$$

where:

K = a constant (see Table 4.2), T = time of exposure in hours, A = area in $cm^2$, W = mass loss in grams, and D = density in $g/cm^3$.

Table 4-2 Constant (K) in corrosion rate equation for desired corrosion rate units

| *Corrosion Rate Units Desired* | *Constant (K) in Corrosion Rate Equation* |
|---|---|
| **mils per year (mpy)** | $3.45 \times 10^6$ |
| **inches per year (ipy)** | $3.45 \times 10^3$ |
| **inches per month (ipm)** | $2.87 \times 10^2$ |
| **millimeters per year (mm/y)** | $8.76 \times 10^4$ |
| **micrometers per year (µm/y)** | $8.76 \times 10^7$ |
| **picometres per second (pm/s)** | $2.78 \times 10^6$ |
| **grams per square meter per hour ($g/m^2h$)** | $1.00 \times 10^4 \times D$ |
| **milligrams per square decimeter per day (mdd)** | $2.40 \times 10^6 \times D$ |
| **micrograms per square meter per second ($\mu g/m^2 s$)** | $2.78 \times 10^6 \times D$ |

# 5. Experiment Results and Discussion

## 5.1. Corrosion Kinetic Tests

### 5.1.1. Test Background

In the operation of WTE facilities, soot blowing by high pressure of air or steam is commonly used either online or offline to clean the ash deposits on the boiler tube surface in order to maintain its heat transfer efficiency. During the semiyearly maintenance, boiler tube examinations are usually conducted by means of nondestructive testing (NDT). NDT are noninvasive techniques to determine the integrity of a material, component or structure or quantitatively measure some characteristic of an object. Based on the magnetic flux leakage technique, the defects on the surface, including hole, pit, and crack, can be inspected, and the boiler waterwall tube loss can be tested using NDT methods [35]. In most NDT methods, the tube needs to be sandblasted to remove the ash deposits and scale from the surface in order to obtain a precise measurement. However, many WTE operators have found that both the soot blowing and sandblasting somehow increase the corrosion phenomena of the boiler tube. They attributed this situation to these cleaning methods because of the exposure of the bare metal to the corrosive gases after the cleaning process. In some area where the ash deposits on the tube surface maintain un-melted the corrosion rate is lower because the ash deposits increase the difficulty of the corrosive gases to penetrate through.

Theoretically, at high temperature parabolic oxidation or a combination of parabolic and linear oxidation is frequently encountered. Reactions may be interface controlled (linear) during initial stages and diffusions limited (parabolic) after extended oxidation [16]. If the highest corrosion rate always occurs right after the tube is soot cleaned or sandblasted, WTE operators will face the dilemma of increasing the thermal efficiency of the boiler (by increasing frequency of cleaning process) or extending the tube life (by lower the frequency of cleaning process).

This kinetic test was the first step of this experimental research to help understand the corrosion mechanism of selected alloys at certain times during the 100-hour test and to discuss the effect of metal temperature on the corrosion rates. The low-carbon steel, SA178A, was tested under a well controlled thermal gradient where the gas temperature was at 750$^{o}$C, and metal temperatures ranged from 480 to 600$^{o}$C. The duration of each test varied from 10, 25, 40, and 100 hours. The testing environment was identical for each test except the duration of the test. The composition of the synthetic corrosive test gas consisted of 8% oxygen, 12% carbon dioxide, 1000 ppm hydrogen chloride, 100 ppm sulfur dioxide, 15% water vapor, with a balance of nitrogen for a total gas flow rate of 500 ml/min. The results presented included the mass loss of samples and their corrosion rates converted from the mass loss accordingly.

### 5.1.2. Results and Discussion

Figure 5-1 shows the mass loss of steel SA178A at different metal temperatures and test durations- 10, 25, 40, and 100 hours. It was very clear that the mass loss increased along with the extension of test duration, and for any given test duration, higher metal temperature caused more mass loss than lower metal temperature. For a given metal temperature, the mass loss did not display a linear correlation to the test duration, especially at the higher metal temperature. The difference of mass loss between 25 and 40 hours was smaller than that between 10 and 25 hours.

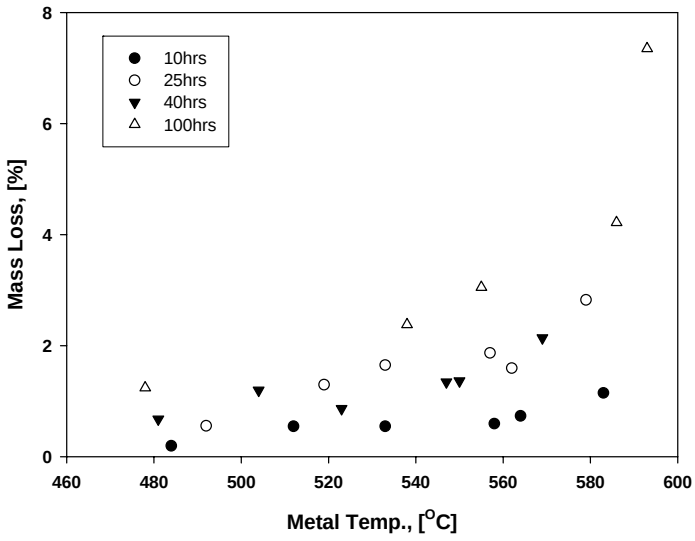


Figure 5-1 Effect of metal temperature on mass loss of samples

Figure 5-2 shows the penetration (thickness loss, mills) of sample SA178A versus test duration for different metal temperatures. Samples were categorized into three groups according to their metal temperatures. Samples with metal temperature ranged between 511 and 565$^{o}$C were put together (the error bar in Figure 5-2 shows the

minimum and maximum mass loss at certain test duration) because their mass loss was within the same level. The penetration curves were found to follow the parabolic time dependence in the three metal temperature scenarios. This result was in agreement with the high temperature corrosion mechanism as described in the reference [16].

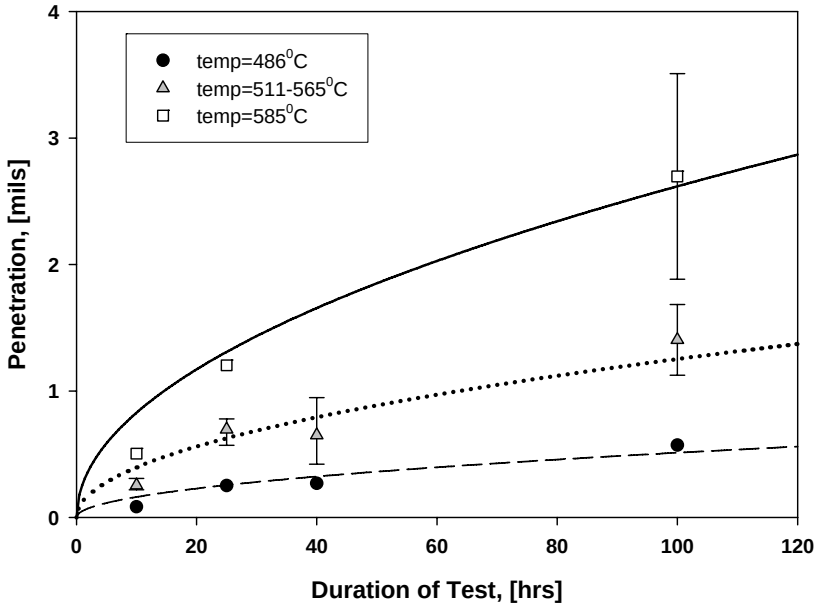


Figure 5-2 The penetration of sample SA178A during different test durations

The parabolic rate equation, as described in Chapter 2.2.1, is shown as follows.

$$dx/dt = K_p\ /x \tag{5-1}$$

$$\mathrm{x}^2 = 2K_p t + C \tag{5-2}$$

where x represents mass loss or thickness of the oxide, t denotes time, $K_p$ denotes the parabolic rate constant and C is the integration constant. In this test, C is zero since the sample has no corrosion at the beginning of the test.

The parabolic rate constant for each metal temperature was calculated according to the experimental data and was shown in Table 5-1. It was found that higher metal temperature caused higher parabolic rate constant.

Table 5-1 Calculated parabolic rate constants of steel SA178A for different metal temperatures

| ***Metal temperature ($^oC$)*** | ***$k_P$ ($mils^2/h$)*** |
|---|---|
| ***585*** | 0.03427 |
| ***511-565 (avg. = 538)*** | 0.00784 |
| ***486*** | 0.00131 |

Many experimental studies of oxidation reactions have shown that the temperature dependence of oxidation rate constants at constant ambient oxygen pressure obeys an Arrhenius equation: [16]

$$k = Ae^{-E_a/RT} \tag{5-3}$$

$$lnk = lnA + \frac{-E_a}{R}\left(\frac{1}{T}\right) \tag{5-4}$$

where k represents the rate constant, A denotes the pre-exponential factor, Ea is the apparent activation energy, R is the gas constant, and T is the temperature of the reaction. Using this equation, the apparent activation energy is determined by plotting ln k as a function of 1/T, in which case the slope of the curve is given by –Ea/R.

Figure 5-3 shows the temperature dependence of parabolic rate constants of SA178A within the 100-hour test by using its parabolic rate constants of three metal temperatures that were calculated from the experimental data (Table 5-1). The calculated overall activation energy of steel SA178A within the 100-hour test was 178 kJ/mol.

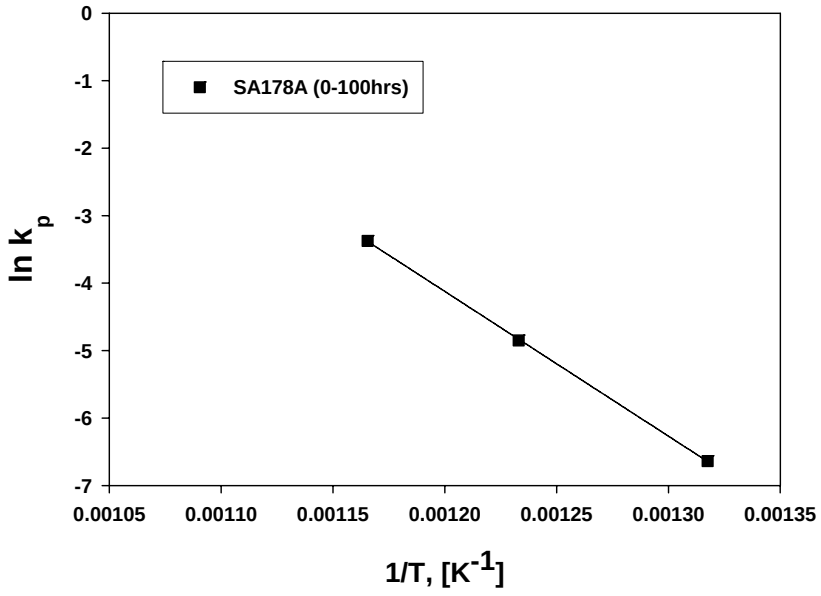


Figure 5-3 Temperature dependence of oxidation rate constant of SA178A within the 100-hour test

In the other section of this research, another two materials, SA213 T11 and NSSER-4, were also tested in the same environment with the kinetic test (results will be presented in the following chapter). Unlike the kinetic tests for alloy SA178A that were repeated for different test durations, these two materials were only test for 100 hours. Therefore, we were not able to obtain the parabolic rate constants as we did for alloy

SA178A. Instead of the parabolic rate constant, the penetrations of these three materials after the 100-hour test were used to plot their temperature dependence shown as Figure 5-4. The parabolic rate equation (Eq. 5-2) shows the relation of the penetration of sample with time. If we use the penetration of samples at the 100$^{th}$ hour, $x_{100}$, the parabolic rate equation will become:

$$x_{100}{}^2 = 2k_p \times 100 \tag{5-5}$$

and the relation of $\ln x_{100}$ with $\ln k_p$ can be interpreted through Eq. 5-6 to 5-8.

$$x_{100} = \sqrt{200k_p} \tag{5-6}$$

$$lnx_{100} = ln\left(200k_p\right)^{1/2} \tag{5-7}$$

$$lnx_{100} = \frac{1}{2}\, ln200 + \frac{1}{2}\, lnk_p \tag{5-8}$$

Therefore, the slops obtained from the cures shown in Figure 5-4 will be only half of that from the curve shown in Figure 5-3. After using the above adjustment, the activation energies of the three materials at the 100$^{th}$ hour calculated from the slops in Figure 5-4 were $E_{a,\ S178A}$= 149kJ/mol, $E_{a,\ 213T11}$=117kJ/mol, and $E_{a,\ NSSER\text{-}4}$=59 kJ/mol. The activation of alloy S178A at 100$^{th}$ hour ($E_{a,\ S178A}$= 149kJ/mol) was close to its overall activation energy within the 100-hour test ($E_{a,\ S178A}$= 178kJ/mol) showing that the 100 hours of exposure to the corrosive environment could not only elucidate the corrosion mechanism but also the likely mode of failure during actual operation. By comparing the activation energies of these three materials, we could infer that the corrosion of the

low-carbon steel, SA178A was more reaction control while the stainless steel, NSSER-4 was more diffusion control.

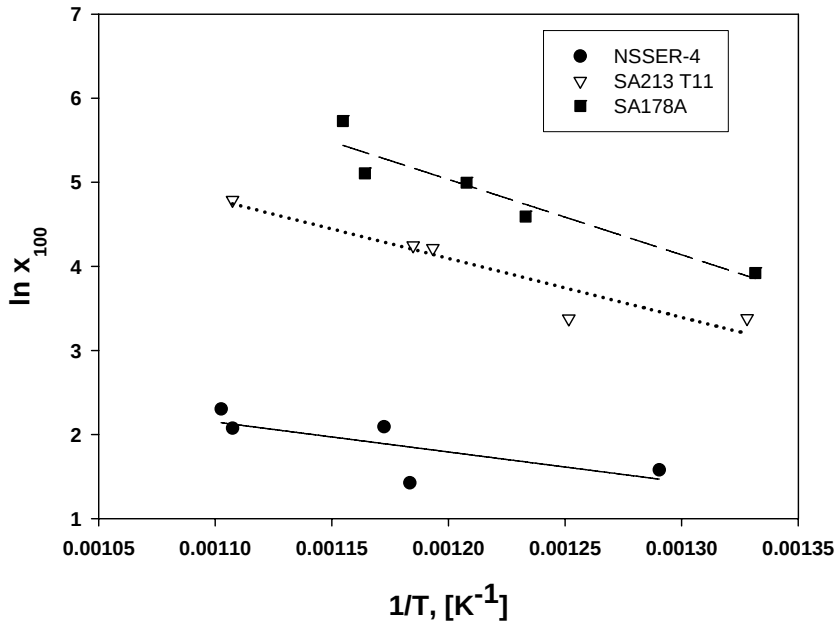


Figure 5-4 Temperature dependence of penetrations of three different materials (SA178A, SA213T11, and NSSER-4) after the 100-hour test

### 5.1.3. Conclusion

The overall reaction process of alloy SA178A during the 100-hour test was found to follow the parabolic time dependence which was often found in high temperature oxidations. The calculated overall activation energy of alloy SA178A within the 100-hour test was 178kJ/mol. The calculated activation energy of alloy SA178A after the 100-hour test was 149kJ/mol, which was close to its overall activation energy showing that the 100 hours of exposure was suitable for the corrosion test. From the compassion of activation energies of three test materials, it was inferred that the corrosion of the low-

carbon steel, SA178A was more reaction control while the stainless steel, NSSER-4 was more diffusion control.

## 5.2. Chlorine Induced Corrosion Mechanisms

### 5.2.1. Test Background

The objective of this test is to use the simulated thermal gradient created by the apparatus mentioned in the previous chapter to investigate the chlorine induced corrosion mechanisms. Three types of commercial tubing (NSSER-4, SA213 T11, and SA178A) were tested under corrosive environments for 100 hours. The composition of the synthetic corrosive gas consisted of 8% oxygen, 12% carbon dioxide, 500 ppm hydrogen chloride, 100 ppm sulfur dioxide, 15% water vapor, with a balance of nitrogen for a total gas flow rate of 500 ml/min. The surface temperatures of the six samples varied from 500-630$^{o}$C, and the thermal gradient (at a furnace temperature of 750$^{o}$C) varied from 120-250$^{o}$C. The post-test investigation consisted of observation of surface and cross-sectional morphology by scanning electron microscopy (SEM) and elemental analysis of corrosion products by energy dispersive spectrometry (EDS). The corrosion rates were acquired by measuring the mass loss of samples after the chemical cleaning.

### 5.2.2. Results

**(1) Alloy NSSER-4 (stainless steel)**

Figure 5-5(a) and (b) are the images of samples after the 100-hour test at metal temperatures of 570$^{o}$C and 630$^{o}$C, respectively. The sample having a lower metal temperature was barely corroded, as judged solely on the basis of its appearance. In contrast, the 60$^{o}$C warmer metal surface was covered with randomly distributed corroded areas (scales) that exhibited a certain level of adhesion without cracking or spallation. From visual observations alone, one could clearly see that for a given temperature in the furnace, a higher metal temperature led to more serious corrosion. Figure 5-5(c) is the SEM image of the external topography of the scale formed on the sample surface shown in Figure 5-5(b). The surface was covered by some congregate oxides and sulphides.

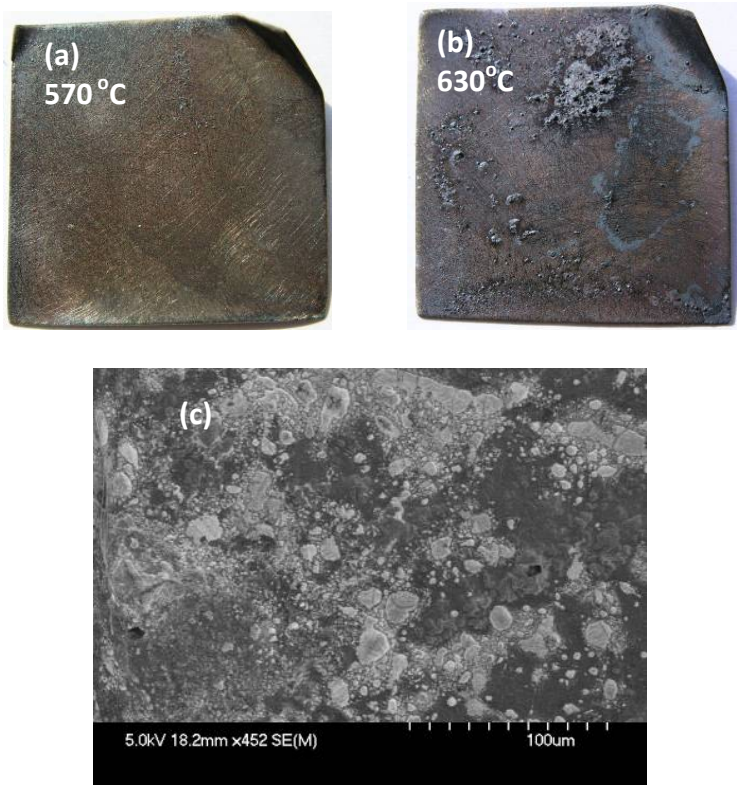


Figure 5-5 Surface morphologies of two samples of NSSER-4 at different metal temperatures after 100-hour test

The elemental analysis of each sample's surface is shown is Figure 5-6(a)-(d). The "corroded area" analysis displayed in these figures corresponds to the area having more deposits on the surface as compared to the "less corroded area". Iron and chromium concentrations of the less corroded areas were higher than those of corroded areas while oxygen and sulfur concentrations showed opposite trends. In addition, there was no clear correlation between composition of scales and metal temperatures. According to thermodynamic calculations, these scales consisted of mostly hematite / magnetite / wustite, ferrous sulphide and chromium hemitrioxide. The other elements such as silicon and nickel did not show similar trends, and chlorine was either not identified or was present at very low concentration on the samples' surface.

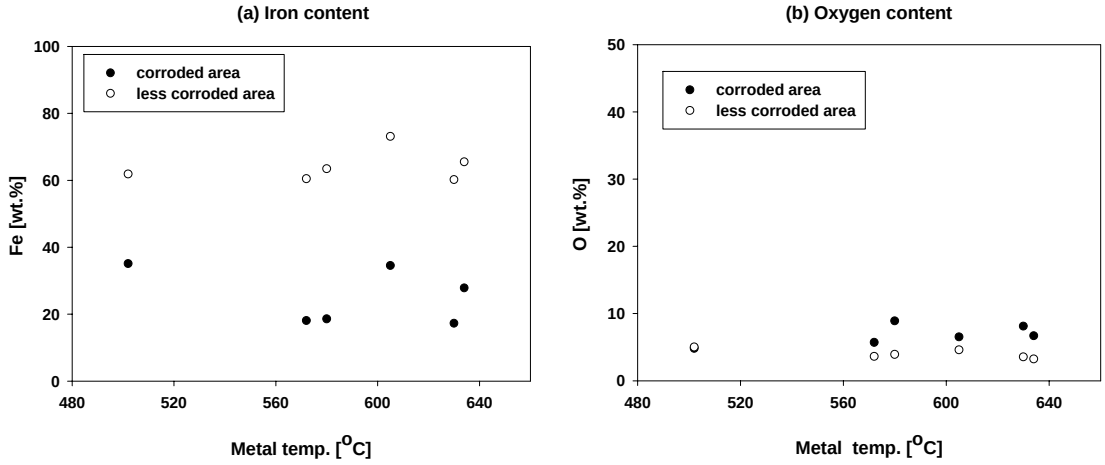

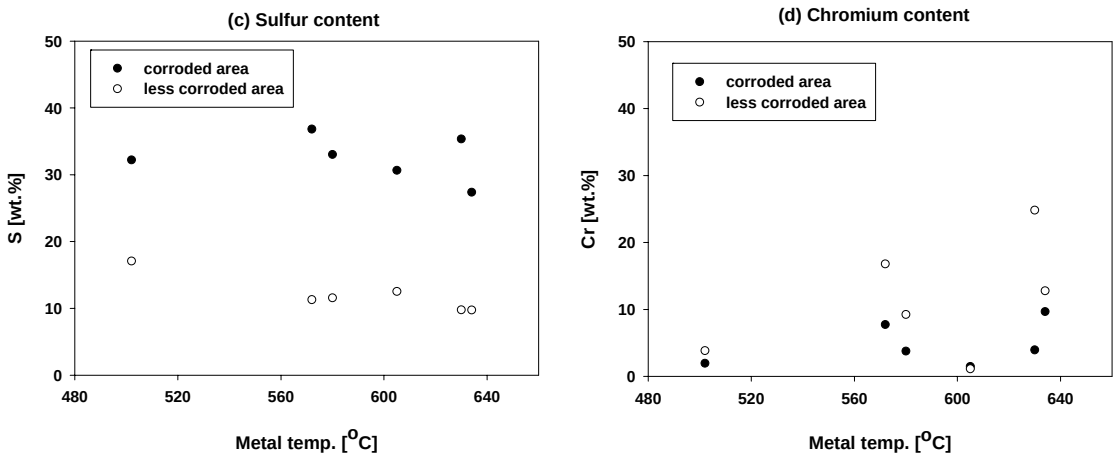


Figure 5-6 Elemental analysis of the samples' surfaces: (a) Fe, (b) O, (c) S, and (d) Cr

Figure 5-7 shows the cross-sectional SEM image of the remaining sample substrate (the most corroded sample in the test) after the chemical cleaning. The accompanying table summarizes the corresponding wt.% composition appearing in Figure 5-7. High chlorine concentration was found on the surface of the remaining substrate, and it decreased with increasing distance below the sample surface while chromium and iron concentrations revealed opposite tendencies. According to thermodynamic calculations, it was assumed that the reaction products on the scale/metal interface consisted of iron chlorides. Combining these calculations with the results of the sample surface elemental analysis mentioned above helped to explain the corrosion mechanism. Chloride (or chlorine) appeared to penetrate the oxide scale through cracks and pores in the loosely bound scale and corrosion products accumulated at the scale/metal interface attributable to thermal and chemical potential driving forces [16].

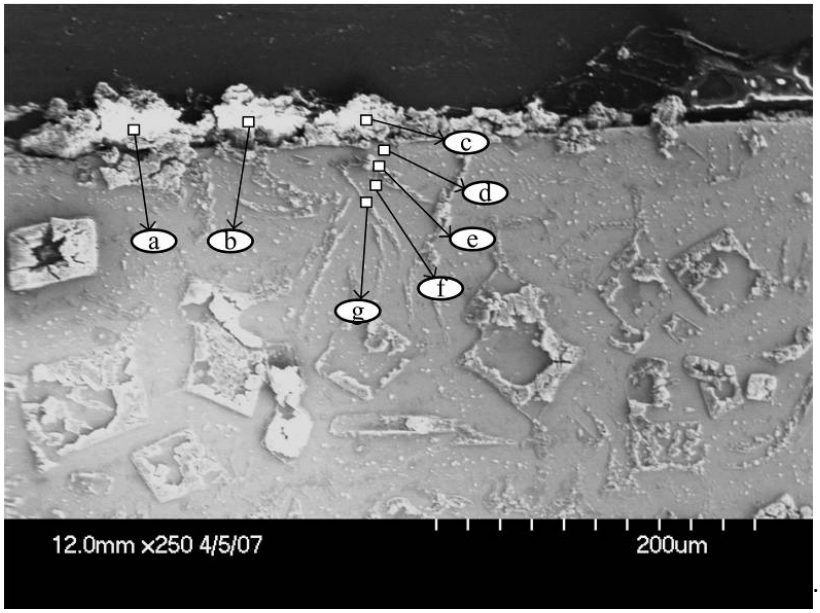


**Composition (wt.%)**

| Area | O | Si | Cl | Cr | Fe | Mn | Ni | P | S |
|---|---|---|---|---|---|---|---|---|---|
| a | 8.85 | 0.01 | 39.53 | 2.28 | 46.99 | 0.00 | 1.48 | 0.35 | 0.52 |
| b | 0.00 | 0.00 | 39.38 | 2.94 | 50.09 | 0.00 | 2.19 | 0.49 | 0.67 |
| c | 0.24 | 0.27 | 41.75 | 3.47 | 52.24 | 0.00 | 1.11 | 0.29 | 0.64 |
| d | 0.00 | 2.38 | 3.16 | 20.48 | 70.79 | 0.00 | 1.36 | 0.36 | 1.47 |
| e | 0.00 | 2.14 | 1.70 | 18.51 | 74.52 | 0.00 | 1.08 | 0.46 | 1.59 |
| f | 0.00 | 2.32 | 1.06 | 18.97 | 74.36 | 0.11 | 1.21 | 0.54 | 1.44 |
| g | 0.00 | 2.39 | 1.84 | 19.12 | 71.43 | 0.00 | 0.07 | 0.34 | 1.55 |

Figure 5-7 Cross-sectional SEM image of the sample and the elemental analysis of each location

The cross-sectional SEM images of the remaining sample substrate are shown in Figure 5-8 (a) and (b) with metal temperatures of 630$^{o}$C and 502$^{o}$C, respectively. It can be seen that the sample substrate is oxidized, and the crack and cavity occurred after the metal chloride diffused outward through the scales.

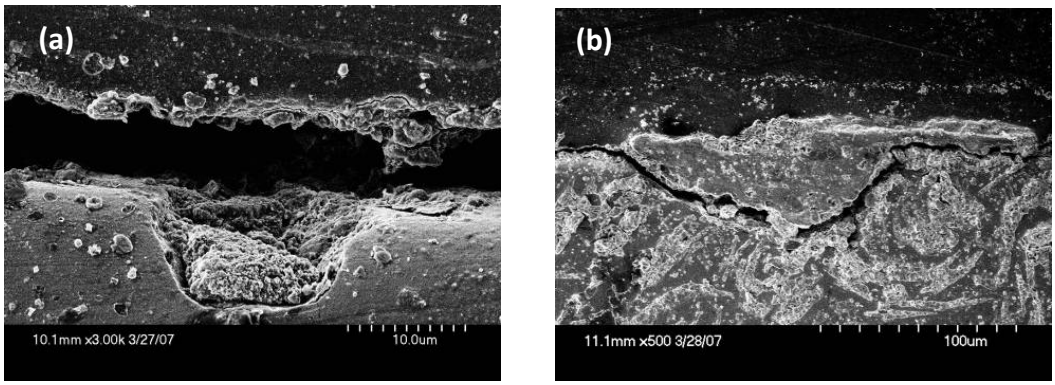


Figure 5-8 Cross-sectional SEM images of the remaining sample substrates: (a) metal temperatures = 630$^{o}$C and (b) metal temperatures = 502$^{o}$C

**(2) Alloy SA213 T11 (low-carbon, intermediate-chrome steel)**

Figure 5-9 (a) and (b) are the images of coupons following a 100-hour test at metal temperatures of 565$^{o}$C and 630$^{o}$C, respectively. In this case, the temperature difference did not seem to result in different levels of corrosion. The entire surface of both samples was corroded and formed a thin flat skin of corrosion products that could easily be peeled off after cooling. Below that remained an inner scale that was more attached to the bare metal.

The elemental analysis of each sample's surface is shown in Figure 5-9(a)-(d). The "outer scale" shown in these figures denotes the oxide scale on the sample surface while the "inner scale" denotes the layer that becomes exposed after the removal of the outer scale. Both the iron and oxygen concentrations of the outer scales were higher than those of the inner scales, especially for the iron concentration difference (>10%) in the higher temperature region. The iron concentration of the inner scale decreased as the metal temperature increased while the oxygen concentration showed an opposite

trend, indicating that as the metal temperature increased more iron from the inner scales became oxidized. In addition, more sulfur and chromium contents were found in the inner scale than in the outer scale as the scale was porous, sulfur could easily diffuse through it to react with metal.


Figure 5-9 Surface morphologies of samples of SA213 T11 after the 100-hour test

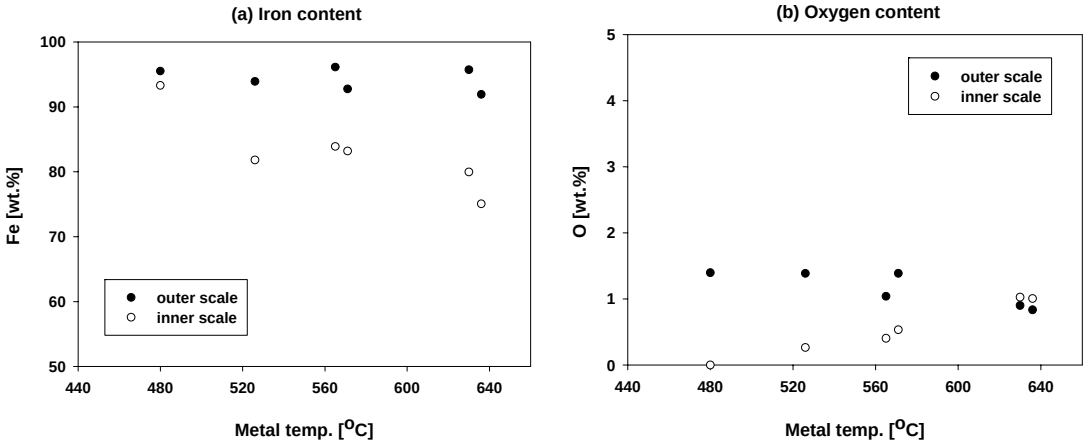

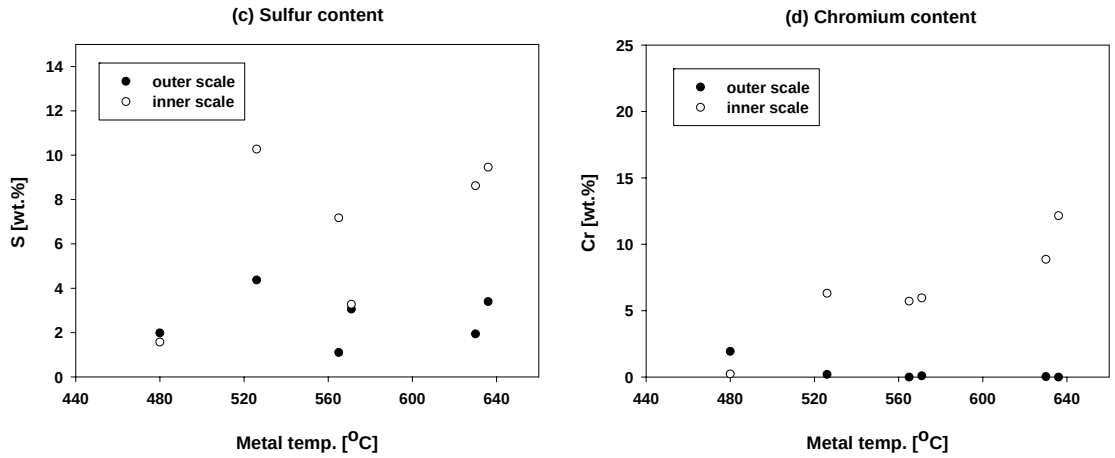


Figure 5-10 Elemental analysis of surfaces of samples SA213 T11: (a) Fe, (b) O, (c) S, and (d) Cr

**(3) Alloy SA178A (low-carbon steel)**

Figure 5-11 (a) and (b) are the images showing the sample surface morphology of alloy SA178A after a 100-hour test with metal temperatures of 540°C and 600°C, respectively. Both metal surfaces were covered with crusty scales, but the scale formed on the higher metal temperature surface was thicker and had a rippled texture. Figure 5-11(c) is the SEM image of the external topography of the scale formed on the sample surface. The needle-like oxide whiskers were porous and exhibited a low contact surface area with the metal substrate.

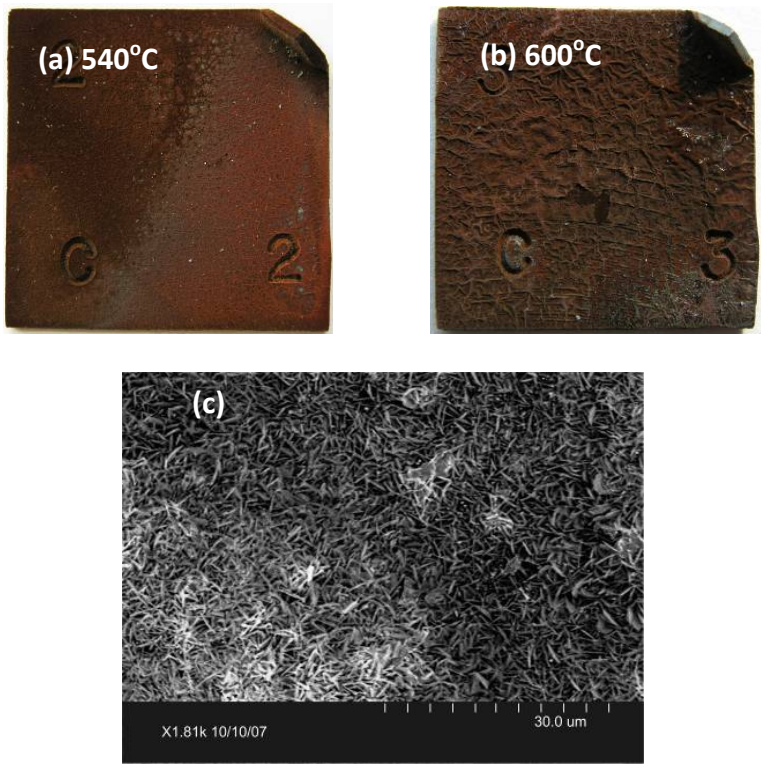


Figure 5-11 Surface morphologies of samples of alloy SA178A after the 100-hour test

The elemental analysis of each sample's surface is shown in Figure 5-12(a)-(d). Unlike the procedure for the previous two metals, the elemental analysis was conducted solely on the sample's surface since the entire sample coupon was covered by the scale. According to Kofstad [16] who has described the reactions under sulfur dioxide and oxygen mixtures, the scales consisted of iron sulfate, magnetite/wustite, and ferrous sulphide. The iron and sulfur concentrations decreased, while the oxygen and chlorine increased with increasing metal temperature. However, the concentration differences of these elements were not obvious with different metal temperatures since the structure and porosity of the scales on the sample surface due to the chlorine and sulfur attacks were observed to be similar under SEM examination. The scale consisted mainly

of magnetite and wustite during the initial stage of experiment did not offer the good protection against the subsequent attack by the corrosive gas.

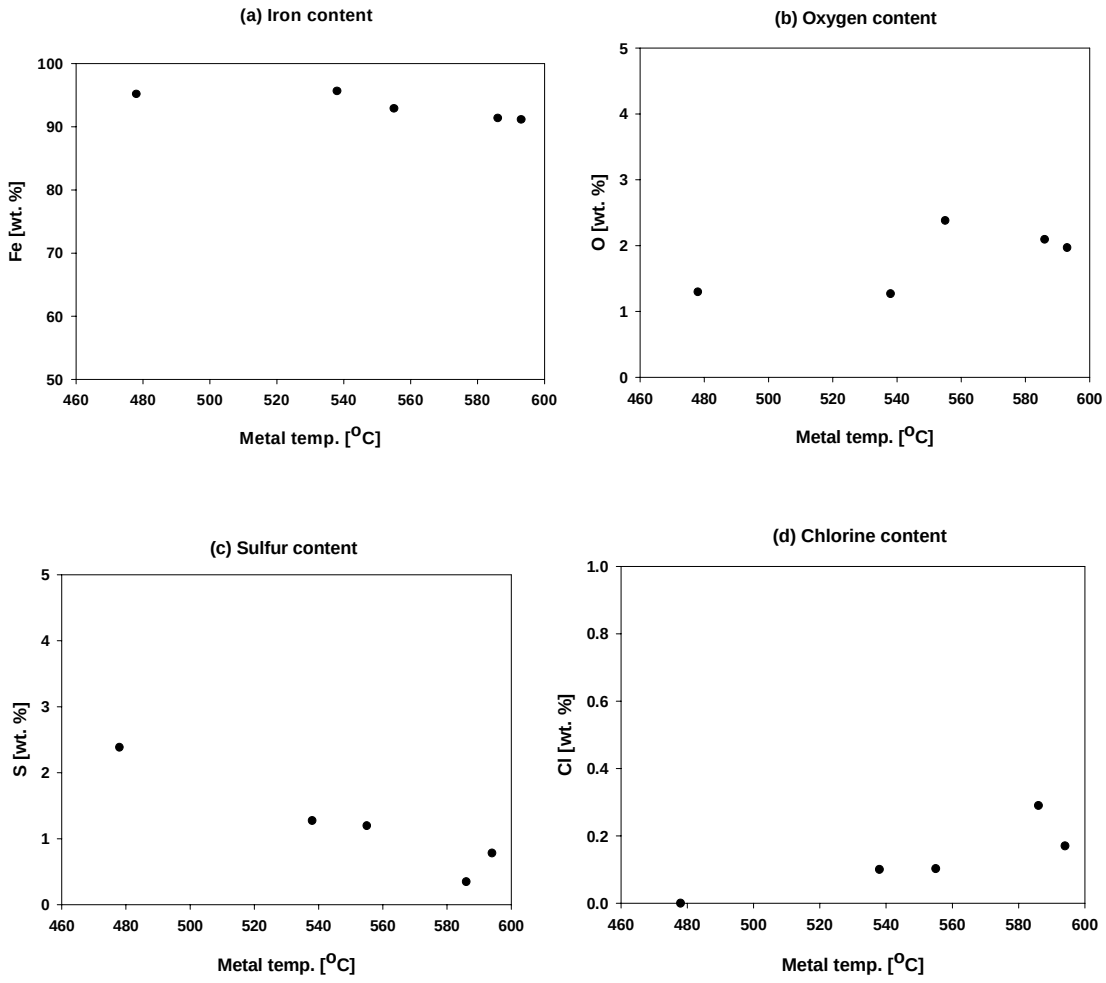


Figure 5-12 Elemental analysis of surfaces of alloy SA178A: (a) Fe, (b) O, (c) S, and (d) Cl

**(4) Comparison of mass loss corrosion rates**

Figure 5-13 shows the mass loss corrosion rate for each of the three metals. The stainless steel NSSER-4 showed very good corrosion resistance of less than 0.25 mm/y (10 mils/y) within the metal temperature range of 500°C to 630°C. When the metal

temperature was below 540°C, the corrosion rates of the steel alloy SA213 T11 were about 0.76 mm/y (30mils/y) and it showed a nearly linear increase with metal temperature above 560°C. The carbon steel SA178A had the highest corrosion rates among these three metals. The effect of metal temperature was manifest especially in the high metal temperature region. These results were in agreement with the practical corrosion rates reported from WTE plants [7].

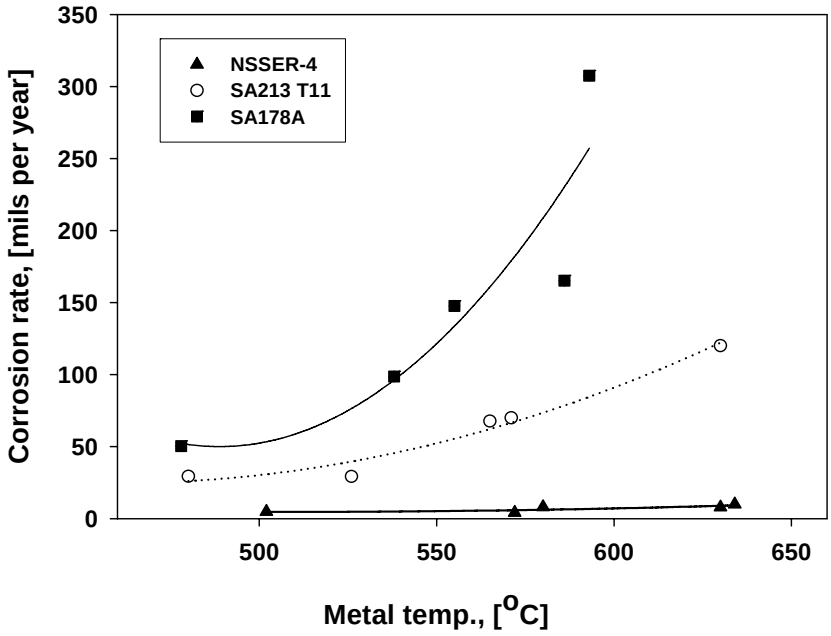


Figure 5-13 Comparison of mass loss corrosion rate

### 5.2.3. Discussion

**(1) Alloy NSSER-4 (stainless steel)**

The NSSER-4 exhibited a good corrosion resistance within the tested metal temperature range of 500-630°C. Chromium and nickel provided good protection

against the sulfur and chlorine attack. The EDS analysis indicated no clear correlation between composition of scales and metal temperatures. Thermodynamic calculations showed that scales formed on the "corroded area" consisted of mostly hematite/ magnetite/wustite, ferrous sulphide and chromium hemitrioxide. High chlorine concentration was found on the surface of the remaining substrate (scale/metal interface), and it decreased with increasing distance below the sample surface while chromium and iron concentrations revealed opposite tendencies. According to thermodynamic calculations, it was assumed that the reaction products on the scale/metal interface consisted of some iron chlorides. Combining these calculations with the results of the sample surface elemental analysis mentioned above helped to explain the corrosion mechanism. Chloride (or chlorine) appeared to penetrate the oxide scale through cracks and pores in the loosely bound scale and corrosion products accumulated at the scale/metal interface. Most of the iron chloride diffused outward through the scale, reacted with the oxygen, and then released the chlorine.

**(2) Alloy SA213 T11 (low-carbon, intermediate-chrome steel)**

Compared to the alloy SA178A, the additive chrome provides it better corrosion resistance, especially to the sulfur attack. At the lower metal temperature region (<540$^{o}$C), the corrosion rates (0.76 mm/y, or 30 mils/y) was acceptable, but the rate increased almost linearly when metal temperature was above 560$^{o}$C. From the EDS analysis, the inner scale consisted of more sulfur and chromium contents but less iron and oxygen contents then the outer scale. This showed that the sulfur was able to

penetrate the scale and reached the scale/metal interface to react with iron and chromium and induced more corrosion.

**(3) Alloy SA178A (low-carbon steel)**

Alloy SA178A was most corroded among all test samples. Its corrosion rate increased rapidly with the increase of metal temperature when the metal temperature was higher than 540$^{o}$C. The scales consisted of iron sulfate, magnetite/wustite, and ferrous sulphide due to the reactions under sulfur dioxide and oxygen mixtures. The iron and sulfur concentrations decreased, while the oxygen and chlorine increased with increasing metal temperature. However, the concentration difference for all the element was negligible since at the initial stage of the experiment, magnetite and wustite were formed on the sample surface, but its porous structure did not offer the good protection to the following chlorine and sulfur attacks.

### 5.2.4. Conclusions

Three commercial metals were tested under prescribed corrosive environment for 100 hours. The stainless steel NSSER-4 exhibited very high corrosion resistance and little effect of metal temperature in the range of 500$^{o}$C to 630$^{o}$C. It was therefore, suitable for the application of superheater tubing. The steel alloy SA213 T11 exhibited acceptable corrosion resistance at the metal temperature of 540$^{o}$C, but its performance degraded dramatically when the metal temperature was above 540$^{o}$C. For the

superheater that is operated at metal temperature up to 540$^{o}$C, SA213 T11 is a more economical solution instead of stainless steel. The carbon steel SA178A had the highest corrosion rate among all of the metals which explained why it was mostly used as waterwall tube (lower metal temperature) with coating material, such as Inconel 625.

The corrosion rates measured in this laboratory test were quite close to the numbers reported from waste-to-energy facilities. Confirmation of the lab test results with actual corrosion rates observed out in the field gave greater confidence in the usefulness of the experimental apparatus and the testing procedure in forecasting long term effects of corrosion factors on superheater tube life.

The elemental analysis of NSSER-4 showed that the elemental concentrations in the corrosion products did not change significantly as a result of varying the metal temperature. The cross-sectional elemental analysis verified the statement that chloride (or chlorine) penetrated the oxide scale through cracks in the scale due to activity driven by chemical potential and temperature gradients. This resulted in deposition that led to accumulation in the metal/oxide scale. The elemental analysis of the other two metals, consisting mostly of iron, showed that more iron was oxidized under higher metal temperatures. The elemental analysis by EDS helped to explain the formation of corrosion products under different metal temperatures. However, to better explain the corrosion mechanisms additional analytical tools such as x-ray diffraction for identifying the chemical compounds should be used.

## 5.3. Effects of Hydrogen Chloride Gas Concentrations on Corrosion Rates of Commercial Tube Alloys under Simulated Environment of WTE Facilities

### 5.3.1. Test Background

Laboratory investigations on the corrosion behavior have been performed in chlorine-containing atmospheres with different temperatures on several metals and alloys [11, 30, 36, 37]. Most of these studies have shown that even small changes of the oxygen/chlorine ratio or temperature can influence the corrosion behavior. A recent in-plant study indicates that significantly increased corrosion rate was observed when extra chlorine in the form of PVC was added to the fuel mix [38]. In the earlier test of this study, an apparatus that can create a controlled thermal gradient between synthetic flue gas and metal surface was developed to examine the corrosion rates of different commercial steels. The experimentally corrosion rates that were in agreement with the annual wastages of boiler tubes in WTE facilities [39] have proved the ability of this apparatus to predict the life of a particular tube alloy. Therefore, this test used the same apparatus and tried to clarify the effects of HCl concentrations on corrosion rates of WTE boilers. Three commercial tubing SA178A, SA213 T11 and NSSER-4 were investigated under a well controlled thermal gradient where the gas temperature was at 700$^{o}$C and metal temperatures ranged from 480 to 580$^{o}$C. The duration of each test was 100 hours. The composition of the synthetic corrosive test gas consisted of 8% oxygen, 12% carbon dioxide, 0-1000 (0, 500 and 1000) ppm hydrogen chloride, 100 ppm sulfur

dioxide, 15% water vapor, with a balance of nitrogen for a total gas flow rate of 500 ml/min. The post-test analysis included observations of surface morphology and elemental composition analysis of corrosion products by means of scanning electron microscope (SEM) and energy dispersive spectroscopy (EDS). The corrosion rates were determined by measuring the mass loss of samples after the chemical cleaning.

### 5.3.2. Results and Discussion

When a metal reacts with a gas containing more than one oxidant, a number of different phases may form depending on both thermodynamic and kinetic considerations. Isothermal stability diagrams, usually constructed with the logarithmic values of the activities or partial pressures of the two nonmetallic components as the coordinate axes, are useful in interpreting the condensed phases that can form. One important assumption in the stability diagram is that all considered species are at unit activity. This assumption places important limitations on the use of the diagrams for alloy systems [8]. The synthetic gas composition inside the furnace during test was calculated by the HSC program [40]. Figure 5-14 shows the concentrations of the major corrosive gases within the testing temperature range. The concentrations of these major corrosive gases were used to point out the testing environment on the stability diagrams for the following analysis of corrosion products.

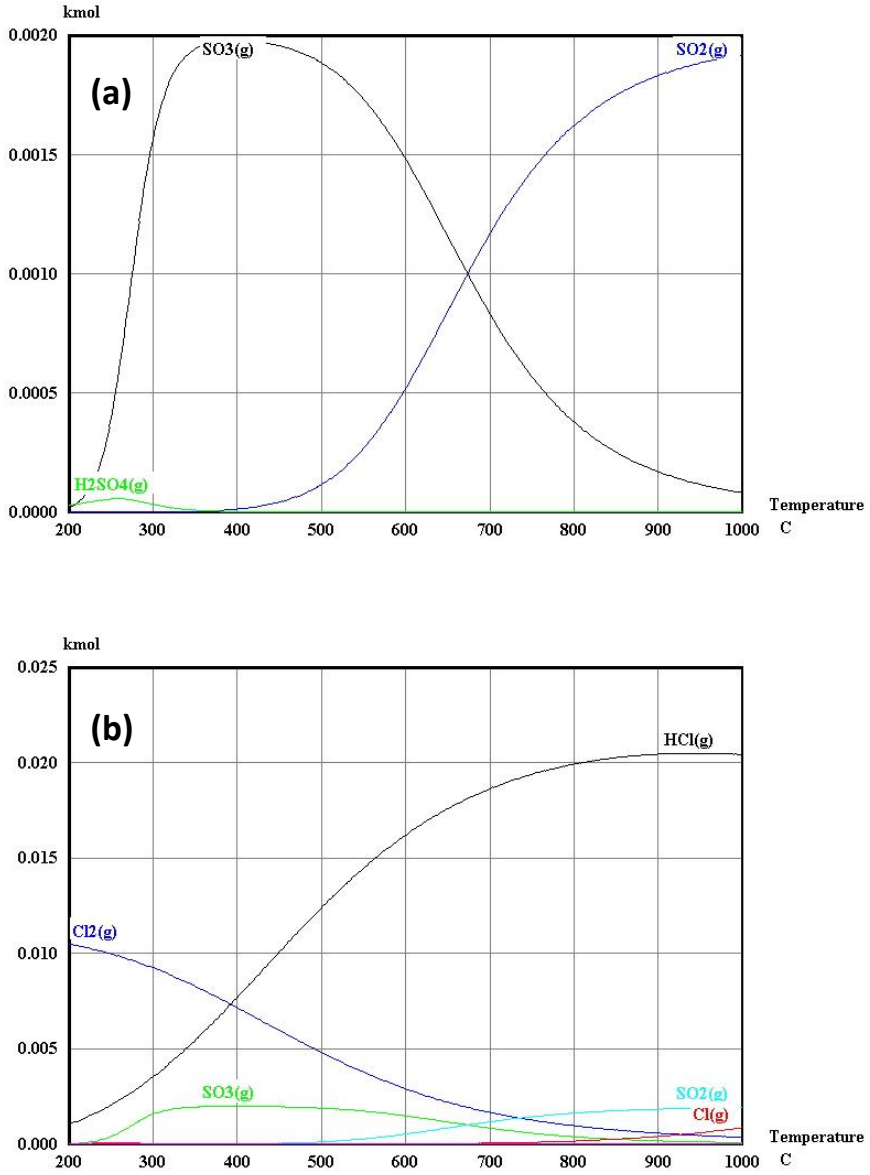


Figure 5-14 The concentrations of the major corrosive gases within the testing temperature range (a) without HCl gas and (b) with 1000ppm HCl gas

**(1) Alloy SA178A (low-carbon steel)**

Figure 5-15(a) is the image of the sample after the 100-hour test with metal temperature of 560$^{o}$C and non HCl-containing gases. A very thin scale was developed on

the metal surface. The SEM image (Figure 5-15(b)) shows that the scale was very porous and consisted of petaline shape oxide. The elemental analysis by EDS indicated the surface of the scale was rich in iron and oxygen with small amounts of sulfur (Figure 5-15(c)). The finding by SEM and EDS, together with thermodynamic calculation and stability diagram shown as Figure 5-16, in which the equilibrium condition of the test was marked, indicated that the oxides were mainly $Fe_2O_3$.

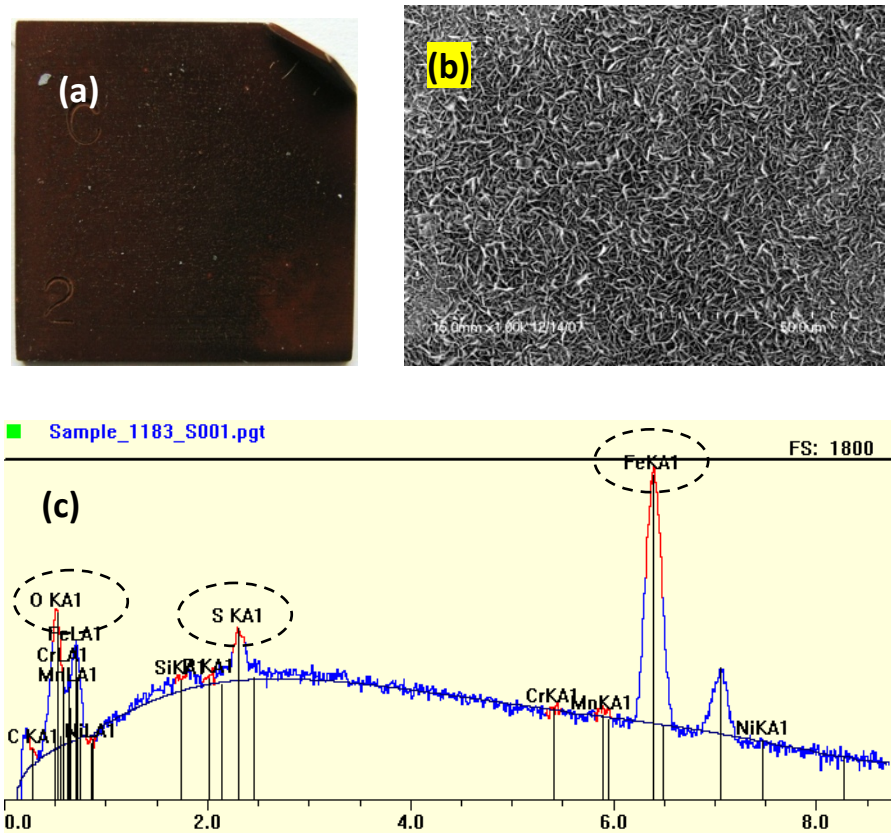


Figure 5-15 (a) Surface morphology of sample SA178A tested at 560°C metal temperature with non HCl-containing gases, (b) SEM images of the scale, and (c) Elemental analysis of the scale

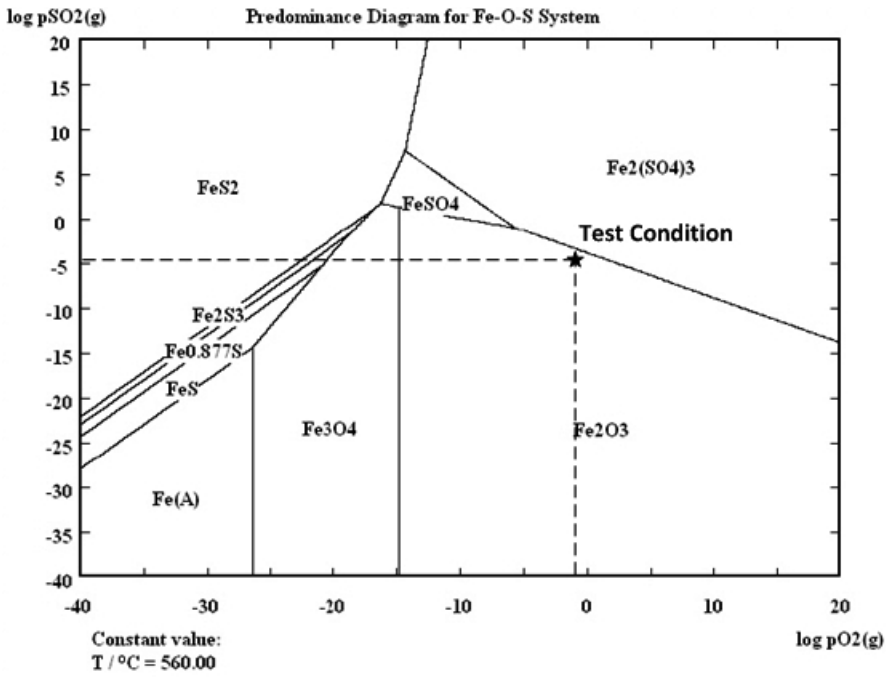


Figure 5-16 Stability diagram of the Fe-$SO_2$-$O_2$ system at 560°C (without HCl) [40]

Figure 5-17(a) is the SEM image of the scale/metal interface of the same sample after the corrosion scale was removed for examination. The scale/metal interface showed a porous grain structure. The stability diagrams (Figure 5-16) inferred only the buildup of $Fe_2O_3$ on the scale/metal interface under the test environment, but the EDS analysis (Figure 5-17(b)) identified high iron and sulfur concentrations with very low oxygen content. The situation occurred because the potential corrosion products, as suggested by the stability diagram shown as Figure 5-16, were according to the sulfur and oxygen concentrations near the surface of the scale. But in practical, the sulfur concentration near the scale/metal interface was expected to be higher since the scale formed was porous and allowed more sulfur to diffuse to the scale/metal interface.

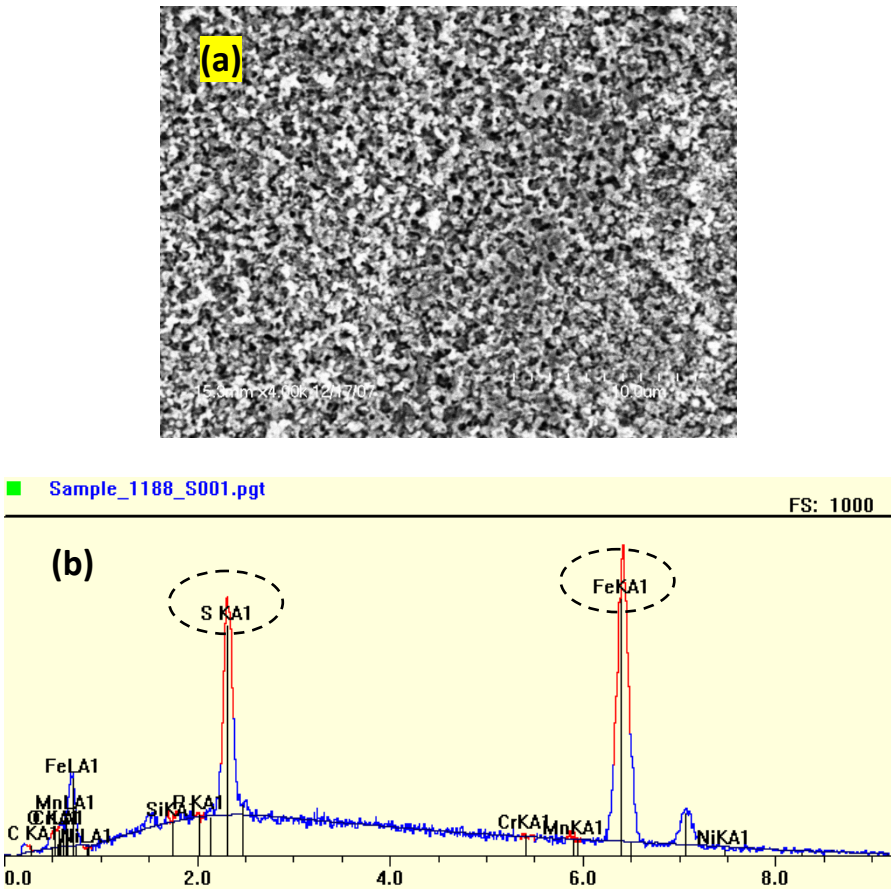


Figure 5-17 (a) SEM images of the scale/metal interface after removal of scale (without HCl), and (b) Elemental analysis of the scale/metal interface

Figure 5-18(a) is the image of the sample after the 100-hour test at metal temperature of 560$^{o}$C and in gas atmosphere containing 1000ppm HCl. Compared to the sample without HCl-containing gases treatment this sample was more corroded as seen from its appearance. The black-reddish scale was thicker and suffered from severe spallation when cooled down. The SEM image (Figure 5-18(b)) also shows porous, petaline shape oxide on the scale. The EDS results shown as Figure 5-18(c) which identified high iron and sulfur concentrations with very low oxygen content inferred the buildup of $Fe_2(SO_4)_3/FeS_2$ on the scale. Compared with the sample without HCl-

containing gases treatment (shown in Figure 5-15(c)), the scale of sample with the additional HCl gas treatment had much higher sulfur content and lower iron and oxygen content.

The stability diagrams for the system Fe-$O_2$-$Cl_2$ and Fe-$O_2$-$SO_2$ at 560$^{o}$C are shown as Figure 5-19(a) and (b) in which the equilibrium conditions of the test were marked. These diagrams showed that the scale consisted of $Fe_2(SO_4)_3$/$Fe_2O_3$ which was in agreement with the findings from EDS.

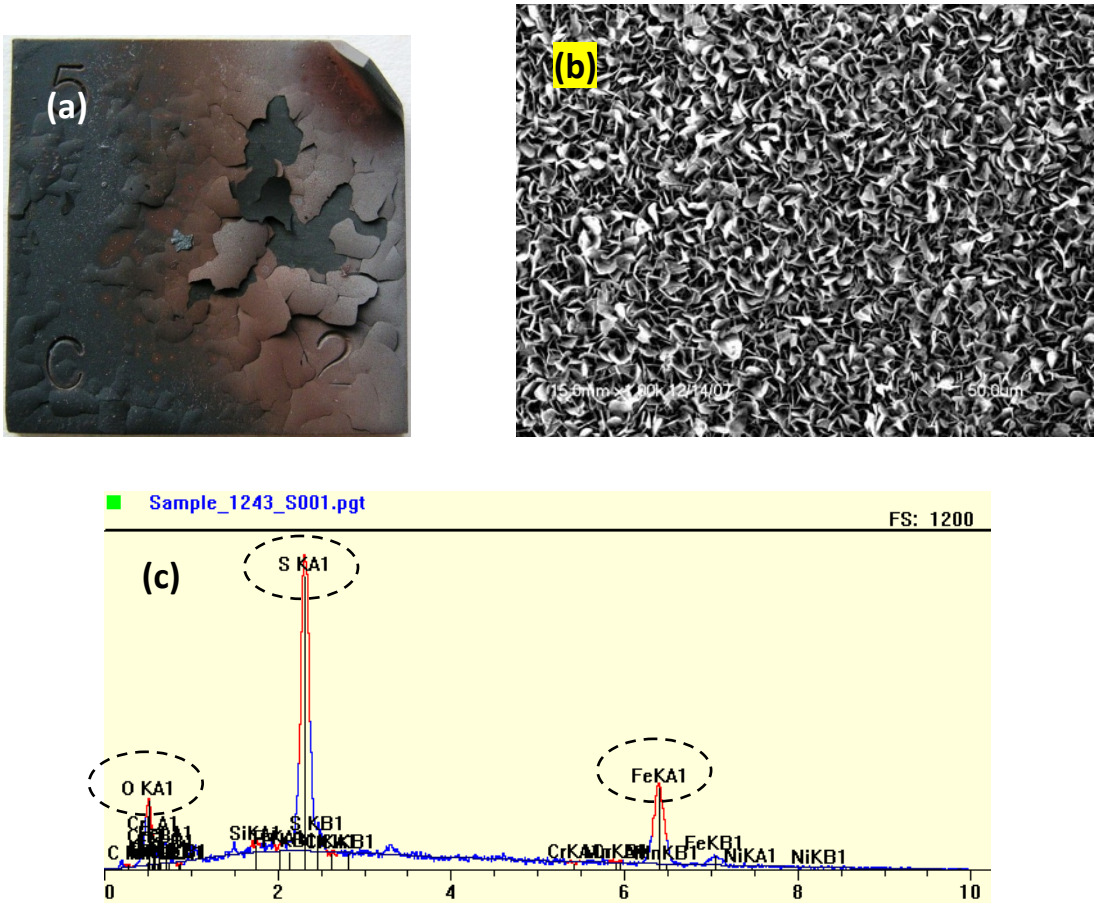


Figure 5-18 (a) Surface morphology of sample SA178A tested with 1000ppm HCl-containing gases, (b) SEM images of the scale, and (c) Elemental analysis of the scale

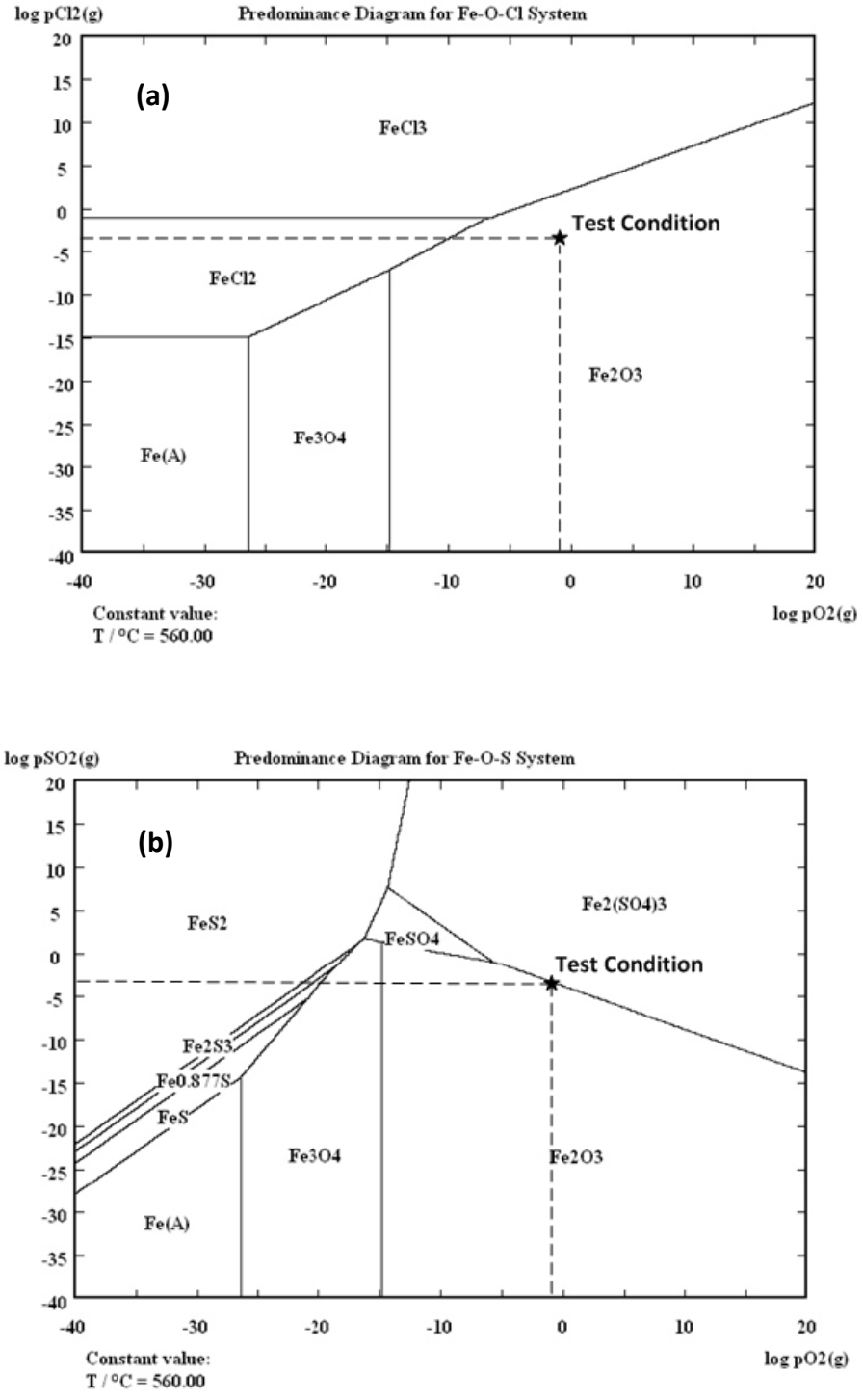


Figure 5-19 Stability diagrams of the system at 560°C (with 1000ppm HCl) (a) Fe-$O_2$-$Cl_2$ and (b) Fe-$O_2$-$SO_2$ [40]

After the removal of the scale, pellet-like oxides were found to cover the whole scale/metal interface (Figure 5-20(a)). Since the scale was more porous and its structure was less complete than the scale treated with non HCl-containing gases, the scale/metal interface suffered more suffer attack. More sulfur was found on the interface in the form of $FeS_2$/$Fe_2S_3$/FeS (Figure 5-20(b)). Besides, significantly less chlorine was found on most of the scale/metal interface due to the high vapor pressure of metal chlorides under this temperature.

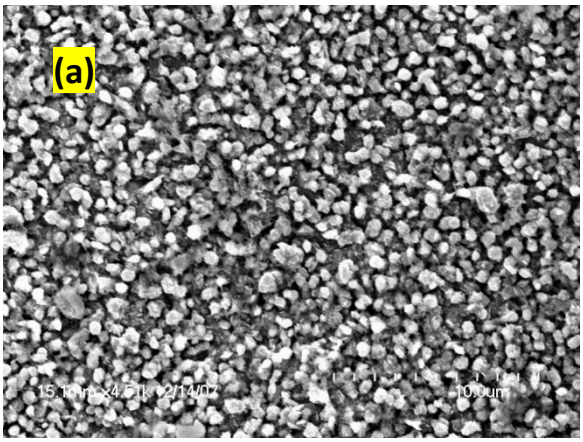


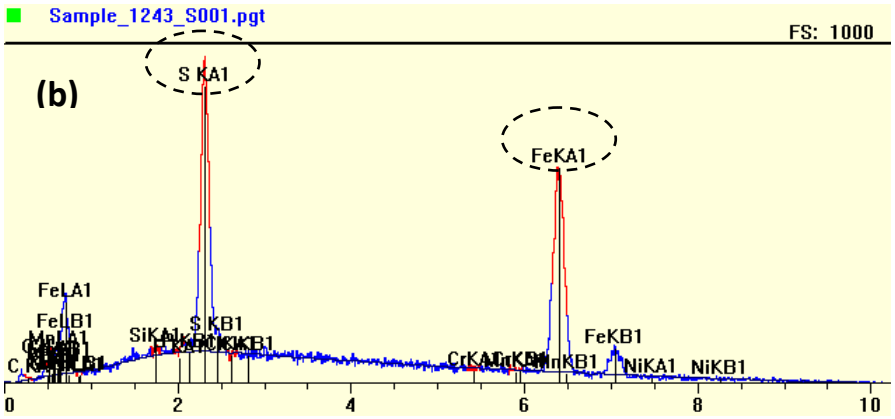


Figure 5-20 (a) SEM images of the scale/metal interface after removal of the scale (1000ppm HCl), and (b) Elemental analysis of the scale/metal interface

Figure 5-21 is the comparison of different elements on the surfaces of scales treated with and without HCl gas. On both tests, iron concentration increased when metal temperature increased, while oxygen and sulfur concentrations decreased. More iron was oxidized at higher metal temperature region. In addition, for each element, the concentration difference between the treating with and without HCl gas under the same metal temperature decreased from the lower to higher metal temperature. This situation indicated that higher metal temperature resulted in the breakdown of the scale in both cases. The metal temperature effect on the corrosion has surpassed the HCl effect.

Regarding the HCl effect on the elemental composition, more porous scales were created because of more severe corrosion attack due to the higher HCl concentration. Sulfur and chlorine were easier to diffuse through the scale and reacted with iron on the scale/metal interface. This was proved by the EDS results that higher sulfur concentration was found both on the scale and scale/metal interface of the sample treated with HCl gas. In addition, some research have found that the presence of HCl will promote the formation of sulfate salts and increase the corrosion [10, 28]. In WTE facilities, the ash deposits usually contain compounds like iron oxides that can catalyze the $SO_2$ in the flue gas to form $SO_3$. Therefore, the partial pressure for $SO_3$ may be high enough to produce pyrosulphate at temperatures between 320 and 480$^0$C according:

$$Na_2SO_4 + SO_3 = Na_2S_2O_7 \quad (5\text{-}9)$$

$$Na_2S_2O_7 + 3Fe = Fe_2O_3 + FeS + Na_2SO_4 \quad (5\text{-}10)$$

At about $500^0$C, sulphates and pyrosulphates can become unstable and react with the protective oxide. At temperature of $550^0$C and higher, the tri-sulphates can attack the metal according:

$$Na_2S_2O_7 + Fe_2O_3 = 2Na_3Fe(SO_4)_3 \quad (5\text{-}11)$$

$$19Fe + 2Na_3Fe(SO_4)_3 = 6Fe_3O_4 + 3FeS + 3Na_2S \quad (5\text{-}12)$$

subsequently:

$$Na_2S + 2O_2 = Na_2SO_4 \quad (5\text{-}13)$$

$$3FeS + 5O_2 = Fe_3O_4 + 3SO_2 \quad (5\text{-}14)$$

$$2SO_2 + O_2 = 2SO_3 \quad (5\text{-}15)$$

The $SO_3$ liberated is available again to react with $Na_2SO_4$ resulting in cyclic corrosion reactions, which are enhanced in the presence of chlorides:

$$2NaCl + SO_2 + O_2 = Na_2SO_4 + Cl_2 \quad (5\text{-}16)$$

$$2KCl + SO_2 + O_2 = K_2SO_4 + Cl_2 \quad (5\text{-}17)$$

$$4FeCl_2 + SO_2 + O_2 = Fe_3O_4 + 4Cl_2 + FeS \quad (5\text{-}18)$$

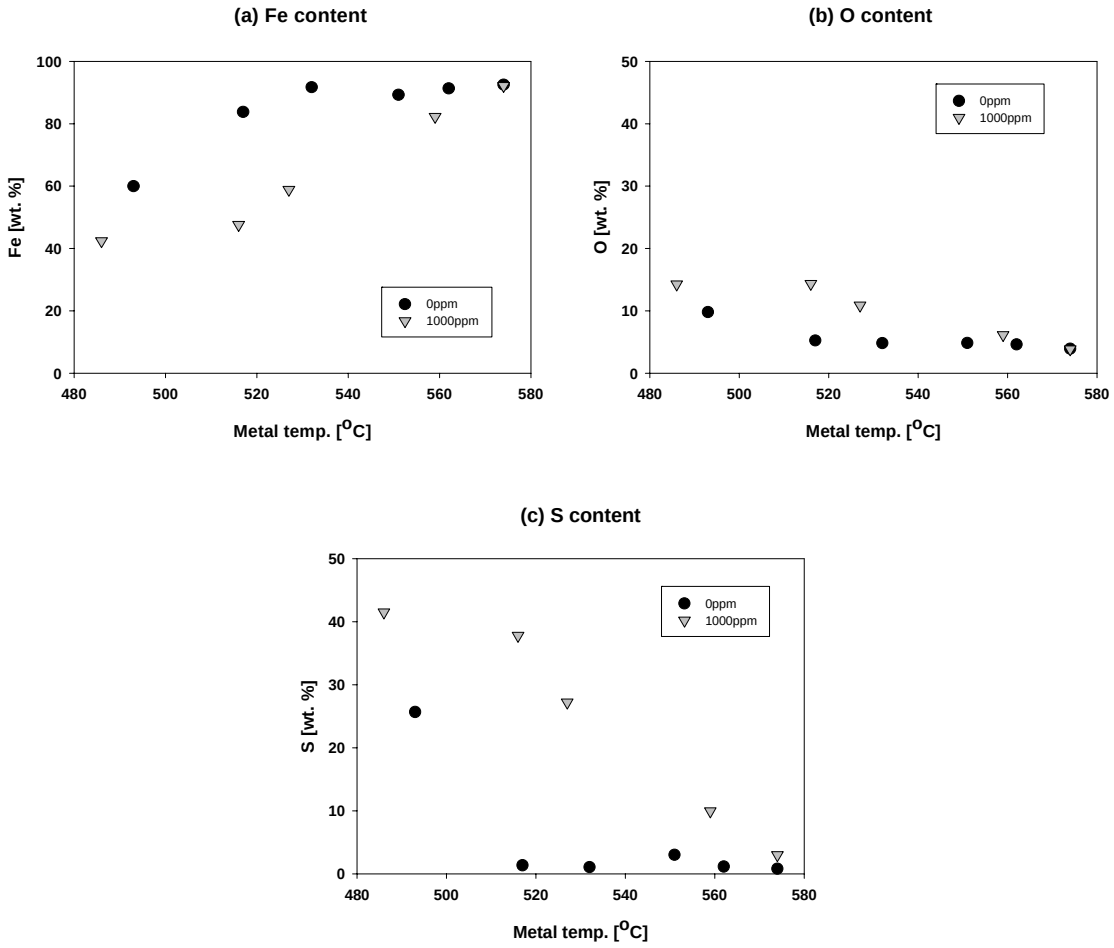


Figure 5-21 Elemental analysis of the scales' surfaces; (a) Fe, (b) O, and (c) S

Figure 5-22 compares the mass loss corrosion rates at different HCl concentrations. The corrosion rates varied from 0.25 to 2.79 mm/y (10-110 mils/y) within the range of testing metal temperatures. Higher HCl concentration caused more corrosion, but the relation of HCl content with corrosion rate was not linear. The corrosion rate increased more when HCl increased from 0 to 500 ppm than increased from 500 to 1000 ppm. In all three tests, the increase of metal temperature increased the corrosion rates. In the tests with HCl gases, corrosion rates increased dramatically when metal temperatures were higher than 560$^{o}$C.

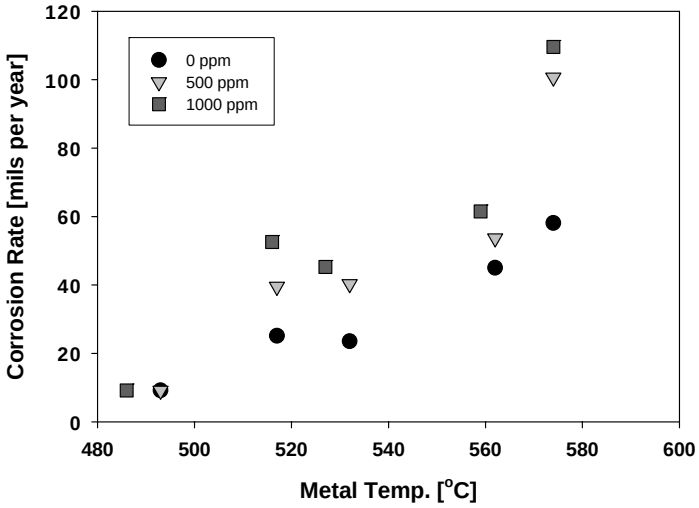


Figure 5-22 Comparison of mass loss corrosion rates

**(2) Alloy SA213 T11 (low-carbon, intermediate-chrome steel)**

Figure 5-23(a) is the image of the coupon of Alloy SA213 T11 after the 100-hour test at metal temperature of 570°C and non HCl-containing gases. The whole metal surface was covered by black-reddish scale which was found very porous and consisted of needle-like oxide whiskers under SEM (Figure 5-23(b)). These oxide whiskers were rich in iron and oxygen with a small amount of sulfur and were expected to be $Fe_2O_3$ /$Fe_2(SO_4)_3$ (Figure 5-23(c)).

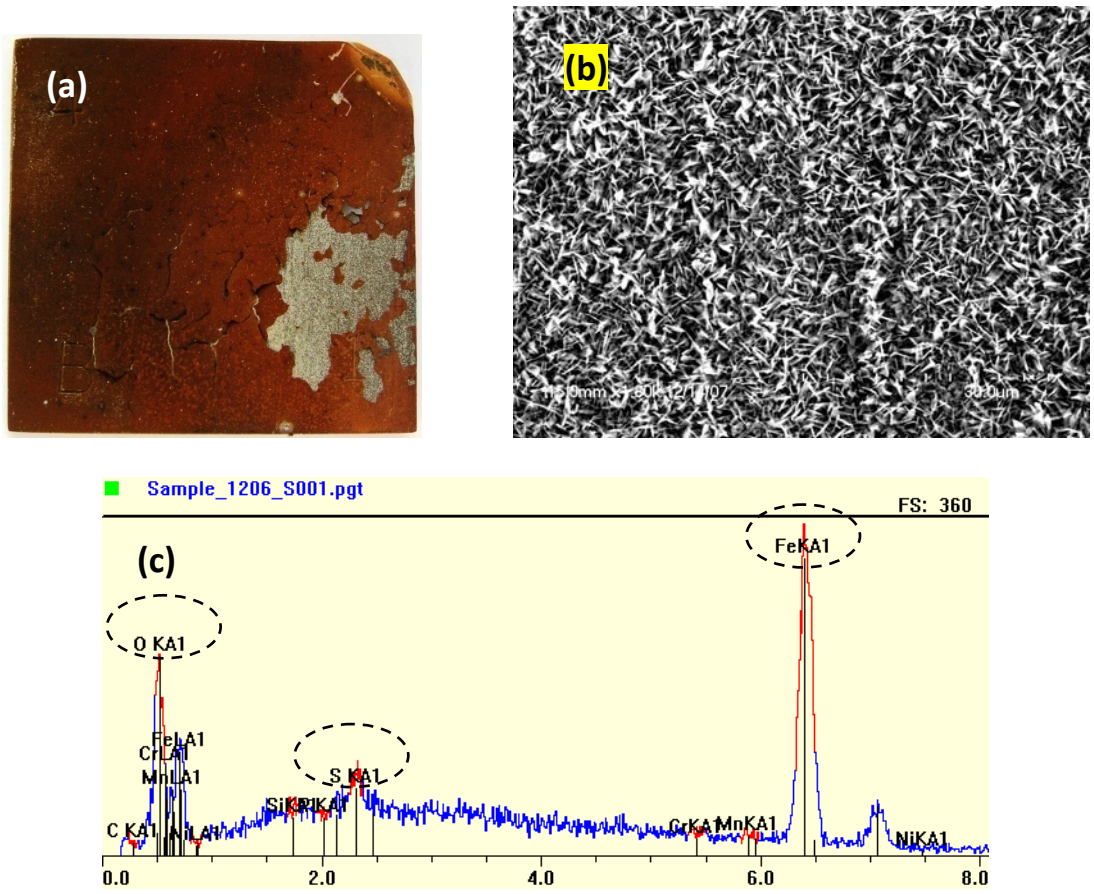


Figure 5-23 (a) Surface morphology of sample SA213 T11 tested at metal temperature of 570°C with non HCl-containing gases, (b) SEM images of the scale, and (c) Elemental analysis of the scale

Figure 5-24 (a) is the SEM image of the same sample after removal of the scale from the surface. The scale/metal interface was porous and contained some cracks. EDS results showed higher iron and chromium contents in the interface that were different from the scale, but the sulfur content was at about the same level (Figure 5-24 (b)). The interface was expected to consist of $Cr_2(SO_4)_3/Cr_2O_3$ and $Fe_2O_3/Fe_2(SO_4)_3$. The stability diagrams (Figure 5-25) showed that the scale might be consisted of only $Cr_2O_3$ and $Fe_2O_3$. However, as mentioned previously, the gas composition near the scale/metal interface

was unknown, and sulfur concentration at this area might be higher than that near the scale surface. If compared to the results of SA178A, the addition of chromium to SA213 T11 protected the metal from being further corroded by sulfur.

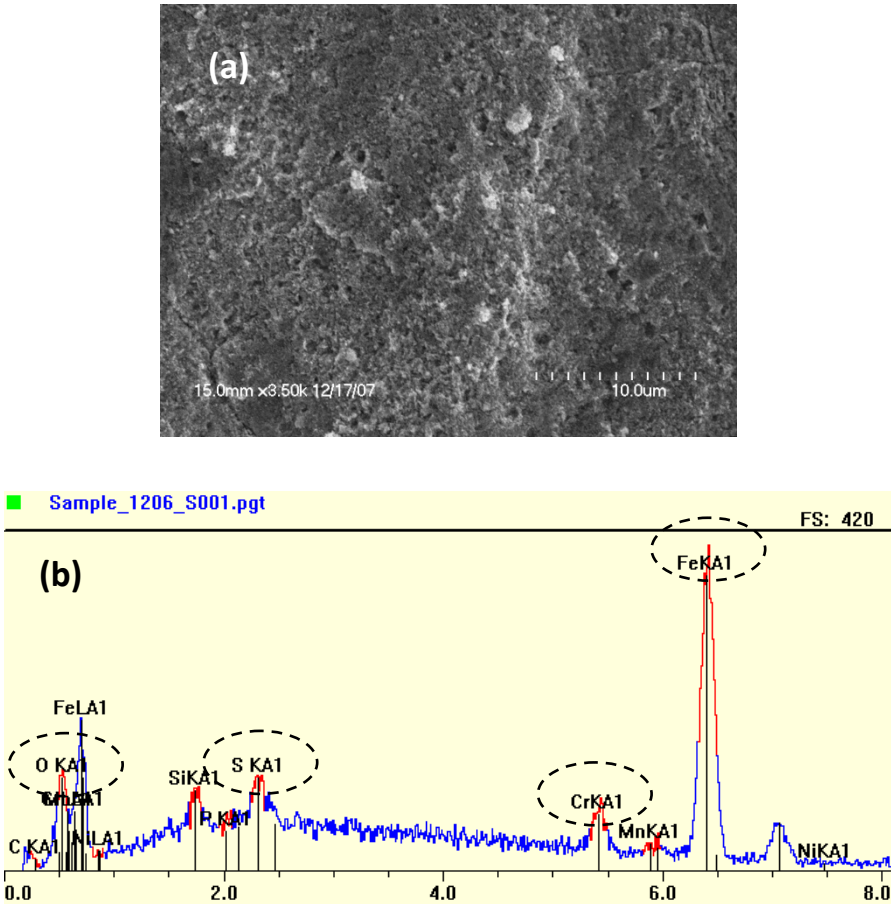


Figure 5-24 (a) SEM images of the scale/metal interface after removal of the scale (without HCl), and (b) Elemental analysis of the scale/metal interface

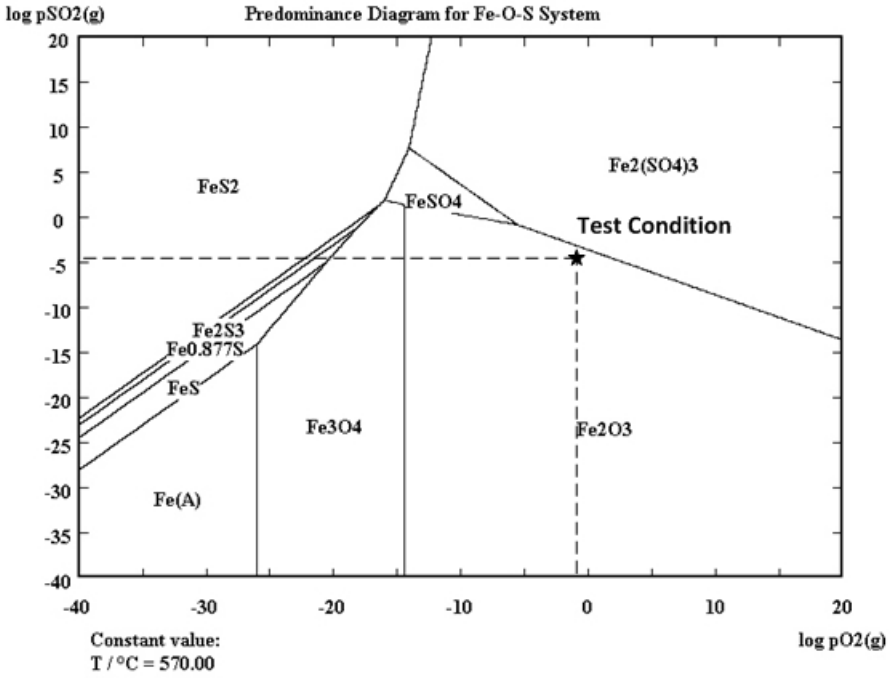


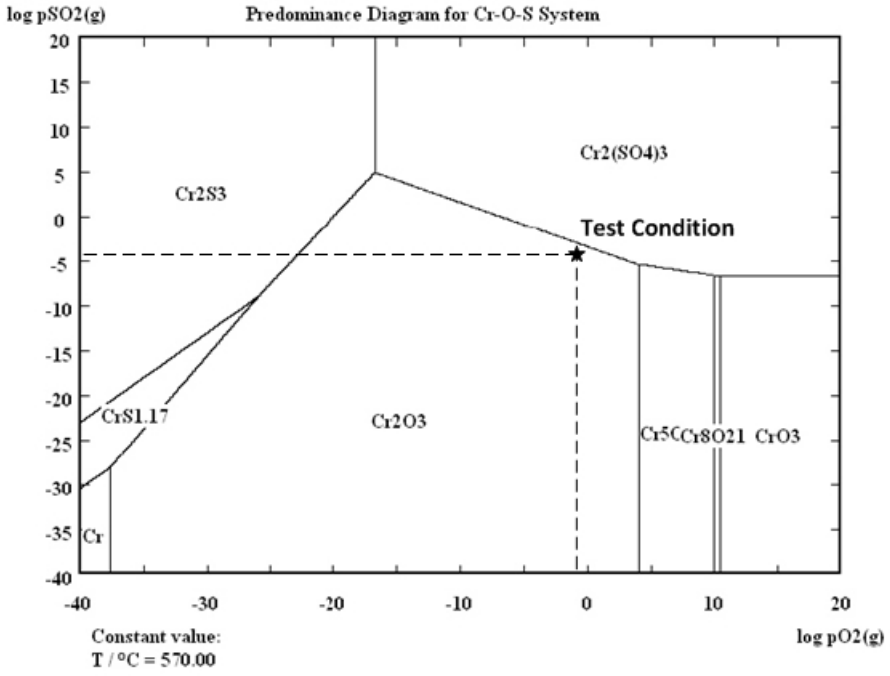


Figure 5-25 Stability diagrams of the system at 570°C (without HCl) (a) Fe-$O_2$-$Cl_2$ and (b) Fe-$O_2$-$SO_2$ [40]

Figure 5-26 (a) is the image of the sample after the 100-hour test at metal temperature of 565°C and in gas atmosphere containing 1000 ppm HCl. A grey-reddish thick scale has grown on the sample's surface and suffered from severe spallation when cooled down. Unlike the scale observed in the absence of HCl, this scale showed some congregate cubic crystals (Figure 5-26 (b)). These crystals were rich in iron, oxygen and sulfur (Figure 5-26 (c)). A small amount of chromium was identified. These crystals were expected to be $Fe_2O_3/Fe_2(SO_4)_3$ and $Cr_2(SO_4)_3/Cr_2O_3$. The stability diagrams shown as Figure 5-27 again indicated slightly different results with EDS on the appearance of sulfate.

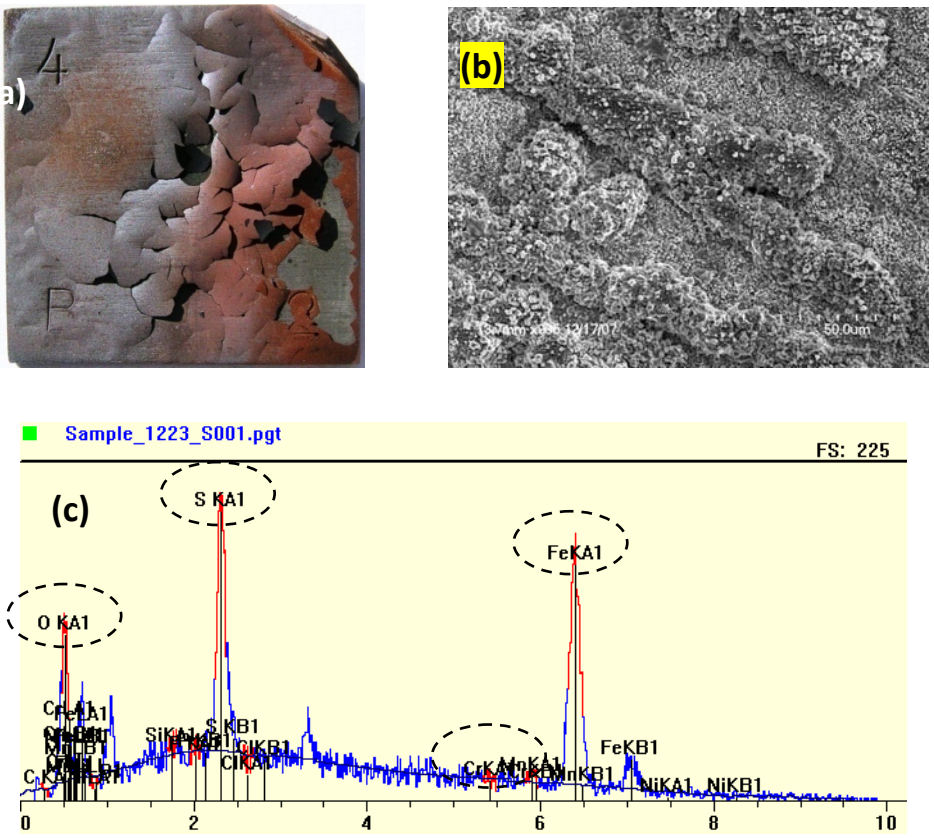


Figure 5-26 (a) Surface morphology of sample SA213 T11 tested at metal temperature of 565°C with 1000ppm HCl-containing gases, (b) SEM images of the scale, and (c) Elemental analysis of the scale

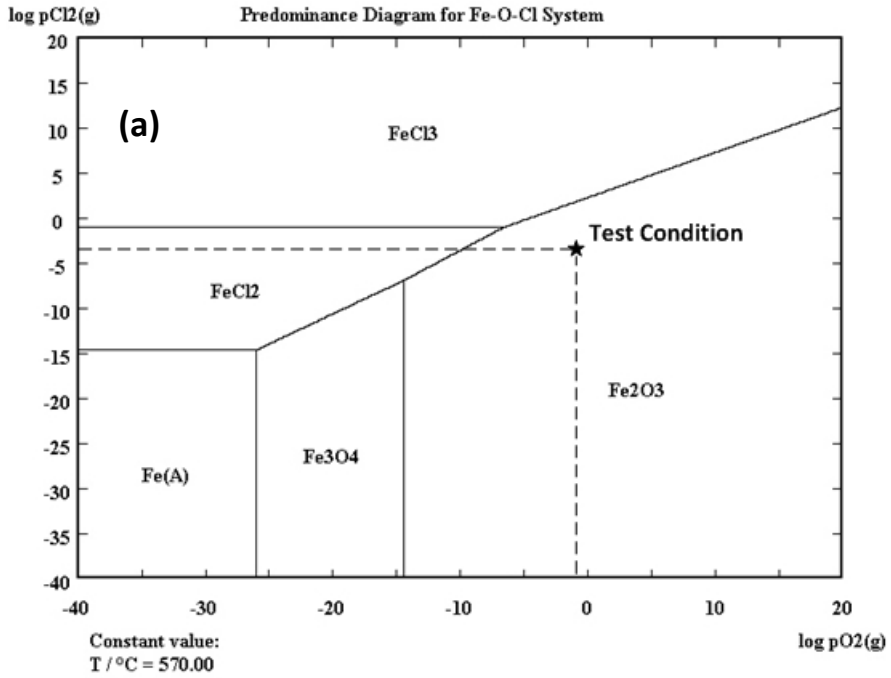
log pCl2(g)
Predominance Diagram for Fe-O-Cl System
(a)
FeCl3
Test Condition
FeCl2
Fe2O3
Fe3O4
Fe(A)
20
15
10
5
0
-5
-10
-15
-20
-25
-30
-35
-40
-40
-30
-20
-10
0
10
20
Constant value:
T / °C = 570.00
log pO2(g)

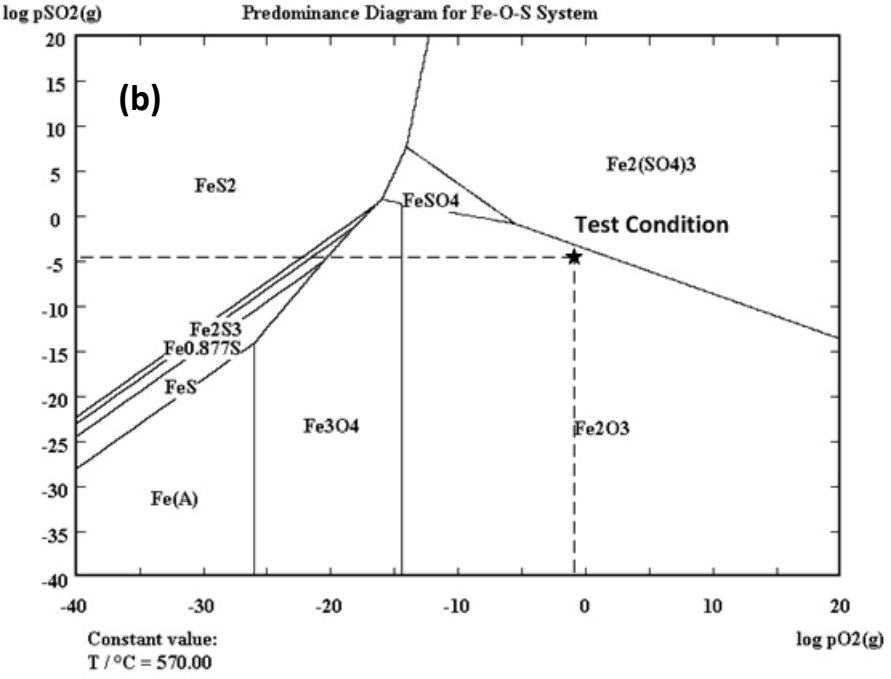
log pSO2(g)
Predominance Diagram for Fe-O-S System
(b)
FeS2
Fe2(SO4)3
FeSO4
Test Condition
Fe2S3
Fe0.877S
FeS
Fe3O4
Fe2O3
Fe(A)
20
15
10
5
0
-5
-10
-15
-20
-25
-30
-35
-40
-40
-30
-20
-10
0
10
20
Constant value:
T / °C = 570.00
log pO2(g)

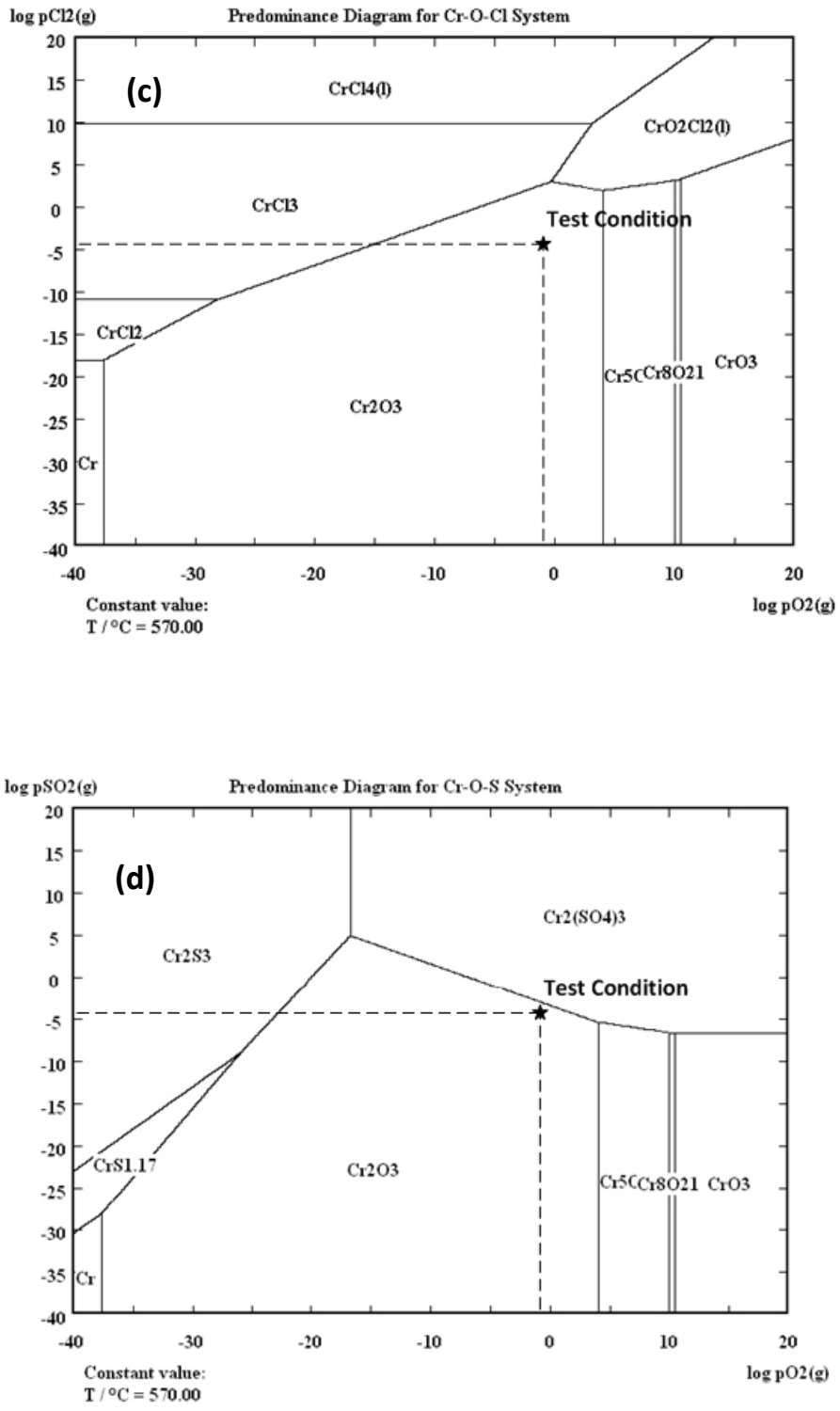


Figure 5-27 Stability diagrams of the system at 570°C (with 1000ppm HCl) (a) Fe-$O_2$-$Cl_2$, (b) Fe-$O_2$-$SO_2$, (c) Cr-$O_2$-$Cl_2$, and (d) Cr-$O_2$-$SO_2$ [40]

Figure 5-28(a) is the SEM image of the same sample after removing the scale from the surface. The scale/metal interface was porous and covered unevenly by congregate oxides. The element composition of the interface was rich in iron, chromium and sulfur, but the sulfur content was slightly lower than that in the scale (Figure 5-28 (b)). The lower sulfur concentration on the interface than on the scale showed the presence of $Cr_2O_3$ could help reduce the sulfur attack to the base metal.

However, when a sample was treated with the additional HCl gas, the sulfur concentration on the scale/metal interface increased substantially. This situation showed that the protection of $Cr_2O_3$ was reduced because of the chlorine attack, and therefore the corrosive gases were easier to reach the scale/metal interface and caused more corrosion.

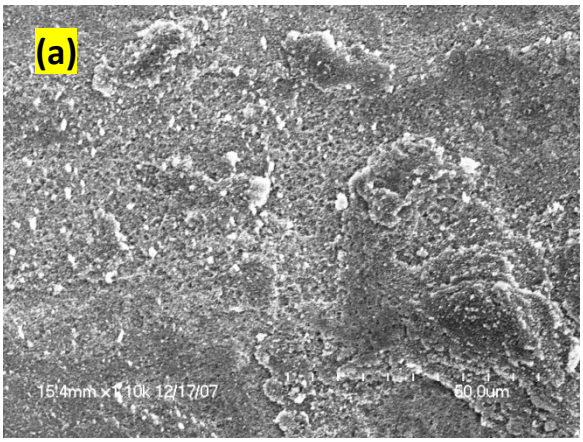

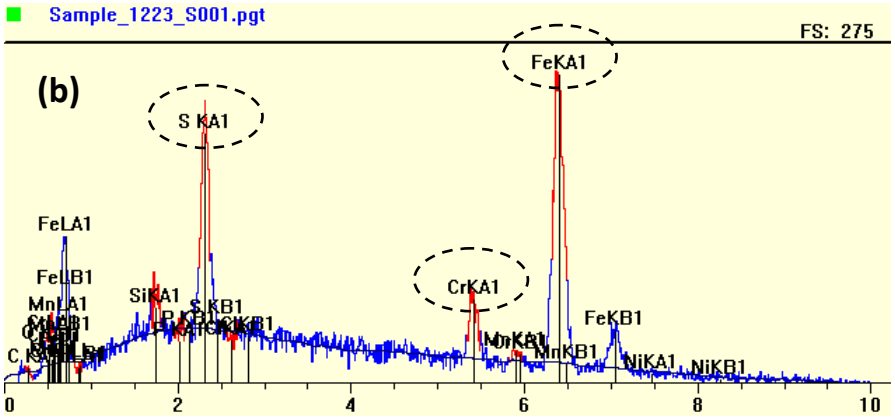


Figure 5-28 (a) SEM images of the scale/metal interface after removal of the scale (1000ppm HCl), and (b) Elemental analysis of the scale/metal interface

Figure 5-29 is a comparison of elemental composition on the surfaces of scales treated with and without HCl gas. The trends of iron, oxygen, and sulfur were similar to those observed on Alloy SA178A except the concentration differences were less. The addition of HCl gas promoted the formation of sulfate as described above. Metal temperature showed less effect on the corrosion in this case. The formation of $Cr_2O_3$ at the initial corrosion stages offered protection of the metal against subsequent sulfur and chlorine attacks.

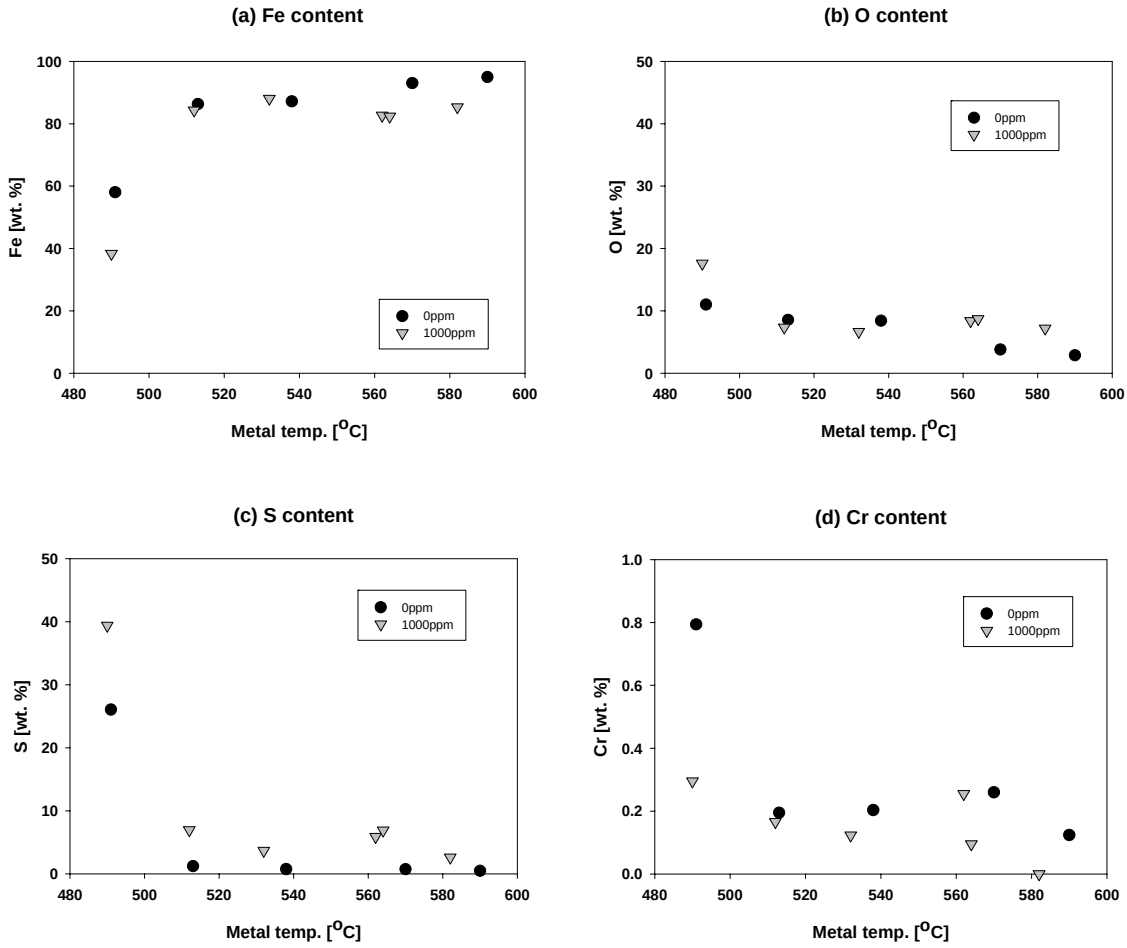


Figure 5-29 Elemental analysis of the scales' surfaces; (a) Fe, (b) O, (c) S and (d) Cr

Figure 5-30 shows the comparison of mass loss corrosion rates at different HCl concentrations in the furnace gas. The corrosion rates varied from 0.38 to 1.93 mm/y (15-76 mils/y) within the range of testing metal temperatures. HCl showed its effect on increasing the corrosion rate, but similarly to Alloy 178A, the relation of corrosion rate and HCl concentration was not linear. However, the HCl effect on corrosion was more noticeable when the metal temperature was higher than 560$^{o}$C.

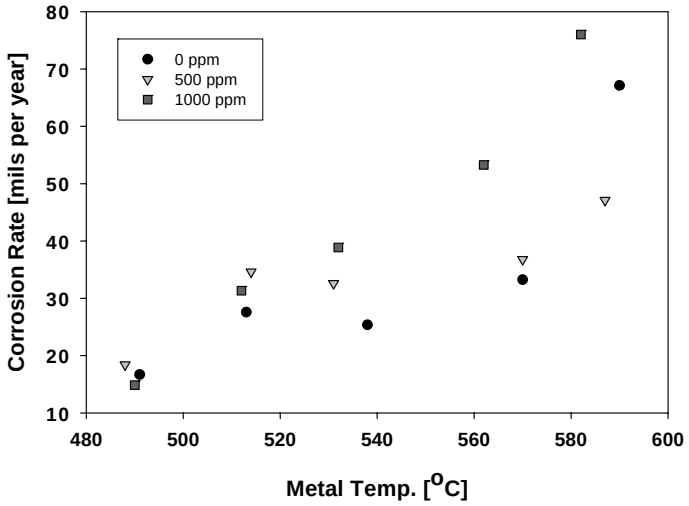


Figure 5-30 Comparison of mass loss corrosion rates

**(3) Alloy NSSER-4 (stainless steel)**

Figure 5-31(a) shows that the sample retained almost its original surface after the 100-hour test at metal temperature of 575°C and non HCl-containing gases. The SEM image shows that only a few spots of oxide were deposited on the surface. Except the sample's original elemental composition, oxygen and sulfur were indentified (Figure 5-31(b) and (c)). The stability diagrams (Figure 5-32) showed that the deposits consisted of $Fe_2O_3$, $Cr_2O_3$, and $NiSO_4$.

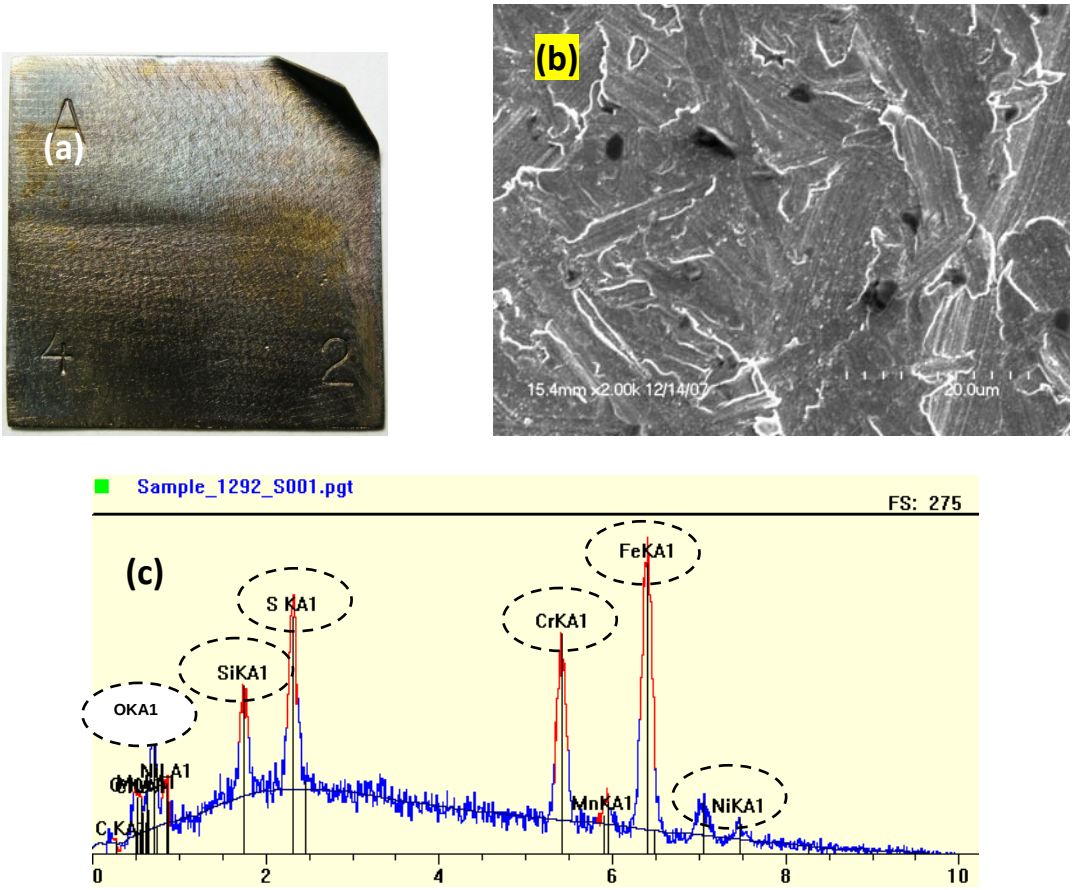


Figure 5-31 (a) Surface morphology of sample NSSER-4 tested at metal temperature of 575$^{o}$C with non HCl-containing gases, (b) SEM images of the scale, and (c) Elemental analysis of the scale

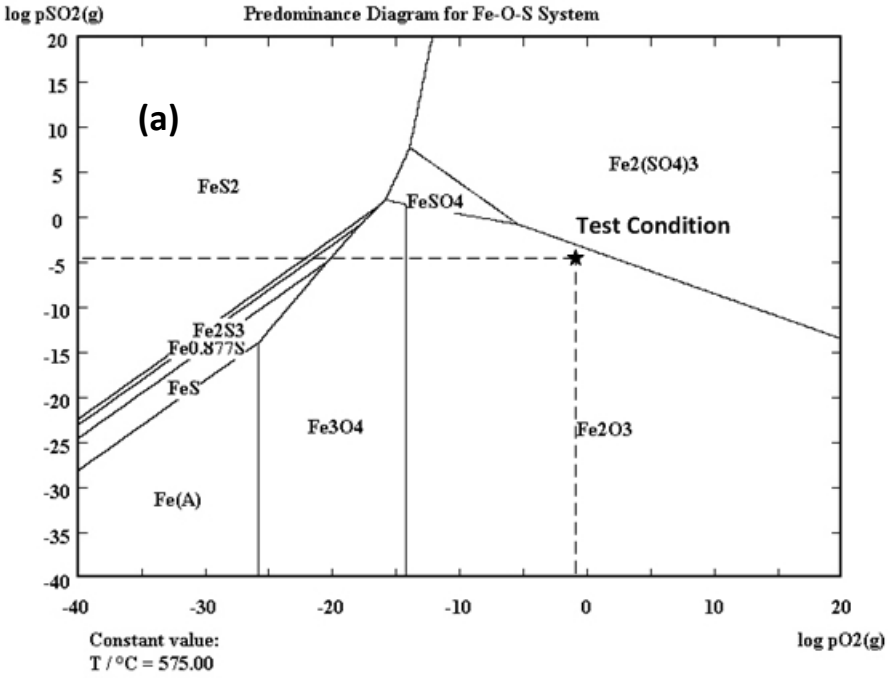
log pSO2(g)
Predominance Diagram for Fe-O-S System
(a)
FeS2
Fe2(SO4)3
FeSO4
Test Condition
Fe2S3
Fe0.877S
FeS
Fe3O4
Fe2O3
Fe(A)
20
15
10
5
0
-5
-10
-15
-20
-25
-30
-35
-40
-40
-30
-20
-10
0
10
20
Constant value:
T / °C = 575.00
log pO2(g)

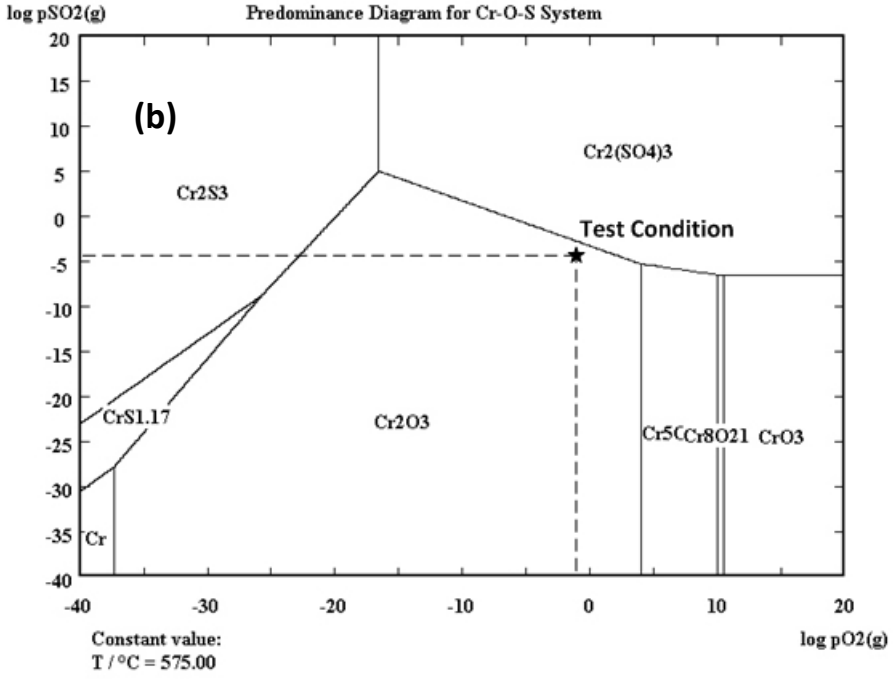
log pSO2(g)
Predominance Diagram for Cr-O-S System
(b)
Cr2S3
Cr2(SO4)3
Test Condition
CrS1.17
Cr2O3
Cr5C
Cr8O21
CrO3
Cr
20
15
10
5
0
-5
-10
-15
-20
-25
-30
-35
-40
-40
-30
-20
-10
0
10
20
Constant value:
T / °C = 575.00
log pO2(g)

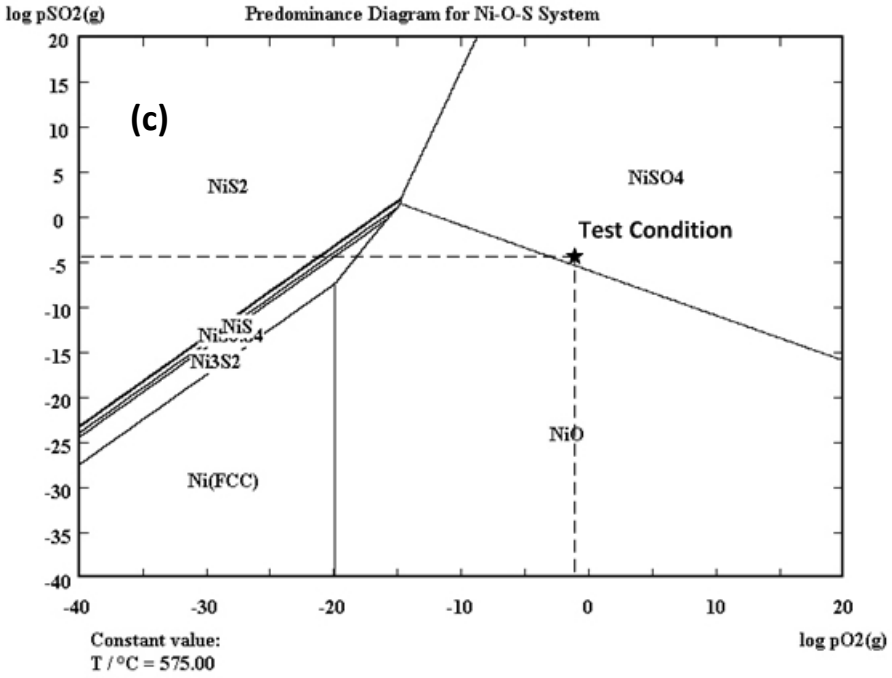


Figure 5-32 Stability diagrams of the system at 575$^{o}$C (without HCl) (a) Fe-$O_2$- $SO_2$, (b) Cr-$O_2$-$SO_2$, and (c) Ni-$O_2$-$SO_2$

The appearance of the sample tested in gas atmosphere containing 1000 ppm HCl did not show much difference with that of the sample reacted in the absence of HCl (Figure 5-33 (a)), but the SEM image showed that many granular crystals that were rich in sulfur were deposited over the all surface (Figure 5-33(b) and (c)). The thermodynamic calculations and stability diagrams (Figure 5-34) indicated that the compounds were mainly $Fe_2O_3$, $NiSO_4$, NiO and $Cr_2O_3$.

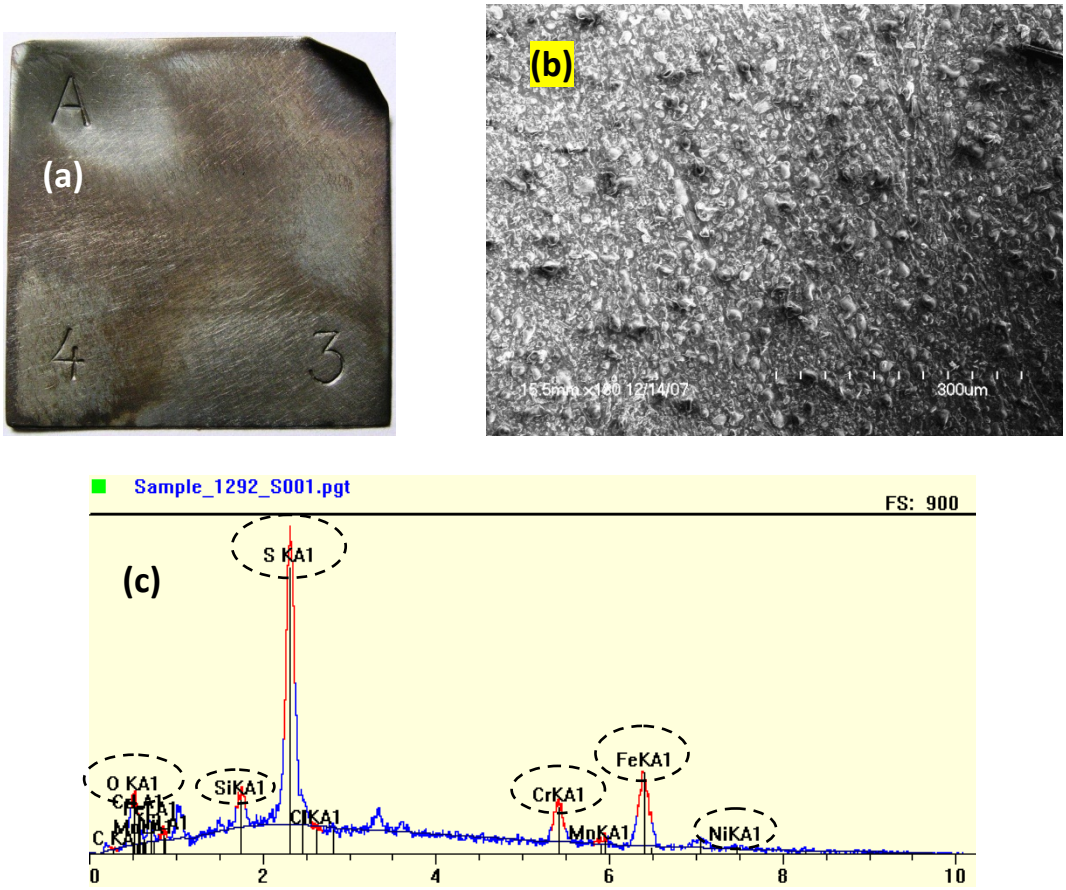


Figure 5-33 (a) Surface morphology of sample NSSER-4 tested with 1000ppm HCl-containing gases, (b) SEM images of the scale, and (c) Elemental analysis of the scale

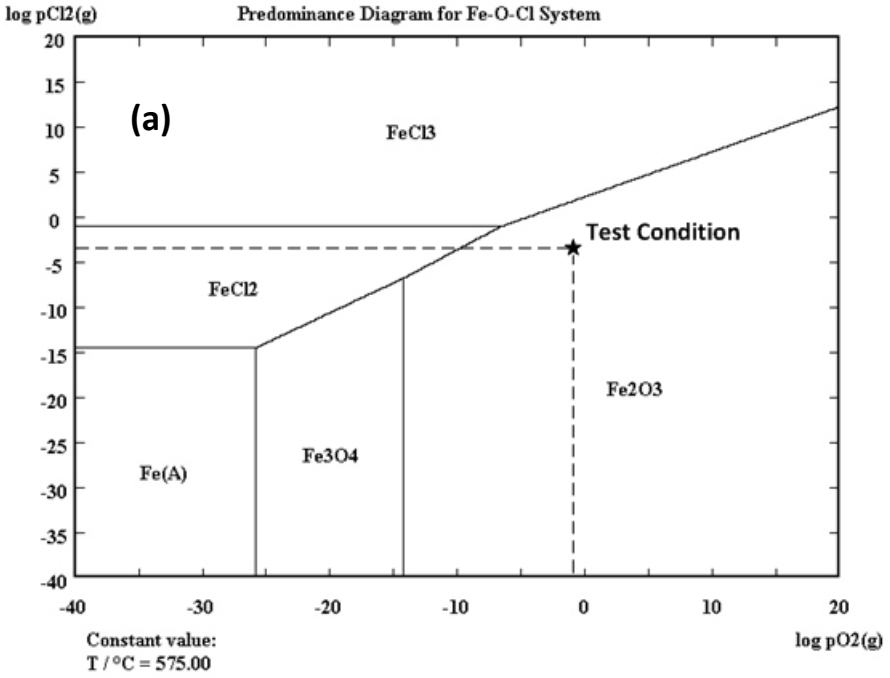
log pCl2(g)
Predominance Diagram for Fe-O-Cl System
(a)
FeCl3
Test Condition
FeCl2
Fe2O3
Fe3O4
Fe(A)
Constant value:
T / °C = 575.00
log pO2(g)

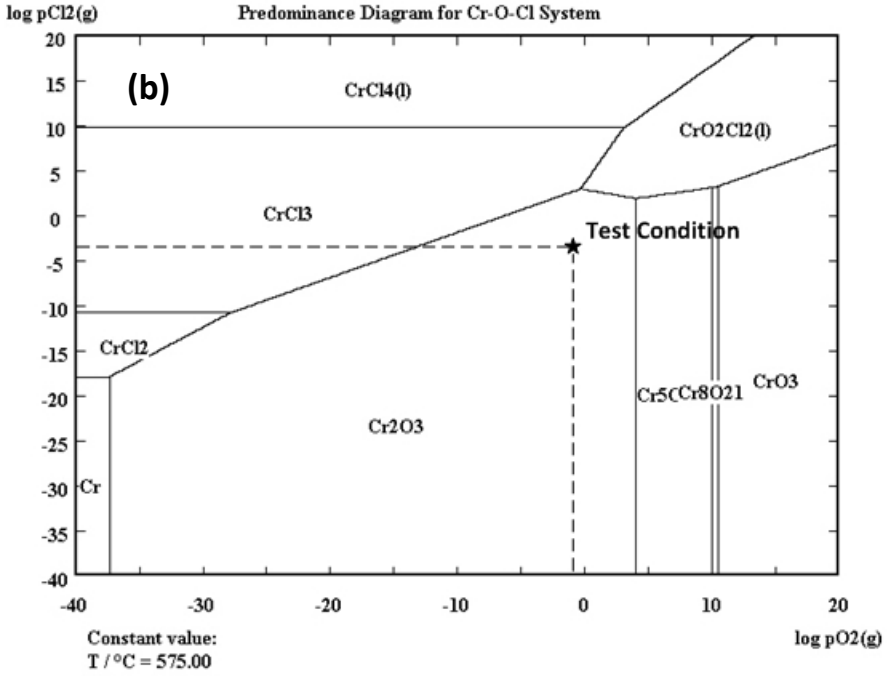
log pCl2(g)
Predominance Diagram for Cr-O-Cl System
(b)
CrCl4(l)
CrO2Cl2(l)
CrCl3
Test Condition
CrCl2
Cr5Cr8O21
CrO3
Cr2O3
Cr
Constant value:
T / °C = 575.00
log pO2(g)

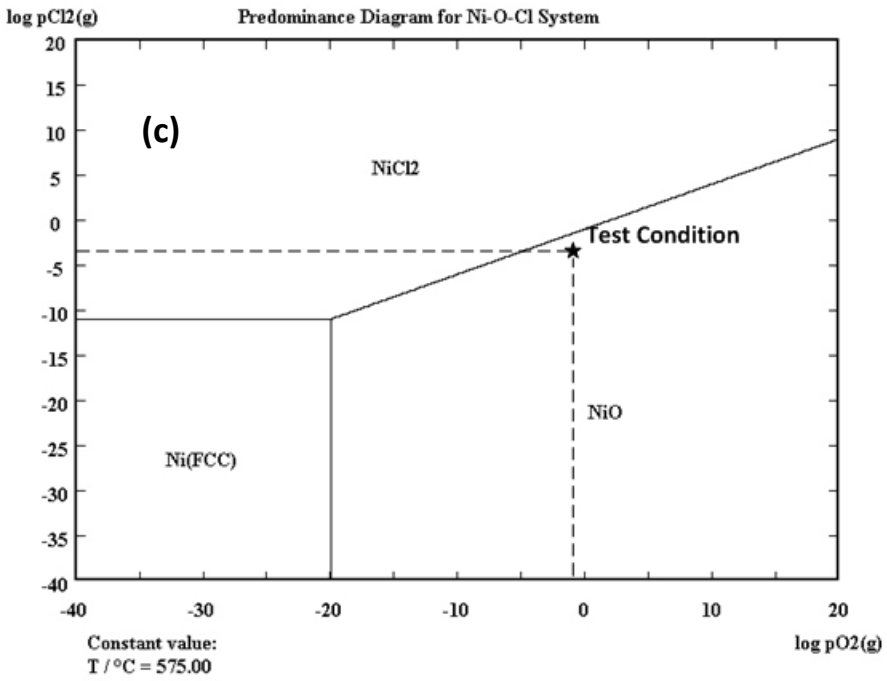


Figure 5-34 Stability diagrams of the system at 575°C (with 1000ppm HCl) (a) Fe-$O_2$-$Cl_2$, (b) Cr-$O_2$-$Cl_2$, and (c) Ni-$O_2$-$Cl_2$

The X-ray diffraction was used to analyze the corrosion product formed on the surface of NSSER-4. The result, shown as Figure 5-35, indicated the presence of nickel sufate, chromium oxide, and nickel oxide on the sample surface. This result was in agreement with the findings from the SEM analysis and the stability diagrams.

Figure 5-35 X-ray diffraction analysis of corrosion product formed on the surface of stainless steel NSSER-4

Figure 5-36 is the comparison of different elements on the surfaces of scales on samples treated with and without HCl gas. The trends of iron, oxygen, sulfur and chromium were similar to that occurred on Alloy SA213 T11. However, unlike previous two alloys, the elemental composition of NSSER-4 did not vary with the metal temperature. This has shown that NSSER-4's ability to maintain its corrosion resistance with the testing temperature profile. Although the presence of HCl gas promoted the formation of sulfate, the formation of NiO and $Cr_2O_3$ during the corrosion process protected the metal against subsequent sulfur and chlorine attacks.

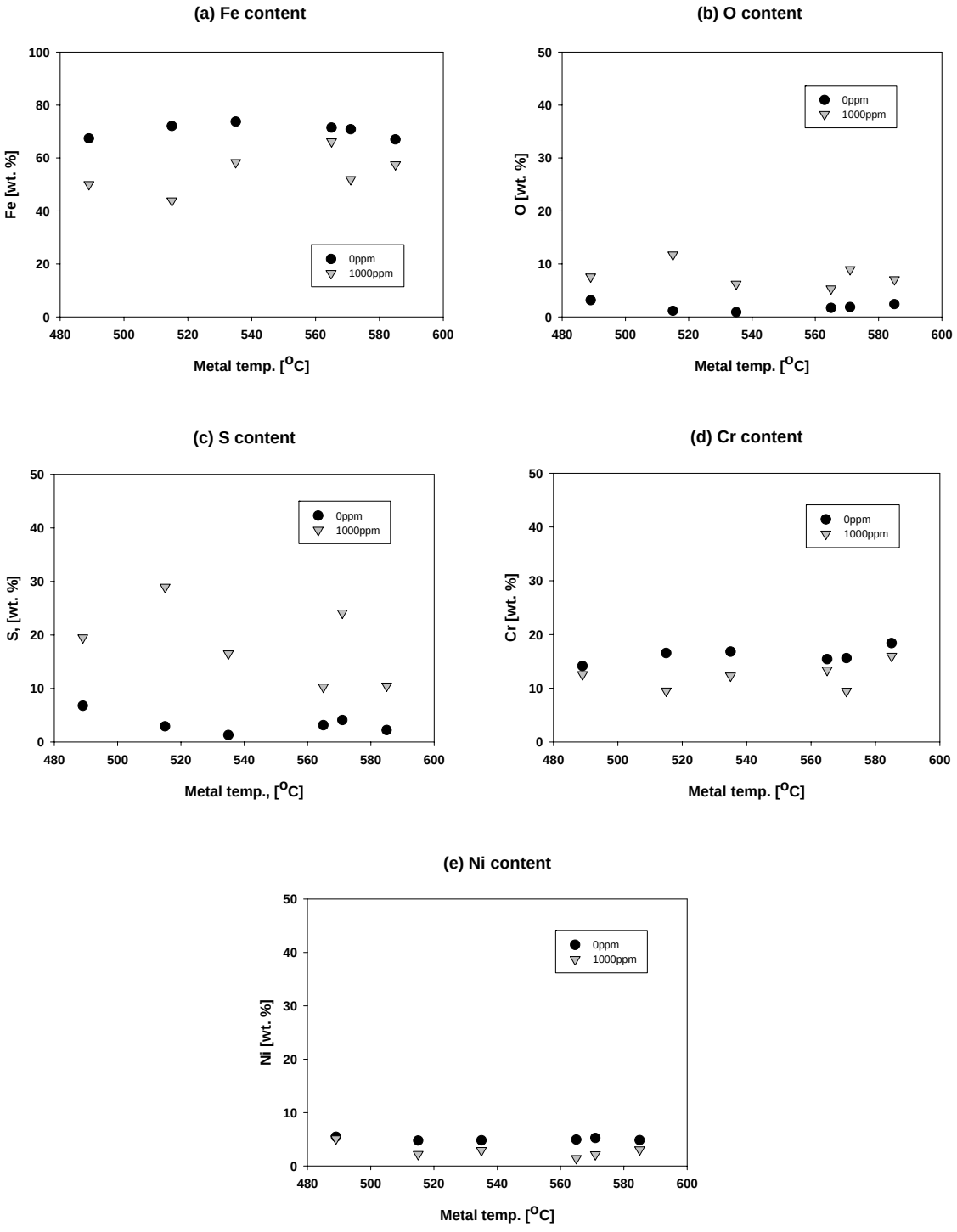


Figure 5-36 Elemental analysis of the scales' surfaces; (a) Fe, (b) O, (c) S, (d) Cr, and (e) Ni

NSSER-4 showed excellent corrosion resistance (under 0.076 mm/y (3.0 mils/y)) within the temperature range of 480$^{o}$C -580$^{o}$C (Figure 5-37). The addition of HCl gas increased the corrosion rate, especially from 0 to 500 ppm. The corrosion rates increased to about 4.5 mils/y when the metal temperature was over 580$^{o}$C, and the effect of HCl gas was also magnified.

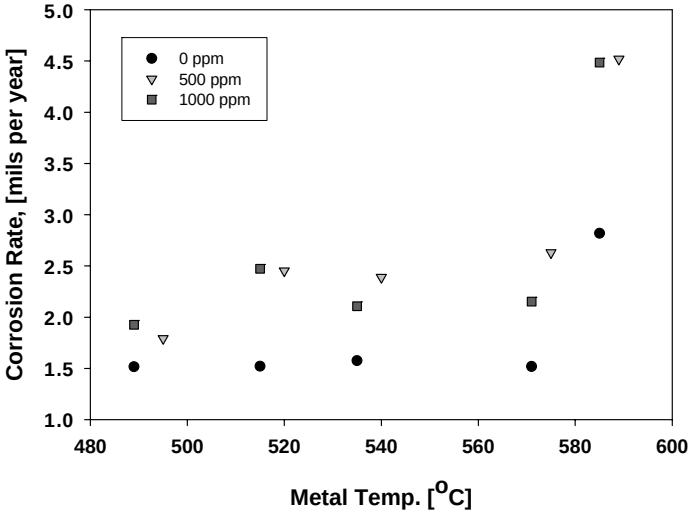


Figure 5-37 Comparison of mass loss corrosion rates

**(4) Comparison of corrosion rates of three materials**

Figure 5-38 shows the comparison of corrosion rates of three materials that were tested under similar condition (metal temperature: SA178—573$^{0}$C, SA213 T11—567$^{0}$C, NSSER-4—586$^{0}$C). The addition of HCl gas increased the corrosion rate of all three materials. The corrosion rates of alloy SA178A increased dramatically when the HCl gas concentration was added from 0 to 500ppm which indicated that this material had poor resistance to chlorine induced corrosion. Alloy SA213 T11 was able to resist

the chlorine induced corrosion when the HCl gas concentration increased from 0 to 500ppm, but its performance degraded when the HCl gas concentration increased more. Stainless steel NSSER-4 showed good corrosion resistance even under higher HCl gas concentration.

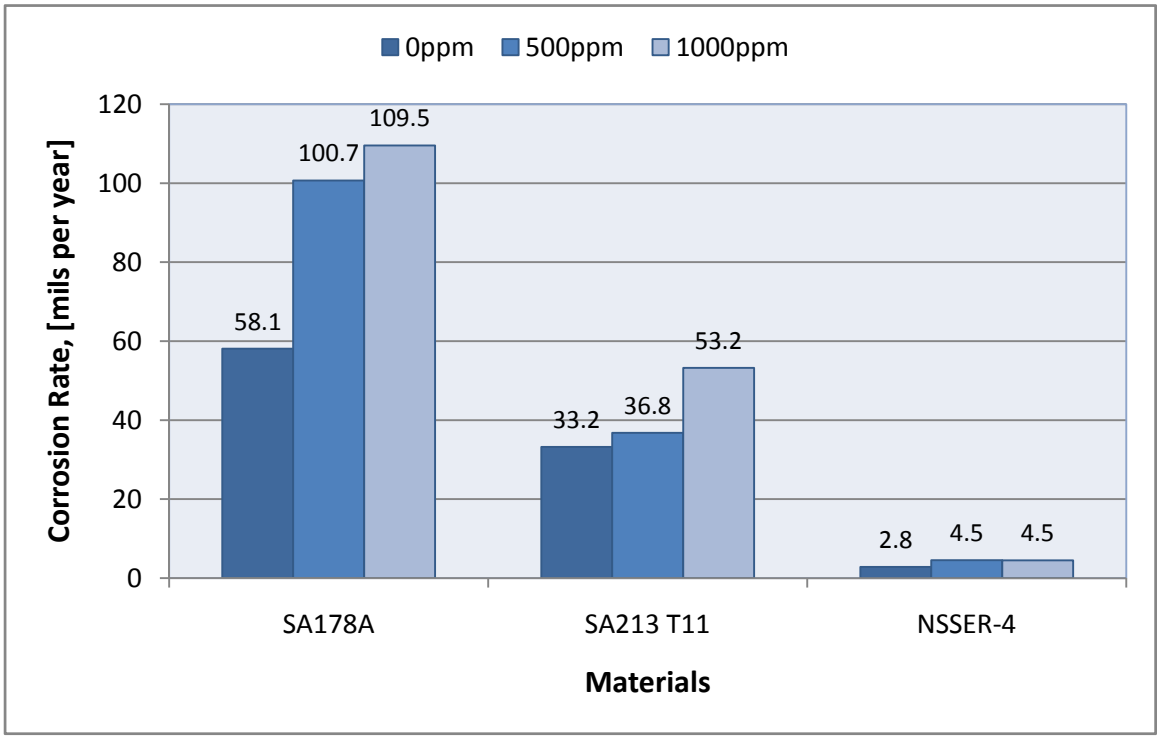


Figure 5-38 The comparison of corrosion rates of three materials

### 5.3.3. Conclusions

The addition of 500 and 1000ppm HCl to the synthetic gas flow used in the corrosion tests increased the corrosion rates of these three test samples, although the relation between the HCl concentration and corrosion rate was not linear. The HCl effects on corrosion rates were more prominent when its concentration changed from 0

to 500ppm. In addition, the HCl effects were accentuated by increasing the metal temperature. When the metal temperature was below 500$^{o}$C, the HCl effect was negligible, while its effect increased significantly when the metal temperature was over 560$^{o}$C.

In order to simulate the gas environment in the WTE facility, another corrosive gas - $SO_2$ was included in the synthetic gas in addition to HCl. The advantage of this approach was that the corrosion rates acquired from the test could reflect the practical situations in WTE facilities. On the other hand, this also increased the complexity of analyzing the corrosion resistance of different elements in a sample and the difficulty of isolating the HCl effect from the overall corrosion rate.

## 5.4. Preliminary Results of HCl/$Cl_2$ Sequestration Tests

### 5.4.1. Test Background

As mentioned earlier, the chlorine content in MSW is about 0.47 to 0.72% (470 to 720 parts per million by volume) [4]. During combustion, nearly all of the chlorine content in the various components of the MSW, both natural organics and chlorinated plastics is volatilized and converted to HCl gas. On the basis of earlier estimates [4] that the MSW contains 0.5% chlorine, nearly half of it due to chlorinated plastics, the HCl concentration in the combustion gases was calculated to be about 580 ppm [5]. Laboratory investigations on the corrosion behavior have shown that even small

changes of the oxygen/chlorine ratio or temperature can influence the corrosion behavior. A recent in-situ study indicated that significantly increased corrosion rate was observed when extra chlorine in the form of PVC was added to the fuel mix [38]. In addition, as noted elsewhere in this thesis, the results of the present study showed that increasing the HCl concentration in the synthetic gas flow through the test chamber from 500 to 1000ppm greatly increased the corrosion rates of test samples.

Since high chlorine concentrations in the WTE combustion chamber are the cause of high corrosion rates and removing high-chlorine waste materials from the municipal solid waste feed to the WTE unit is not feasible, a way should be found to decrease HCl concentration in the combustion chamber.

A process has been proposed at Columbia University to reduce HCl concentration in flue gas of WTE combustion chambers. This method injects, through a system of pneumatic or pressure nozzles located at a level above the combustion grate of the WTE or in front of the superheater section of the boiler, where metal is subjected to most severe corrosion (Figure 5-39), a slurry of calcium hydroxide that reacts with HCl to form calcium chloride as per the following chemical reaction:

$$Ca(OH)_2 + 2HCl(g) = CaCl_2 + 2H_2O(g) \qquad (5\text{-}19)$$

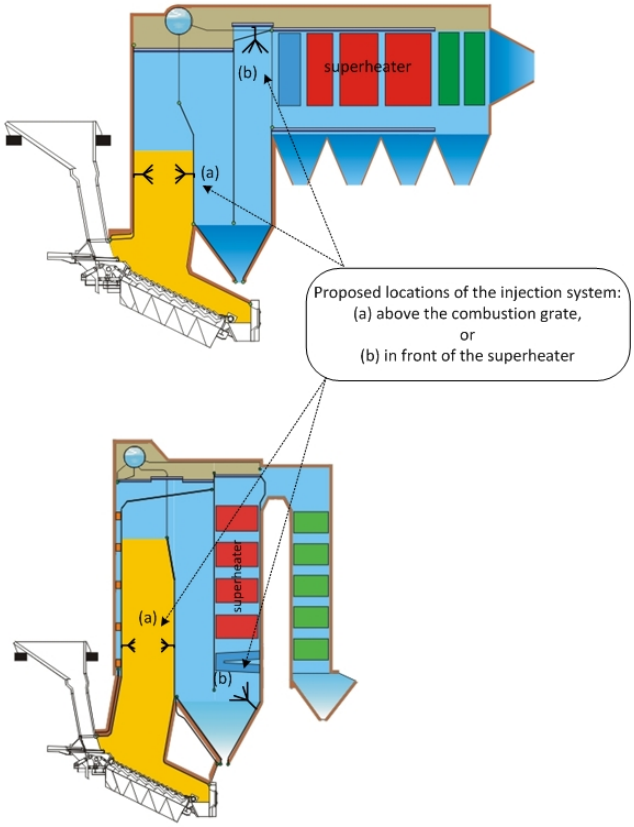


Figure 5-39 Schematic of WTE unit with proposed locations of injection system [41]

The chemical reaction involved in the proposed process for chlorine sequestration is the same as that used in the semi-dry scrubber section of the Air Pollution Control system that follows the WTE boilers. As mentioned in the Chapter 1.1, the HCl and $SO_2$ concentration in the flue gas of WTE facilities can be as high as 580 ppm and 100 ppm, respectively. As part of the 1990 Clean Air Act mandates, EPA promulgated new air pollution control standards for large WTE facilities (daily combustion of MSW more than 250 tons) in 1995. These standards required facilities to implement the Maximum Available Control Technology (MACT). The emission allowance

of HCl and $SO_2$ under MACT regulations is 29 ppm or 95% removal of HCl and 29ppm or 75% removal of sulfur dioxide [42]. In order to meet the MACT regulations, most WTE facilities have adopted the semi-dry scrubber systems to control their acid gases and particulate emissions.

In a semi-dry scrubber system, a finely atomized lime slurry of $Ca(OH)_2$ is injected in the dry scrubber via spray lance/nozzle assemblies to react with the acid gases and generate calcium sulfite/sulfate/chloride reaction products. The particulate matter is then collected in the baghouse that is installed after the scrubber system. The removal efficiency of acid gases in a dry scrubber system is more than 95% [42].

According to the information provided by the engineer of Covanta Energy Corp. [43], WTE plants consume between 9.1 to 13.6 kg (20-30 lbs) of lime (about 95% CaO) per ton of MSW processed. The CaO is converted to $Ca(OH)_2$, (slaking) yielding a concentration of about 10 wt.% $Ca(OH)_2$. This slurry is then atomized into the scrubber system with dilution water. The flowrate of the dilution water is controlled to maintain the desired outlet temperature of the scrubber system, which is typically about 150$^{o}$C (300$^{o}$F). Adding the dilution water just prior to the atomizers reduces the $Ca(OH)_2$ concentration to just a few percent.

The proposed injecting location for the proposed sequestration process is either at a level right above the combustion grate of the WTE or in front of the superheater section where the flue gas temperature (700-1100$^{o}$C) is much higher than that entering the dry scrubber system (150$^{o}$C). Table 5-2 shows that the formation of calcium chloride is highly favored thermodynamically over the whole temperature range in a WTE

combustion chamber. Therefore, in both proposed locations, under the prevailing flue gas temperatures, the injection of calcium hydroxide in the combustion zone will complex hydrochloric gas and chlorine molecules and thus reduce corrosion phenomena.

Table 5-2 Thermodynamic properties of calcium chloride reaction [40]

| T (°C) | deltaH (kJ) | deltas (J/K) | deltaG (kJ) | K | Log(K) |
|---|---|---|---|---|---|
| **100** | -109.088 | 27.154 | -119.220 | 4.900E+016 | 16.690 |
| **200** | -110.166 | 24.607 | -121.809 | 2.809E+013 | 13.449 |
| **300** | -111.487 | 22.081 | -124.143 | 2.065E+011 | 11.315 |
| **400** | -112.974 | 19.693 | -126.230 | 6.251E+009 | 9.796 |
| **500** | -114.577 | 17.474 | -128.087 | 4.512E+008 | 8.654 |
| **600** | -116.243 | 15.448 | -129.731 | 5.776E+007 | 7.762 |
| **700** | -117.908 | 13.642 | -131.184 | 1.102E+007 | 7.042 |
| **800** | -121.042 | 10.011 | -131.785 | 2.600E+006 | 6.415 |
| **900** | -123.960 | 7.410 | -132.652 | 8.070E+005 | 5.907 |
| **1000** | -126.720 | 5.151 | -133.278 | 2.941E+005 | 5.469 |
| **1100** | -129.336 | 3.173 | -133.692 | 1.219E+005 | 5.086 |
| **1200** | -131.819 | 1.427 | -133.920 | 5.609E+004 | 4.749 |
| **1300** | -134.178 | -0.123 | -133.984 | 2.813E+004 | 4.449 |
| **1400** | -136.420 | -1.506 | -133.901 | 1.516E+004 | 4.181 |
| **1500** | -138.552 | -2.743 | -133.688 | 8.681E+003 | 3.939 |

### 5.4.2. Experimental Matrix

| *Test sample* | | *Test environment* | | *Injection system* | | | |
|---|---|---|---|---|---|---|---|
| materials | metal temperature | gas composition | gas (furnace) temp. | air pressure | fluid pressure | fluid capacity | $Ca(OH)_2$ conc. |
| SA178A, SA213 T11, and NSSER-4 | 700°C | 8% $O_2$, 12% $CO_2$, 15% Water Vapor, 500 ppm HCl, 100 ppm $SO_2$, and balance $N_2$ | 750°C | 20.7 kPa (3 psi) | 34.5 kPa (5 psi) | 64.4 $cm^3$/min (0.017 gallons/min) | 0.16% (2 times of the stoichiometry, the outlet HCl concentration would be zero if fully reacted) |

### 5.4.3. Results and Discussion

As mentioned in Chapter 4.2.3, coupons (2.6 cm X 2.6 cm) of three different metals were suspended at the end zone of the reaction tube so as to ensure maximum contact time and reaction between the injected slurry particles and the flue gas. Unlike previous corrosion tests in this study, there was no thermal gradient created by the cooling air. The metal temperatures reached in the HCl sequestration test (approximately 700$^{o}$C) were much higher than in the temperature gradient tests (400-550$^{o}$C), therefore, the corrosion rates were much higher than those reported in Chapters 5.1.2. and 5.2.2. Table 5-3 shows the total mass loss (both sides of the coupon are corroded) and the reduction in corrosion rate effected by the injection of the $Ca(OH)_2$ droplets into the reaction tube as determined after the 50-hour test.

Without the injection of calcium hydroxide slurry, samples of alloy SA178A and SA213 T11 showed mass loss of 57% and 62%, respectively (mass loss per surface area was 0.133 and 0.197 g/cm$^2$, respectively). These results confirmed that corrosion rates by HCl at high metal temperature are indeed catastrophic, and that corrosion continues unabated by volatilization of successive metal layers at the gas-metal interface. However, it is interesting to note that the sample of stainless steel NSSER4 showed excellent corrosion resistance, even under these conditions with mass loss of only 0.89% (mass loss per surface 0.001 g/cm$^2$).

With the injection of calcium hydroxide slurry maintained at a fixed ratio with respect to the inlet HCl concentration ($Ca(OH)_2$ : HCl = 2 : 1), the overall mass loss for the SA178, SA213 T11, and NSSER-4 coupons was reduced to 39%, 56%, and 0.62%,

respectively (mass loss per surface area was 0.093, 0.161, and 0.0006 $g/cm^2$, respectively). The corresponding mass loss reduction during the 50-hour test was 17.87%, 6.42% and 0.27%.

Another test was carried out that attempted to increase the ratio of $Ca(OH)_2$ to HCl from 2 to 4 (concentration of $Ca(OH)_2$ slurry form 0.16% to 0.32%) to investigate if the corrosion rate would be further reduced. Unfortunately, the test was not successful because the concentration of the slurry was too high to be used in the spray system. The nozzle head got stuck and required cleaning every 5-10 minutes.

Table 5-3 Corrosion reduction of test samples after 50 hours at metal temperature of 700°C

| | *SA178A* | | *SA213 T11* | | *NSSER-4* | |
|---|---|---|---|---|---|---|
| ***Baseline (no $Ca(OH)_2$)*** | mass loss per surface area ($g/cm^2$) | overall mass loss (%) | mass loss per surface area ($g/cm^2$) | overall mass loss (%) | mass loss per surface area ($g/cm^2$) | overall mass loss (%) |
| | **0.133** | **56.67** | **0.197** | **62.40** | **0.0010** | **0.89** |
| ***$Ca(OH)_2$ : HCl = 2 : 1*** | mass loss per surface area ($g/cm^2$) | overall mass loss (%) | mass loss per surface area ($g/cm^2$) | overall mass loss (%) | mass loss per surface area ($g/cm^2$) | overall mass loss (%) |
| | **0.093** | **38.80** | **0.161** | **55.98** | **0.0006** | **0.62** |
| ***Corrosion reduction*** | | mass loss reduction (%) | | mass loss reduction (%) | | mass loss reduction (%) |
| | | **17.87** | | **6.42** | | **0.27** |

### 5.4.4. Conclusions on chlorine sequestration tests

The injection of calcium hydroxide slurry to react with $HCl/Cl_2$ gas has shown to reduce corrosion phenomena effectively in the combustion chamber. The blank test that was conducted without the chemical slurry injection showed that samples of the steel alloys SA178A and SA213 T11 were corroded rapidly due to the high HCl concentration and elevated metal temperature ($700^oC$). However, even under these extreme conditions, the stainless steel NSSER 4 resisted corrosion very well. Its overall mass loss per surface area was 64 times lower than SA178A and 70 times lower than SA213 T11.

With the chemical slurry injection, the overall mass loss of the three alloys tested was reduced by 0.3-18%. These results confirmed the known fact that HCl is the main contributor to corrosion, by the formation of ferrous chloride that continues to volatilize with catastrophic effects. Also, the results showed that chemical reaction between the $Ca(OH)_2$ and HCl is effective in sequestering chlorine in the form of $Ca(OH)_2$ and reducing HCl concentration under the environment of the WTE combustion chamber.

Although the injection system in the combustion will help to decrease the concentration of acidic gas in flue gas, its main purpose is to help reduce the corrosion phenomena; it is not, aimed to replacing the semi-dry scrubber in the air pollution control system. However, the installation of the injection system in the combustion chamber is expected to reduce the amount of calcium hydroxide needed in the

subsequent in the semi-dry scrubber since part of the acidic gas has been removed in advance.

The results of this study are encouraging enough to warrant further and more detailed study of calcium hydroxide injection in the combustion chamber, such as the mixing of the injected slurry particles and the flue gas, the optimal injecting ratio, the injecting location, and cost-benefit analysis of such a process in an actual WTE plant. However, it is believed that the results of these tests can provide WTE engineers with useful information in developing a new method of combating corrosion in WTE boilers.

# 6. Conclusion

The corrosion survey of about 50 WTE facilities in the U.S. showed that the most common material for the waterwall tubing in the combustion chamber was low-carbon steel SA178A (>99%Fe), and its average wastage rate was 1.62 mm/y (63.8 mils/y). All of the WTE facilities that participated in the survey applied Inconel 625 (58%Ni-20-23%Cr-8-10%Mo) cladding to the waterwall, and the average wastage rate of 0.14 mm/y (5.5 mils/y) was reported. The average lifetime of service for Inconel 625 was about 5-10 years. In most plants, higher HCl and $SO_2$ concentration led to higher coverage of the Inconel 625 cladding. If the coverage of Inconel 625 cladding is taken as an indicator of the corrosion rate, we can describe higher HCl and $SO_2$ concentrations as the contributors to higher corrosion rates.

Low-carbon, intermediate-chrome alloys SA213 T11 (Fe-1.05%Cr-0.08%C) and SA213 T22 (Fe-2.21%Cr-0.1%C) were most widely used for superheater tubes. The average wastage rate varied widely from 0.01 to 3.81 mm/y (0.002 to 150 millls/y) among WTE facilities. Some WTE facilities applied a small portion of Inconel 625 on superheater. Unlike the waterwall, the lifetime of superheater tubes was more unpredictable. As indicated by the wastage rates mentioned above, superheater tubes may last for years, or as little as three months. Also, the respondents to the survey generally agreed that the application of Inconel 625 did not improve performance too much. Both the higher HCl and $SO_2$ concentrations led to higher wastage rate of superheater tubing.

The yearly maintenance cost per boiler unit due to corrosion ranged from $18,000 to $1.2 million (2003 dollars; the highest cost of $1.2 million was due to the plant's recent replacement of the boiler), and the reported maintenance cost due to corrosion ranged from as low as $0.23 to $8.17 per ton of MSW combusted. For the high corrosion rate plants, the corrosion costs accounted for about 1/3 of the total maintenance cost.

In the first set of corrosion tests conducted in this study, an apparatus that created a controlled thermal gradient between synthetic flue gas and metal surface was developed to examine the corrosion rates of different commercial alloys. The experimentally determined corrosion rates were in agreement with the annual wastages of boiler tubes in WTE facilities and have proven the ability of this apparatus to predict the life of a particular tube alloy.

The stainless steel alloy NSSER-4 (Fe-17.3%Cr-13.1%Ni-2.5%Si) that is produced by the Japanese company, exhibited the excellent corrosion resistance and little effect of metal temperature on the corrosion rate and composition of corrosion product in the temperature range of 500-630$^{o}$C. Although this alloy is not available in the current U.S. steel industry, it is still highly recommended to be applied as the superheater tubing when higher metal temperature is required. The low-carbon, intermediate-chrome steel, SA213 T11, exhibited acceptable corrosion resistance at metal temperature up to 540$^{o}$C, but its performance degraded dramatically when the metal temperature was above 540$^{o}$C. For superheater tube operated at metal temperature lower than 540$^{o}$C, SA213 T11 is a more economical solution instead of stainless steel. The carbon steel SA178A

had the highest corrosion rate among all of the metals. This explains why it is mostly used as waterwall (i.e., at relatively lower metal temperatures) and, also, it is cladded with Inconel 625.

The cross-sectional elemental analysis verified the theory that chloride (or chlorine) penetrated the oxide scale through cracks in the scale to react with the base metal due to activity driven by chemical potential and temperature gradients. This results in formation and volatilization of iron chloride and also on the formation and accumulation on the metal/oxide scale.

The addition of 500 and 1000ppm HCl to the synthetic gas flow used in the corrosion tests increased the corrosion rates of test samples. The presence of HCl promoted the formation of sulfate salts that also increased the corrosion. However, the relation between the HCl concentration and corrosion rate was not linear: the HCl effects on corrosion rates became more prominent as its concentration was increased from 0 to 500ppm. In addition, the HCl effects were accentuated by increasing the metal temperature.

The results of the chemical rate test showed that the overall reaction process of alloy SA178A during the 100-hour test followed the parabolic time dependence which was often found in high temperature oxidations. The calculated overall apparent activation energy of alloy SA178A within the 100-hour test was 178kJ/mol. The calculated activation energy of alloy SA178A after a single 100-hour test was 149kJ/mol, which was close to its overall activation energy showing that the 100 hours of exposure was suitable for the corrosion test. From the compassion of activation energies of three

test materials, it was inferred that the corrosion of the low-carbon steel, SA178A was more reaction control while the stainless steel, NSSER-4 was more diffusion control.

The injection of calcium hydroxide slurry to react with $HCl/Cl_2$ gas was shown to reduce corrosion phenomena effectively in the combustion chamber. These accelerated corrosion tests were conducted at temperatures of about $700^{o}C$, which is substantially higher than the controlled temperature gradient test. The observed reduction of overall mass loss ranged from 0.3-18% in three different test materials. In these accelerated corrosion tests, the stainless steel alloy, NSSER-4, exhibited its superiority: Its mass loss was 0.001 grams per square centimeter, which is 133 to 197 times lower than the two steel alloys used widely in WTE boilers. The installation of the injection system in the combustion chamber would be beneficial to reduce the corrosion phenomena of the boiler tube and the amount of lime slurry injected in the semi-dry scrubber since part of the acidic gas has been removed in advance.

# References


1. Themelis, N.J., Y.H. Kim, and M.H. Brady, *Energy recovery from New York City municipal solid wastes.* Waste Management & Research, 2002. **20**(3): p. 223-233.
2. *Integrated Waste Services Association*. [cited 2007; Available from: www.wte.org/worldwide.
3. Themelis, N.J. and P.A. Ulloa, *Methane generation in landfills.* Renewable Energy, 2007. **32**(7): p. 1243-1257.
4. Albina, D.O., K. Millrath, and N.J. Themelis. *Effects of Feed Compositions on Boiler Corrosion in Waste-to-Energy Plants*. in *12th North American Waste To Energy Conference (NAWTEC 12)*. 2003. Florida, USA.
5. Themelis, N.J., *Chlorine Balance in a Waste-To-Energy Facility*. 2005, Earth Engineering Center.
6. Adams, B., et al. *Seghers Boiler Prism: a Proven Primary Measure against High Temperature Boiler Corrosion*. in *12th North American Waste to Energy Conference*. 2004. Savannah, U.S.A.
7. Albina, D.O., *Theory and experience on corrosion of waterwall and superheater tubes of Waste-To-Energy facilities*, in *Department of Earth and Environmental Engineering*. 2005, Columbia University.
8. Roberge, P.R., *Handbook of Corrosion Engineering*. 2000: Mc Graw Hill.
9. Lee, S.-H., N. Themelis, and M. Castaldi, *High-Temperature Corrosion in Waste-to-Energy Boilers.* Journal of Thermal Spray Technology, 2007. **16**(1): p. 104-110.
10. Rademarkers, P., W. Hesseling, and J.v.d. Wetering, *Review on corrosion in waste incinerators, and possible effect of bromine*. 2002, TNO Industrial Technology.
11. Kawahara, Y., *Evaluation of high-temperature corrosion life using temperature gradient corrosion test with thermal cycle component in waste combustion environments.* Materials and Corrosion, 2006. **57**(1): p. 60-72.
12. Holcomb, G.R., *Hot corrosion in a temperature gradient.* Materials and Corrosion, 2000. **51**(8): p. 564-569.
13. Covino, B.S., et al., *Corrosion in a Temperature Gradient*. 2001, Albany Research Center, U.S. Department of Energy: Albany.
14. Holcomb, G.R., B.S. Covino, and J.H. Russell, *Oxidation in a temperature gradient*, in *15th Annual Conference on Fossil Energy Materials*. 2001: Oak Ridge National Laboratory.
15. Kawahara, Y., et al., *Demonstration test of new corrosion-resistant superheater tubings in a high-efficiency waste-to-energy plant.* Corrosion' 2000, 2000: p. 265.

16. Kofstad, P., *High temperature corrosion*. 1988, London ; New York: Elsevier. x, 558 ill. 23 cm.

17. Kawahara, Y., Y. Yamada, and K. Seki. *Proceedings of High Temperature Corrosion and Protection*. 2000. Lusutsu, Japan.

18. Spiegel, W., *Praxisnahe Unterstutzung der Betreiber bei der Optimierung und nachhaltigen Nutzung der bayerischen MV-anlagen*. 2002, CheMin GmbH: Augsburg, Germany.

19. Wilson, A., U. Forsberg, and J. Noble, *Experience of composite tubes in municipal waste incinerators.* Corrosion 97, 1997: p. 153.

20. Solomon, N.G., *Erosion-resistant coatings for fluidized bed boilers.* Materials Performance, 1998. **37**(2): p. 38-43.

21. Uusitalo, M.A., P.M.J. Vuoristo, and T.A. Mantyla, *Elevated temperature erosion-corrosion of thermal sprayed coatings in chlorine containing environments.* Wear, 2002. **252**(7-8): p. 586-594.

22. Higuera, V., et al., *Influence of the thermal-spray procedure on the properties of a nickel-chromium coating.* Journal of Materials Science, 2002. **37**(3): p. 649-654.

23. Al-Fadhli, H.Y., et al., *The erosion-corrosion behaviour of high velocity oxy-fuel (HVOF) thermally sprayed inconel-625 coatings on different metallic surfaces.* Surface and Coatings Technology. **In Press, Corrected Proof**.

24. Fukuda, Y., K. Kawahara, and T. Hosoda, *Application of high velocity flame sprayings for superheater tubes in waste incinerators.* Corrosion 2000, 2000: p. 264.1-264.14.

25. Martin, J.D. and K. Robbins. *Evaluation of chloride corrosion reduction with chemical additives at Maine Energy Recovery*. in *13th NAWTEC*. 2005. Orlando, FL.

26. Smyriniotis, C.R. and C. Collier, *Slag Inhibition Success Utilizing Targeted In-Furance Injection at Western Farmers Cooperative Hugo Station*, in *PRB Coal Users' Group Annual Meeting, Electric Power 2004 Conference*. 2004: Baltimore, MD.

27. Zwahr, H. *Ways to improve the efficiency of waste to energy plants for the production of electricity, heat and reusable materials*. in *11th North American Waste To Energy Conference* 2003. Tampa, FL.

28. Kawahara, Y., *High temperature corrosion mechanisms and effect of alloying elements for materials used in waste incineration environment.* Corrosion Science, 2002. **44**(2): p. 223.

29. Covino, B.S., Jr. , et al., *The Role of Ash Deposits in the High Temperature Corrosion of Boiler Tubes*, in *Corrosion 2003*. 2003, NACE International, 1440 South Creek, Houston, TX 77084-4906 USA: San Diego, CA

30. Stott, F.H. and C.Y. Shih, *The influence of HCl on the oxidation of iron at elevated temperatures.* Materials and Corrosion, 2000. **51**(5): p. 277-286.

31. Mohanty, B.P. and D.A. Shores, *Role of chlorides in hot corrosion of a cast Fe-Cr-Ni alloy. Part I: Experimental studies.* Corrosion Science, 2004. **46**(12): p. 2893.

32. N. Otsuka, Y.F.Y.K.T.H., *Laboratory corrosion tests for simulating fireside wastage of superheater materials in waste incinerators.* Materials and Corrosion, 2000. **51**(4): p. 236-241.

33. Spiegel, M., *Influence of gas phase composition on the Hot Corrosion of steels and nickel-based alloys beneath a (Ca-Na-K)-sulfate mixture containing PbSO4 and ZnSO4.* Materials and Corrosion, 2000. **51**(5): p. 303-312.

34. *Catalog 70 US*, S.S. Co., Editor. 2008.

35. Lu, X., G. Liu, and S. Luan. *The development of the boiler water wall tube inspection*. in *Electric Utility Deregulation and Restructuring and Power Technologies, 2008. DRPT 2008. Third International Conference on*. 2008.

36. A. Zahs, M.S.H.G., *The influence of alloying elements on the chlorine-induced high temperature corrosion of Fe-Cr alloys in oxidizing atmospheres.* Materials and Corrosion, 1999. **50**(10): p. 561-578.

37. Asteman, H. and M. Spiegel, *Investigation of the HCl (g) attack on pre-oxidized pure Fe, Cr, Ni and commercial 304 steel at 400 [degree sign]C.* Corrosion Science, 2007. **49**(9): p. 3626-3637.

38. Persson, K., et al., *High temperature corrosion in a 65 MW waste to energy plant.* Fuel Processing Technology, 2007. **88**(11-12): p. 1178-1182.

39. Lee, S. H. and M.J. Castaldi, *High temperature corrosion resistance of different commercial alloys under various corrosive environments*, in *The North American Waste-to-Energy Conference* 2007: Miami, FL.

40. *HSC Chemistry*. 2008, Outotec: Espoo, Finland.

41. 03/20/2008 [cited 2008 03/01]; Drawings of various boiler designs]. Available from: http://www.martingmbh.de/index_en.php?level=2&CatID=6.31&inhalt_id=27.

42. Wark, K., C.F. Warner, and W.T. Davis, *Air Pollution: Its Origin and Control* 3ed. 1997: Prentice Hall.

43. Goff, S., *Dry scrubbing operation in WTEs Corrosion Research*, J.T. Nickolas, Editor. 2008: New Jersey.

# Appendix 1: WTERT Corrosion Questionnaire

## Waste-To-Energy Research and Technology Council

### Corrosion Data Questionnaire

Corrosion is a major cost in the operation of WTE facilities and the subject of a major research effort by the WTERT Council for 2005. In addition to the analysis of published data and experimental work, this project can benefit much by the experience of the operators of WTE facilities. The objective of this questionnaire is to collect data and benefit from the accumulated experience of the operators of WTE facilities that are members of ISWA. The identity of each plant responding to this Questionnaire will be maintained confidential but the results of the analysis will be made available to all plants and companies participating in this Survey.

Please return the completed Questionnaire and other documents requested to Prof. Nickolas J. Themelis (njt1@columbia.edu) who will assign an identification number to each responding WTE and maintain the identity of each plant confidential. Any questions related to the questionnaire or additional information that you think is relevant to the study (e.g., past corrosion studies by the plant or the company), should be sent to Prof. Themelis or contact Mr. Shang-Hsiu Lee (sl2304@columbia.edu, (212)-854-0305).

**Date:**

**Plant name/Company**:

**Respondent's (name and e-mail)**:

**Type of WTE** (mass burn, RDF):

**Unit #** (Please select the most representative unit in your plant):

**Grate technology** (Martin, Von Roll, Roller Grate, Seghers, etc.):

**Unit actual daily capacity**: (tons/day)

**Unit days of operation/year**: (days)

**Total air input**: (scfm), or (lb/h)

**Steam generation**: Design: (lb/hr) Actual: (lb/hr)

**Boiler outlet steam temperature**: (F)

**Boiler diagram:** Please attach boiler diagram showing steam / water /flue gas layout and approximate location of secondary air nozzles

**Waterwall Data:**

Average number of days between shutdowns because of corrosion: (days)

Frequency of unexpected shutdowns because of corrosion: (times/year)

Details of Tubing:

a) Base Metal:

b) Tube diameter: thickness: and spacing:

Refractory Lining:

a) Type of refractory:

b) How is the refractory applied (as castable or tile):

c) Anchoring system/s used:

d) Has the use of refractory improved performance:

e) Height above the grate where “best choice” switches from refractory to alloy cladding:

f) Height of the furnace above the grate (at feed end):

Alloy Cladding:

- Type:

- Thickness:

- Area of coverage above refractory lining (height, wall areas, etc):

Approximate percent of waterwall cladded:

- 1st pass:

- 2nd pass:

- 3rd pass:

What is the average lifetime of alloy cladding (if used):

What is the saturation temperature in the steam/water mix in the waterwall and the corresponding drum pressure:

Flue gas conditions:

What is the temperature (measured or estimated) at the exit of the furnace? first pass: (F) second pass: (F) third pass: (F)

What is the typical operating oxygen concentration? Design: (%)

Actual: (%)

c) How are these temperatures measured (unshielded short thermocouple, IR measuring device, shielded aspirating pyrometer traverse, other):

Maximum observed wastage rate due to corrosion: (mils/year) (Please specify the corroded material, e.g. the corrosion rate of Inconel)

Estimated weight of new metal used for waterwall: (lb/yr)

**Superheater Tube Data:**

Average number of days between shutdowns because of corrosion:

1st superheater: (days) 2nd superheater: (days) 3rd superheater: (days)

Frequency of unexpected shutdowns because of corrosion: (times/year)

Details of tubing:

a) Base Metal:

b) Tube diameter: thickness: spacing:

Cladding:

a) Type or types of alloys used:

b) Cladding (thickness):

Percent of superheater tube cladded: 1st superheater: (%) 2nd superheater: (%) 3rd superheater: (%)

Superheater Conditions if known (if more than one superheater please specify):

What are the steam inlet temperature: (F) pressure: (psia) mass flow rate: (lb/h)

What are the steam outlet temperature: (F) pressure: (psia) mass flow rate: (lb/h)

What are the estimated flue gas conditions (temperature, velocity) at inlet of superheater: (F) outlet of superheater: (F)

Maximum observed wastage rate: (mils/year)

Estimated weight of new metal used for superheaters: (lb/yr)

What is average lifetime of the superheater bundle?

**Furnace and Boiler Questions.**

Please list the principal types of corrosion that you have observed in furnace and boiler (i.e. flame impingement, erosion-corrosion, molten salts corrosion, acid gas condensation (HCl and $SO_x$), acid gas attack ($SO_x$), stress induced corrosion, etc) and also at which location in your process is this type of corrosion the most problem?

Please describe briefly tube-cleaning method in your plant: Do you think this method and the frequency of cleaning affect tube life:

What is the duration in days between cleaning cycles (offline and online) of fire side deposits? Offline: (days) Online: (days)

How often does the boiler come off line due to grate slagging or low furnace clinkers:

**Combustion Air, $NO_x$ Reduction and Cleaning Technique Questions:**

Ratio of primary air to secondary air:

Is there a flue gas recirculation system: If yes, what is the estimated % recirculation: (%)

Are auxiliary burners used: If yes, do you think they contribute to corrosion:

Are chemicals added in the furnace for emission reduction: If yes, please state type and flow rates used: Do you think such chemicals have an effect on corrosion:

Typical HCl concentration (inlet of APC): (ppm)

Typical $SO_2$ concentration (inlet of APC): (ppm)

**Overall:**

Estimated yearly scheduled downtime: (days)

Estimated non-scheduled downtime due to corrosion: (days)

Estimated yearly maintenance cost for unit due to corrosion: (Please specify the cost, e.g. the replacement of superheater bundle, alloy cladding, etc.)

Has the facility carried out fuel characterization: If so please attach results.

Has the facility carried out R&D on corrosion: If the answer is Yes, please send results, comments and any conclusions to Prof. Themelis indicating whether you like the facility to be anonymous in the communication of such results to other ISWA members.

***Many thanks for your contribution to this Survey. Please return questionnaire, drawing and any previous study/report on corrosion to***

Prof. Nickolas J. Themelis
WTERT, Earth and Engineering Center
Columbia University
500 West, 120th Street, #918 Mudd
New York, New York, 10027
Tel: (212)-854-2138 Fax:(212)-854-5213
(E-mail: njt1@columbia.edu)

To understand more about WTERT, please visit: http://www.columbia.edu/cu/wtert/

# Appendix 2: Results of the WTERT Corrosion Questionnaire

The responses of each question are summarized below. The author communicated with the survey respondents to ensure the accuracy of the information. The questions are underlined. Because not all the responses of each question are applicable, each analysis result presented below is followed by the effective number of samples shown in the bracket.

**(1) Basic information of the facility:**

(a) Type of WTE: mass burn (13), RDF (1).

(b) Grate technology: rotary combustor (4), roller grate (1), reciprocating grate (8), and traveling grate (1).

(c) Ave. unit actual daily capacity: 439 tons/day, StdDev: 217 tons/day (14).

(d) Ave. unit days of operation: 331 days/y, StdDev: 12 days/y (14).

(e) Ave. total air input: 108,587 kg/h (239,394 lbs/h), StdDev: 73,877 kg/h (162,871 lbs/h) (13).

(f) Ave. steam generation: 55,649 kg/h (122,685 lbs/h), StdDev: 28,817 kg/h (63,570 lbs/h) (13).

(g) Ave. boiler outlet steam temperature: 386$^{o}$C, StdDev: 5$^{o}$C (14).

**(2) Waterwall tube data:**

(a) Base material of tubing: SA178a (12), SA210al (1), and SA192 (1).

(b) Ave. tube diameter: 76.2 mm (3 inches), StdDev: 7.62 mm (0.3 inches) (14).

(c) Ave. tube thickness: 4.58 mm (0.18 inches), StdDev: 0.76 mm (0.03 inches) (14).

(d) Ave. tube spacing: 73.9 mm (2.91 inches), StdDev: 40.9 mm (1.61 inches) (9).

(e) Type of refractory: 12 facilities use refractory lining in the combustion chamber. There is a big diversity of types of refractory which include Bluemax ram, Inconel 625, Resco 70Hs, Onyx 80, etc.

(f) Has the use of refractory improved performance: Yes (2), No (4), and No reference (3).

(g) Alloy cladding: Inconel 625 (14).

(h) Thickness of alloy cladding: 1.78 mm (0.07 inches), StdDev: 0.152 mm (0.006 inches) (14).

(i) Ave. approximate cladding percentage of waterwall ($1^{st}$ pass): 65%, StdDev: 26.6% (10).

(j) Ave. approximate cladding percentage of waterwall ($2^{nd}$ pass): 10%, StdDev: 6.1% (5).

(k) Ave. approximate cladding percentage of waterwall ($3^{rd}$ pass): 1.4%, StdDev: 2.2% (5).

(l) The Ave. saturation temperature in the steam/water mix in the waterwall and the corresponding drum pressure: $266^{o}$C, StdDev: $2.85^{o}$C (14), 5260 kPa (763 PSIG), StdDev: 1172 kPa (170 PSIG) (12).

(m) Ave. flue gas temperature at the exit of the furnace (1st pass): 806°C, StdDev: 41.1°C (13).

(n) Ave. flue gas temperature at the exit of the furnace (2nd pass): 662°C, StdDev: 113.1°C (8).

(o) Ave. flue gas temperature at the exit of the furnace (3rd pass): 513°C, StdDev: 86.2°C (9).

(p) Ave. operating oxygen concentration (design): 8.07%, StdDev: 1.82% (13).

(q) Ave. operating oxygen concentration (actual): 7.88%, StdDev: 1.53% (14).

(r) Ave. maximum observed wastage rate of cladding material (Inconel 625) due to corrosion: 0.14 mm/y (5.5 mils/y), StdDev: 0.13 mm/y (5.1 mils/y) (5).

(s) Ave. maximum observed wastage rate of base tubing due to corrosion: 1.62 mm/y (63.8 mils/y), StdDev: 0.46 mm/y (18.0 mils/y) (4).

**(3) Superheater tube data:**

(a) Base material of tubing: SA213 T11 and T22 are the most popular materials (9). The others include SA106B, SA178A and SA355.

(b) Ave. tube diameter: 49.78 mm (1.96 inches), StdDev: 8.89 mm (0.35 inches) (14).

(c) Ave. tube thickness: 5.59 mm (0.22 inches), StdDev: 1.78 mm (0.07 inches) (14).

(d) Ave. tube spacing: 125.98 mm (4.96 inches), StdDev: 40.13 mm (1.58 inches) (9).

(e) Alloy cladding: Inconel 625 (6), stainless steel shield (5), and none (2).

(f) Thickness of alloy cladding: 1.78 mm (0.07 inches), StdDev: 0.102 mm (0.004 inches) (7).

(g) Ave. approximate cladding percentage of 1st superheater: 2.7%, StdDev: 3.6% (9).

(h) Ave. approximate cladding percentage of 2nd superheater: 33.4%, StdDev: 41.3% (9).

(i) Ave. approximate cladding percentage of 3rd superheater: 25%, StdDev: 50% (4).

(j) Ave. steam inlet temperature, pressure, and mass flow rate of 1st superheater: 261°C, StdDev: 3.8°C, 754 PSIG, StdDev: 149 PSIG, and 121768 lbs/h, StdDev: 65367 lbs/h (14).

(k) Ave. steam outlet temperature, pressure, and mass flow rate of 1st superheater: 398°C, StdDev: 28.2°C, 5199 kPa (705 PSIG), StdDev: 903 kPa (131 PSIG), and 53,481 kg/h (117,906 lbs/h), StdDev: 28,871 kg/h (63,651 lbs/h) (14).

(l) Ave. flue gas inlet temperature of 1st superheater: 699°C, StdDev: 142°C (13).

(m) Ave. flue gas outlet temperature of 1st superheater: 492°C, StdDev: 74.2°C (11).

(n) Ave. maximum observed wastage rate due to corrosion: 1.32 mm/y (51.8 mils/y), StdDev: 1.41 mm/y (55.4 mils/y) (7).

**(4) Furnace and boiler data:**

(a) The principal types of corrosion observed in furnace and boiler and also at which location in process is this type of corrosion most prevalent: Flame impingement (6), erosion-corrosion (10), molten salts corrosion (7), stress corrosion (2), and soot blower damage (2).

(b) Tube cleaning method in the plant: Soot blowing (10), water pressure washing (4), explosive blasting (3), grit blasting (1), stick blasting (2), string blasting (3), and rappers (1).

(c) Does the cleaning method affect tube life: Yes (Soot blowing, 10).

**(5) Combustion air, $NO_X$ reduction and clean technologies:**

(a) Ratio of primary air to secondary air: 3.1 (12) and no secondary air (2).

(b) Flue gas recirculation: No (14).

(c) Are chemicals added in the furnace for emission reduction? No (5), aqueous ammonia for $NO_X$ reduction (6), and urea for $NO_X$ control (3).

(d) Do you think such chemicals have an effect on corrosion: Yes (4, Aqueous ammonia (3) and urea (1)).

(e) Typical HCl concentration (inlet of APC): 544 ppm, StdDev: 110.4 ppm (8).

(f) Typical $SO_2$ concentration (inlet of APC): 108 ppm, StdDev: 59.4 ppm (13).

**(6) Overall operating information**

(a) Estimated yearly scheduled downtime: 20.3 days, StdDev: 6.4 days (14).

(b) Estimated non-scheduled downtime due to corrosion: 8.6 days, StdDev: 9.16 days (14).

(c) Estimated yearly maintenance cost for unit due to corrosion: $273,140, StdDev: $387,895 (8).